AD-A242 082
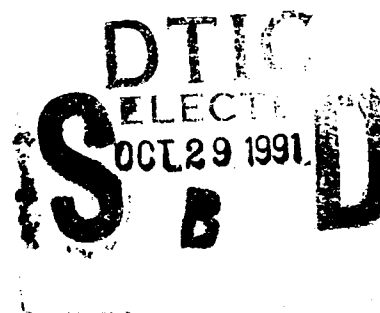

Technical Report 1430
May 1991

Radio Wave Propagation in Horizontally Inhomogeneous Environments by Using the Parabolic Equation Method

A. E. Barrios

91-14111

91 10 25 058

NAVAL OCEAN SYSTEMS CENTER
San Diego, California 92152-5000

J. D. FONTANA, CAPT, USN
Commander

R. T. SHEARER, Acting
Technical Director

ADMINISTRATIVE INFORMATION

SUMMARY

OBJECTIVE

Investigate the validity of a parabolic equation (PE) model for predicting radio field strengths in horizontally inhomogeneous environments by performing comparisons between the model and experimental data.

RESULTS

Excellent agreements were found at VHF and UHF frequencies with good agreement in S- and X-bands. In some cases, the predicted curves for the S-band comparisons underestimated that of the measured data at large ranges. This may be the result of phenomena such as surface roughness, backscatter, etc., not accounted for in the model. Discrepancies may also result from the presence of evaporation ducts not included in the environmental inputs to the model because of a lack of detailed measurements. This would account for lower predicted signal levels at higher frequencies.

CONTENTS

1.0 INTRODUCTION

Many field-strength prediction models for tropospheric radiowave propagation over the ocean have been written, based on the limitation that the environment is laterally homogeneous. It was found that the assumption of a horizontally stratified troposphere led to valid propagation assessments 86% of the time [1]. While the troposphere over the sea does exhibit horizontal homogeneity over relatively long distances in most cases, meteorological conditions occur occasionally in which the environment may change drastically in just a few kilometers, such as at air-mass boundaries associated with wave cyclones and land/ocean interfaces [2]. It is safe to say that horizontally varying environments do occur 14% of the time. This paper addresses the validity of the parabolic equation (PE) model for handling these environments.

The more conventional method of modeling electromagnetic wave propagation in the troposphere is performed by normal mode theory, but most modal techniques are based on a horizontally stratified atmosphere. A parabolic equation method, originally developed by Fock in 1946, allowed the environment to vary with range as well as height [3].

Two methods can be used to solve the PE. One method approximates the derivatives in the PE by finite differences. The other solves the PE (with some approximations) by the split-step Fourier method developed by Hardin and Tappert [4]. The split-step method requires a constant vertical mesh size because of the Fast Fourier Transforms (FFT) used, which may require large data arrays for sufficient sampling. The main advantage the split-step method has over finite difference is that it is more efficient at higher frequencies. The disadvantage is that, with higher frequencies, one needs to have a larger transform size (smaller vertical mesh size). The finite-difference method has the advantage that variable height and range steps can be used to keep the number of data points stored at a minimum. Over the relatively long distances at which one is interested in looking, the split-step method is more numerically efficient because of the FFTs employed. The split-step algorithm thus allows real-time predictions based on current environment descriptions.

While the acoustic community has been using PE modeling for some time, it was only recently (within the last decade) that the radar community has applied the PE method to tropospheric radiowave propagation [5--8].

The importance of the split-step PE method is not only that it provides an exact solution to field equations (within the limits of the operator approximation) for a homogeneous atmosphere in a relatively short time, but that it can also predict (with relatively small errors) field strengths for laterally inhomogeneous environments. The importance of taking into account an environment that varies with ange will become apparent as case studies are presented between experimental data and the predicted fields.

A parabolic equation model for the personal computer (PEPC) was developed by Professor Fred Tappert of the University of Miami in conjunction with the Naval Ocean Systems Center (NOSC), San Diego, during 1989 and 1990. Comparisons between predicted PE fields and measured radio and meteorological profiles on over-water paths from Guadalupe Island to San Diego in 1947 and 1948 are presented [9]. Some comparisons also were made against experimental data taken from the Canterbury Project [10]. The appendix contains a list of profiles used for the figures presented in this report.

2.0 BACKGROUND

2.1 REFRACTIVE EFFECTS

The refractive index, n, of air is defined as the ratio of the velocity of propagation of an electromagnetic (EM) wave in a vacuum to that in air. Since EM waves travel more slowly in air than in a vacuum, this ratio is always greater than one. At the Earth's surface, the numeric value of n is usually between 1.000250 and 1.000400. A more convenient number to use is the refractivity, N, which is defined as $N = (n - 1)10^6$. Normal surface N values then range from 250 to 400. Refractivity can be expressed as a function of atmospheric pressure, air temperature, and humidity as follows:

$$N = (77.6P)/T + (3.73*10^5 e)/T^2$$

where P is the pressure in millibars, T is the temperature in degrees Kelvin, and e is the vapor pressure in millibars. In a "standard" well mixed atmosphere, both temperature and humidity decrease with increasing height such that N decreases at the rate of about 39 N-units per kilometer. An EM wave propagating initially horizontal to the Earth's surface will be refracted downward, but with a rate of curvature less than that of the Earth. If the air temperature should increase with height, or the humidity decrease abnormally fast with altitude, N will decrease faster than normal with height. If N decreases faster than 157 N-units per kilometer, an EM wave will be refracted downward with a radius of curvature greater than the Earth's surface. When this occurs, the EM wave can be trapped in a surface duct. The EM wave is first refracted downward toward the surface and, if the surface is sufficiently smooth, the wave is specularly reflected. This process can be repeated to ranges far beyond the normal horizon. Such continuous refractions/reflections form a surface-based duct and allows radar detections at greatly extended ranges.

A more convenient method for expressing the refractivity to determine the occurrence of ducting is with the use of modified refractivity, or M-units. M is defined in terms of N as

$$M = N + 0.157 h$$

for h in meters. Modified refractivity accounts for the curvature of the Earth and ducts can be determined by inspection of M plotted versus height. Whenever M decreases with height, a trapping layer is formed and indicated by a negative M-gradient. Examples of N and M plotted versus height for a standard atmosphere (118 M-units per kilometer) are given in figure 1. In this figure, M increases with altitude and no trapping layer or duct is formed. Figure 2 shows a plot where M decreases with height and forms a trapping layer (in this case, a surface-based duct). If the M value at the top of the trapping layer is less than that at the surface, then a surface-based duct is formed. If the M value at the top of the trappin; layer is greater than that at the surface, an elevated duct is formed; the vertical extent of the duct is determined by the height below the trapping layer where the M value is equal to M at the top of the trapping layer. Two other terms are used to describe N- or M-gradients other than standard or trapping, namely subrefractive and superrefractive. Superrefractive means more bending than standard refraction but less than trapping. Subrefractive means less refraction than standard. These atmospheres generally do not have the spectacular effect on EM system performance that ducting does.
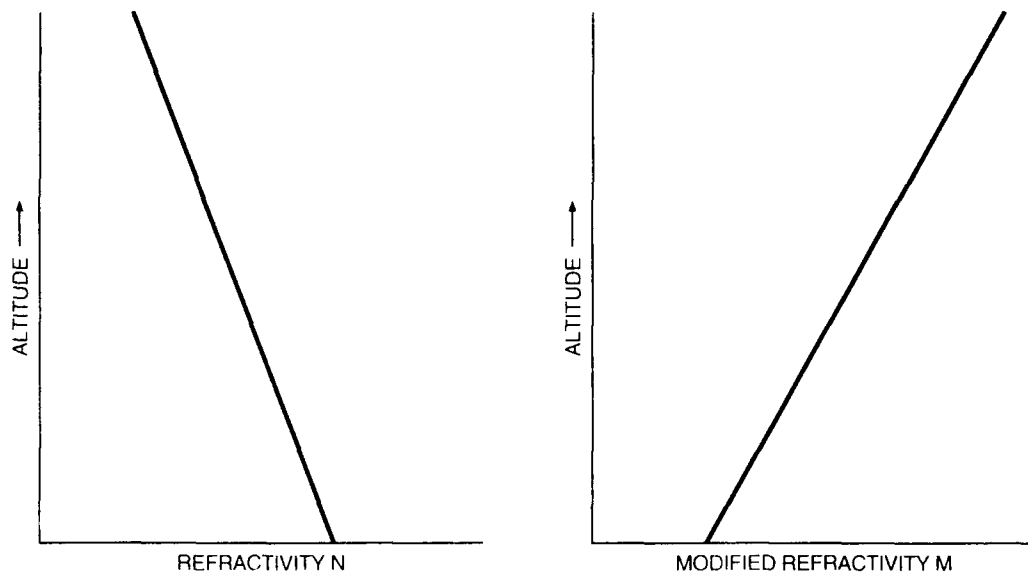
Figure 1. Refractivity N and modified refractivity M versus altitude for a standard atmosphere.
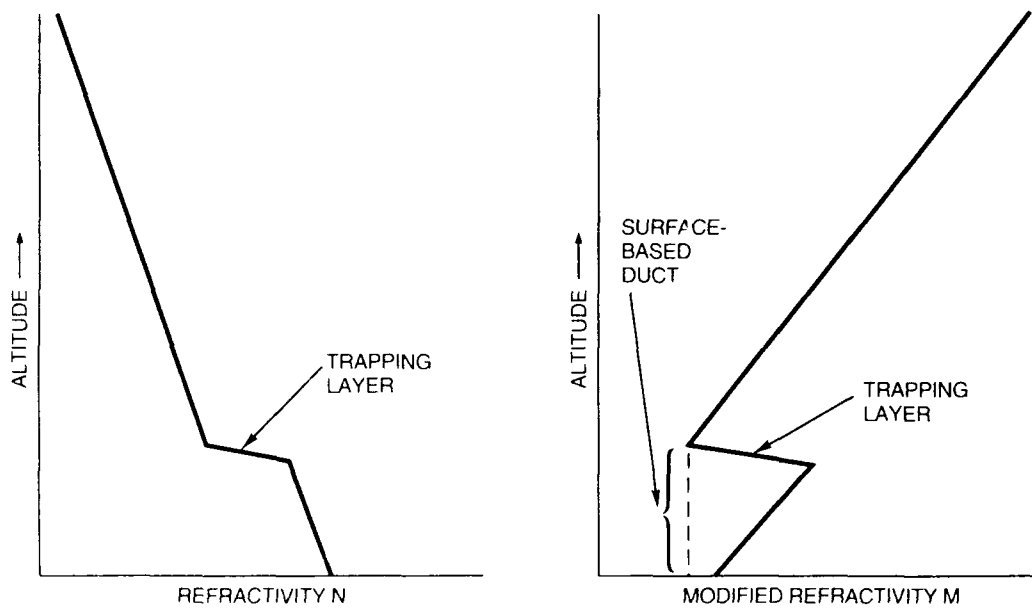
Figure 2. Refractivity N and modified refractivity M versus altitude for a surface-based duct created by an elevated trapping layer.

Another measure of refractivity that was widely used in the 1940s is the B-unit, defined as

B = N + 0.039 h

for h in meters. Thus, for a standard atmosphere, B would be invariant with height.

The two distinct types of surface ducts that affect naval EM systems are surface-based ducts from elevated layers and evaporation ducts. Surface-based ducts from elevated layers are formed by a sharp change in the index of refraction gradient between a cool, moist marine air mass and a dryer, warmer air mass above it. These ducts generally affect all systems with frequencies greater than about 100 MHz, provided both transmitter and receiver/target are in or near the duct. These ducts tend to be on the order of 100 to 300 meters thick. This type of duct is quite common off the Southern California coast, where the same temperature inversions that cause smog to be trapped in the Los Angeles air basin also create strong surface-based ducts at sea. The duct has a dramatic effect on the signal level well beyond the horizon but, generally, does not greatly affect the signal level within and near the horizon. Quite often, a "skip zone" is formed where ranges just beyond the horizon are in the normal shadow zone, while slightly greater ranges are illuminated by energy that has been refracted down by the trapping layer. The range to, and extent of, the skip zone is obviously a complex function of the duct height, the M-unit gradients, and the transmitter height. An example of such a skip zone is given in figure 3, which is a raytrace diagram for a 25-meter transmitter antenna in a 100-meter surface-based duct. The trapping layer is represented by the shaded area. The skip zone is from approximately 12 to 17 nmi. For comparison, the raytrace of figure 4 is at the same transmitter height but under standard atmospheric conditions.
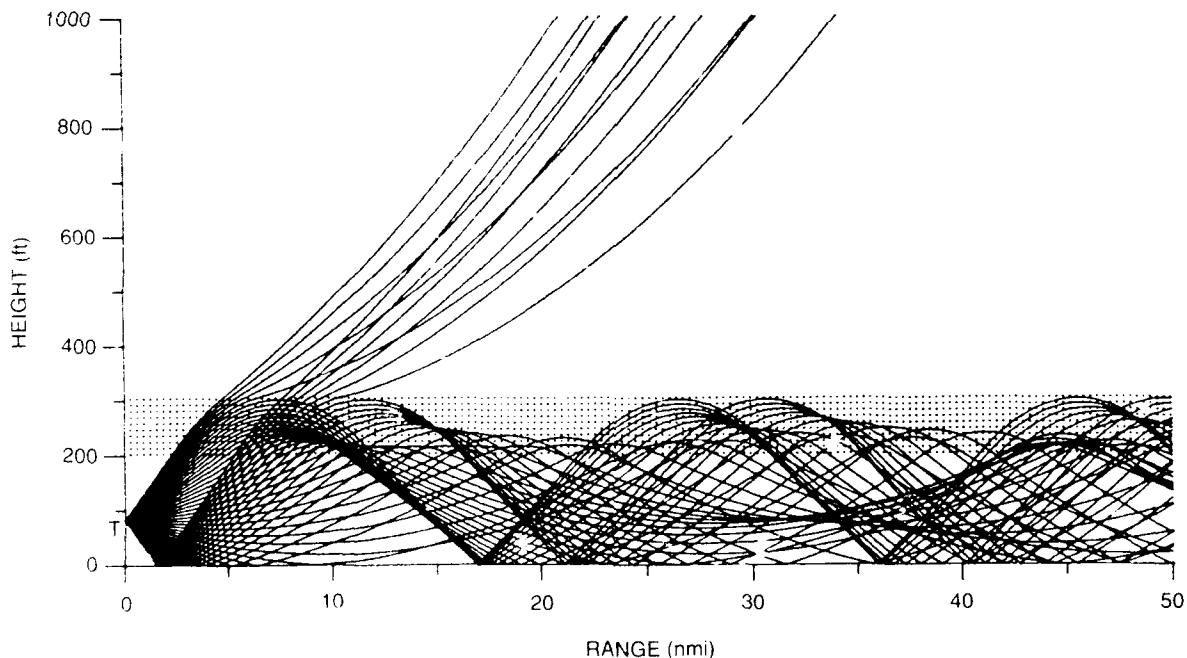
Figure 3. Raytrace diagram for a transmitter at 25 meters (m) in a 100-m surface-based duct resulting from an elevated layer.
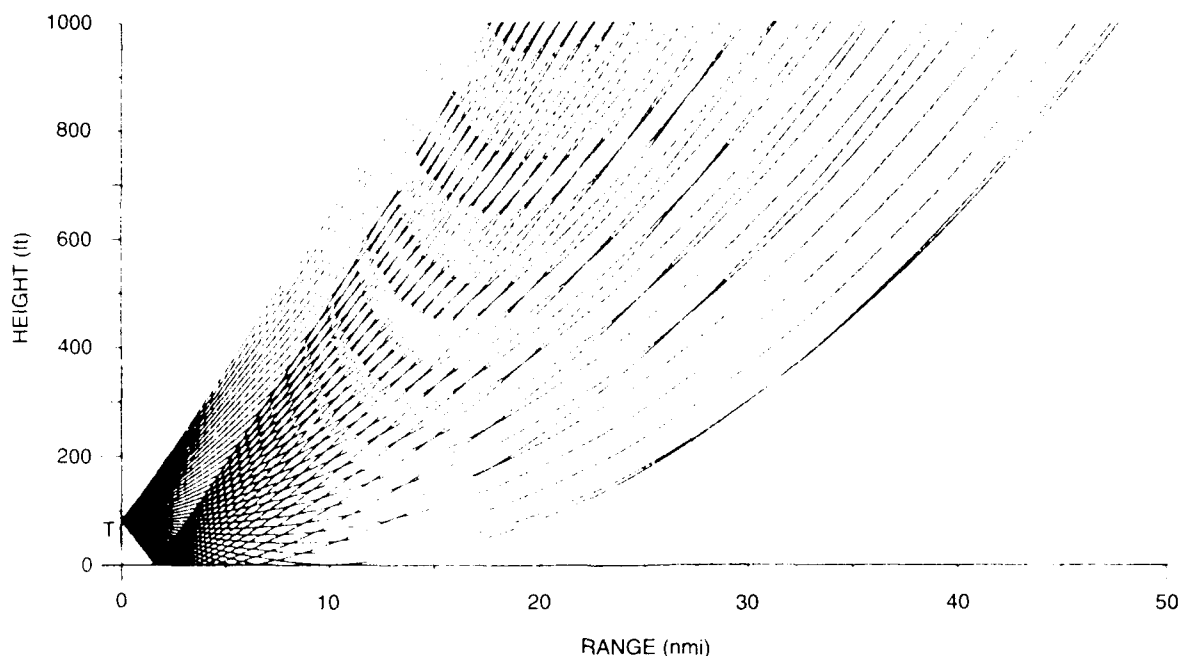
Figure 4. Raytrace diagram for a transmitter at 25 m, standard atmosphere conditions.

Evaporation ducts are created by a rapid decrease in humidity from the air/sea interface. These ducts are limited by boundary-layer mechanics to perhaps 50 meters, although heights of less than 20 meters are the most common. Figure 5 is an example of a typical evaporation-duct M-unit profile. The evaporation-duct height corresponds to the minimum on the M-unit profile and is a measure of the strength of the duct. Unlike the surface-based duct resulting from an elevated layer, the radar and the target do not have to be "in" the duct for enhanced signal levels to be observed. These ducts primarily affect EM systems with frequencies greater than 3 GHz and, if a surface-based duct from an elevated layer is present, it will be the dominant propagation mechanism for ranges well beyond the horizon.
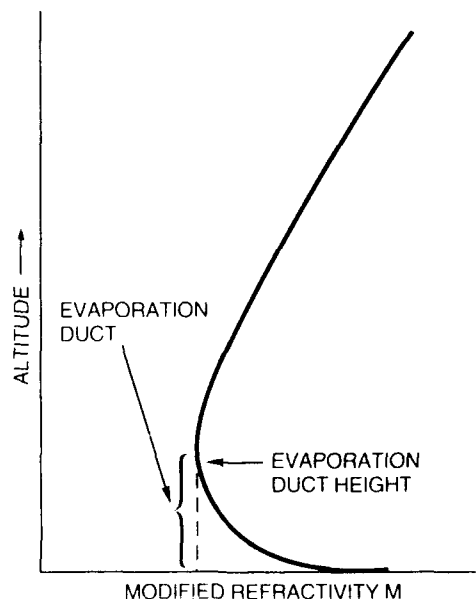
Figure 5. M-profile for a typical evaporation duct.

5

2.2 SPLIT-STEP PE MODEL

A brief discussion will be given of the PE method and how the program calculates field strength. For more detailed descriptions of the theory, see [3, 4, 11]. In the following discussion, the troposphere is assumed to vary in range and height only, making the field equations independent of azimuth. The Earth's surface will be considered perfectly conducting, and only horizontal polarization will be addressed.

As with every electromagnetic wave problem, one begins with Maxwell's equations for steady-state sinusoidal (harmonic) time-varying fields. Second-order partial differential equations (p.d.e.) for the electric and magnetic fields can be derived from the coupled first-order differential equations by the usual method. For a horizontally polarized electric dipole, the only nonzero component of the electric field is $E\varphi$ (r,θ), where r, θ, φ represent spherical coordinates. To write the second-order p.d.e. in the form of the scalar Helmholtz wave equation, a change of variable is used

$$\psi(r,\theta) = \sqrt{r\sin\theta} \ E\varphi(r,\theta) \tag{1}$$

and, changing from spherical to rectangular coordinates by using $z = r - a$ and $x = a\theta$ (applying the Earth-flattening transformation, valid for $z/a \ll 1$, $x/a \ll 1$), one obtains the two-dimensional elliptic wave equation

$$\left[\frac{\partial^2}{\partial x^2} + \frac{\partial^2}{\partial z^2} + k_o^2 \ m(x,z) \right] \psi(x,z) = 0 \tag{2}$$

$$m(x,z) = n(x,z) + z/a$$
$$k_o = 2\pi/\lambda$$

where now

$$\psi(x,z) \cong \sqrt{x} \ E\varphi(x,z) \tag{3}$$

and x represents the horizontal spatial coordinate (range), z is the vertical coordinate (height), a is the Earth's radius, k_o is the vacuum wavenumber, and $m(x,z)$ is the modified index of refraction taking into account the Earth's curvature and neglecting small terms, since we are only interested in the field at large ranges $(kx \gg 1)$.

In much of the literature that has been published on the theoretical description of the derivation of the PE, the parabolic approximation is stated in two ways. The first method removes rapid phase variations (on the basis that one is only interested in field variations that are large compared to a wavelength) by performing an envelope transformation

$$\psi(x,z) = u(x,z) \ e^{ik_o x} \tag{4}$$

which is substituted in equation 2 to give

$$\left[\frac{\partial^2}{\partial x^2} + \frac{\partial^2}{\partial z^2} + 2ik_o \frac{\partial}{\partial x} + k_o^2 \ (m^2 - 1) \right] u(x,z) = 0. \tag{5}$$

6

The horizontal variation in u(x,z) is now assumed to be slow

$$\left|\frac{\partial^2 u}{\partial x^2}\right| \ll 2 k_o \left|\frac{\partial u}{\partial x}\right| \tag{6}$$

in which case one is justified in neglecting the second-order partial derivative in the horizontal component in equation 5. The second method is to define an operator $Q(x)$ and factor equation 2:

$$\left[\frac{\partial}{\partial x} - i k_o Q(x)\right]\left[\frac{\partial}{\partial x} + i k_o Q(x)\right] \psi(x,z) + i k_o \left[\frac{\partial}{\partial x}, Q(x)\right] \psi(x,z) = 0 \tag{7}$$

$$Q(x) = \sqrt{\frac{1}{k_o^2} \frac{\partial^2}{\partial z^2} + m^2} \tag{8}$$

where

$$\left[\frac{\partial}{\partial x}, Q(x)\right] = \frac{\partial Q}{\partial x} - Q \frac{\partial}{\partial x}. \tag{9}$$

The quantities in brackets in equation 7 represent the equations for outward and inward propagating waves, respectively. Since we are only interested in outward propagating waves, we use

$$\frac{\partial}{\partial x} \psi(x,z) = i k_o Q(x) \psi(x,z). \tag{10}$$

After substitution of equation 4, the final equation we must solve is

$$\frac{\partial}{\partial x} u(x,z) = i k_o \tilde{Q}(x) u(x,z) \tag{11}$$

where

$$\tilde{Q}(x) = Q(x) - 1. \tag{12}$$

7

This is now reduced to an initial value problem that neglects backscattering and can be solved by "marching out" in range. Equation 11 is referred to in the literature as the general parabolic equation (GPE), and is exact for a range-independent environment.

While it is not incorrect to make the assumption given by equation 6, the assumption necessarily restricts accurate solutions to the field to near-horizontal directions or small propagating angles. The second method has the advantage that approximations can be made for backscattered waves; the different methods of approximating or "splitting" the operator $\tilde{Q}(x)$ lead to different parabolic equation propagators.

For the simplest case, assume that the index of refraction in $\tilde{Q}(x)$ is range independent (m is constant); then the field at some range $x + \Delta x$ can be found from $u(x)$;

$$u(x + \Delta x) = e^{ik_o \int_x^{x + \Delta x} \tilde{Q}(x)dx} u(x) \sim e^{ik_o \Delta \tilde{Q}(x)} u(x). \tag{13}$$

At this point, $\tilde{Q}(x)$ can be "split" to get ultimately a form for $u(x + \Delta x)$ suitable for numerical computation on a computer. Let us define two new variables a and b:

$$a = \frac{1}{k_o^2} \frac{\partial^2}{\partial z^2}; \quad b = m^2 - 1. \tag{14}$$

$\tilde{Q}(x)$ can now be written as a function of a and b as

$$\tilde{Q}(x) = (1 + a + b)^{1/2} - 1. \tag{15}$$

The two most widely used approximations for $\tilde{Q}(x)$ are

$$\tilde{Q}_1(x) = (1/2)a + (1/2)b \tag{16a}$$

$$\tilde{Q}_2(x) = (1 + a)^{1/2} + [(1 + b)^{1/2} - 1] - 1 \tag{16b}$$

where in $\tilde{Q}_1(x)$ the term under the radical in equation 15 has been expanded in a binominal series with higher-order terms dropped. This approximation leads to the standard parabolic equation (SPE). $\tilde{Q}_2(x)$ leads to the wide-angle parabolic equation (WAPE) originally derived by Feit and Fleck [12] to study propagation in optical fibers, and later applied to acoustic propagation by Thomson and Chapman [13].

Thomson and Chapman have done extensive error analysis for the approximations $\tilde{Q}_1(x)$ and $\tilde{Q}_2(x)$ and have stated that $\tilde{Q}_2(x)$ gives much more accurate numerical predictions at higher angles. However, their application was toward acoustic propagation, in which severe ducting conditions (large gradients) in the ocean can trap modes corresponding to relatively large propagation angles. For the electromagnetic case, large gradients found in the troposphere are two orders of magnitude smaller than that found in the ocean. So while the acoustic problem may need more accuracy at higher angles, for the small propagation angles important in the electromagnetic case, Dockery [14] found no significant

8

improvement between the SPE propagator and the WAPE propagator. Therefore, the remainder of this section will be dealing with the approximation given by $\tilde{Q}_1$ (x).

$\tilde{Q}_1$ (x) can now be used in equation 13:

$$u(x + \Delta x, z) = e^{ik_o \Delta x (A + B)} u(x,z)$$ (17)

where

$$A = (1/2)a; \quad B = (1/2)b.$$

The second-order partial derivative in the exponent can easily be handled by using Fourier transforms. The Fourier transform is defined as

$$U(x,p) = \mathscr{F}[u(x,z)] = \int_\infty^\infty u(x,z) e^{-ipz} dz$$ (18a)

$$u(x,z) = \mathscr{F}^{-1}[U(x,p)] = \frac{1}{2\pi} \int_\infty^\infty U(x,p) e^{ipz} dz$$ (18b)

where the transform variable p is $k_o \sin \theta$, θ being the propagation angle above the horizontal. Using the transform property that

$$\frac{\partial^n u(x,z)}{\partial z^n} \xrightarrow{\mathscr{F}} (-ip)^n U(x,p)$$ (19)

and noting that A and B commute (A + B = B + A)

$$u(x + \Delta x, z) = e^{ik_o \Delta x B} \left[e^{ik_o \Delta x A} u(x,z) \right]$$ (20)

equation 17 can now be solved to give

$$u(x + \Delta x, z) = e^{ik_o \frac{\Delta x}{2} (m^2 - 1)} \mathscr{F}^{-1} \left\{ e^{-i \frac{\Delta x}{2} \frac{p^2}{k_o}} \mathscr{F}[u(x,z)] \right\}.$$ (21)

Equation 21 is the formula that must be computed at each range step, Δx, based on the field at the previous range.

When the refractive index, m, is range dependent, the quantities A and B no longer commute, in which case the steps leading to the right-hand side of equation 13 become more complicated. Approximations and assumptions have to be made in which one finally obtains the same equation for the

field (equation 21), but with a somewhat complicated error term. This error term depends on the range step size, Δx, the frequency, and the refractive index gradients. Therefore, one can make the errors associated with a range-dependent m in equation 21 small by taking a sufficiently small step size and assuring that m(x,z) varies slowly with range.

2.3 PROPAGATION FACTOR AND PATH LOSS

The final step is to determine the pattern propagation factor, F, once the field u(x,z) has been computed. The pattern propagation factor is defined as the ratio of the magnitude of the field at a point in space $|\vec{E}|$, to the magnitude of the field at the same point under free-space conditions, $|\vec{E}_o|$:

$$F = \left| \frac{\vec{E}}{\vec{E}_o} \right| . \tag{22}$$

The field attributable to a horizontally polarized source in free space, located on the vertical axis, is proportional to (in spherical coordinates)

$$E_o \approx \frac{e^{ik_oR}}{R} \left(\frac{r}{R} \sin\theta \right) \tag{23}$$

$$R = (r^2 + r_o^2 - 2r\,r_o\cos\theta)^{1/2}$$

where r_o is the distance to the source from the point of reference and θ is the angle with respect to the vertical between the source and field point. Recalling equation 1, the propagation factor is now written

$$F = \left| \frac{E_\phi}{E_o} \right| = \frac{|\psi(r,\theta)|R^2}{(r\sin\theta)^{3/2}} \tag{24}$$

where the normalizing constant is absorbed in $|\psi(r,\theta)|$. Changing from spherical to Cartesian coordinates, R becomes

$$R = [x^2 + (z-z_o)^2]^{1/2} = x\left[1 + \frac{(z-z_o)^2}{x^2}\right]^{1/2} \approx x \quad \text{for} \quad \frac{(z-z_o)}{x} \ll 1 \tag{25}$$

and the denominator becomes

$$r\sin\theta = a\sin\theta \approx a\theta \approx x \quad \text{for} \quad x/a \ll 1 \tag{26}$$

to obtain for F

$$F = |\psi(x,z)|\sqrt{x} = |u(x,z)|\sqrt{x} . \tag{27}$$

10

$u(x,z)$ is a complex function, possessing a real and imaginary component

$$u(x,z) = u_x + i\, u_y \tag{28}$$

In dB, F is then

$$10 \log F^2 = 10 \log [(u_x^2 + u_y^2) \times]. \tag{29}$$

Path loss, in dB, is defined as

$$\text{loss} = -10 \log \left[\frac{\lambda^2 \, F^2}{(4\pi\, x)^2} \right]. \tag{30}$$

Using equation 29, path loss is calculated as

$$\text{loss} = -10 \log \left[\frac{\lambda^2 \, (u_x^2 + u_y^2)}{(4\pi)^2 \, x} \right]. \tag{31}$$

2.4 NUMERICAL IMPLEMENTATION

The Fourier transform in equation 21 is implemented by using an FFT algorithm. The transform size is kept at a fixed number. The maximum propagating angle above the horizontal and the maximum height is made to depend on the frequency, thereby limiting the program to low-altitude, small-angle propagation effects at high frequencies. The sample size is based on Nyquist's criterion

$$z_{max} * p_{max} = \pi N \tag{32}$$

where z_{max} is the maximum height in the calculation domain and $p_{max} = k_o \sin\theta_{max}$, θ_{max} being the full angular width above and below the horizontal for a full complex transform. Due to the nature of the DFT, the field is abruptly truncated at z_{max}, resulting in reflections from the nonphysical upper boundary. Filters are used to attenuate the field smoothly at large heights and large propagation angles, to keep reflections from entering the physical portion.

The field at any point above the Earth can be found by using image theory and the appropriate boundary conditions. For a perfectly conducting surface and horizontal polarization, the field must vanish at the surface: $u(x,0) = 0$. The next step is to find an initial field $[u(0,z)]$ for which equation 21 can then be used to "march" the field out in range. One begins by noting that the field at range zero is essentially the antenna aperture distribution, and that the far-field antenna pattern and its aperture distribution are a Fourier transform pair:

$$u(o,z) \xleftarrow{\ \mathscr{F}\ } U(o,p) = f(p). \tag{33}$$

The antenna pattern $f(p)$ is assumed to be symmetric about $p = 0$ (0 elevation angle). Introducing a source height and elevation angle is easily done by using the Fourier transform shift properties

$$u(z - z_s) \xrightarrow{\mathscr{F}} e^{-ipz_s} f(p).$$ (34a)

$$e^{ip_o z} u(0,z) \xrightarrow{\mathscr{F}} f(p - p_o).$$ (34b)

where z_s is the source height and p_o is $k_o \sin \theta_{e1}$, θ_{e1} being the elevation angle.

Zero elevation angle was used in all results presented in this report. A uniform aperture distribution (essentially an omnidirectional antenna [f(p) = 1]) was used for the antenna pattern, making the initial field in p-space

$$U(0,p) = f(p) e^{-ipz_s} - f(-p) e^{ipz_s} = -2iC_n \sin(pz_s)$$ (35)

where C_n is the normalizing constant and the two terms on the right-hand side of U(0,p) represent the real and image fields, respectively. Note that U(0,p) is an odd function, resulting from a horizontally polarized source with the boundary condition for a perfectly conducting surface. The initial field for a vertically polarized source and its boundary condition ($\partial u/\partial z|_{z=0} = 0$) leads to an even function.

A troposcatter model is included in PEPC and was taken from Yeh [15] and Rice, et al. [16]. For a full description of the model, refer to NOSC TD 1342 [17], pp 116–120.

To keep the error term (associated with a nonconstant m in equation 21) small, we must keep Δx small. Δx is made to depend on the wavelength, thereby forcing the program to take small range steps at large frequencies where it is needed. For a range-dependent environment, a new profile is obtained at each range step from interpolation of user-specified profiles. The method of interpolation will be discussed in section 3.2.

3.0 VALIDATION OF PE MODEL

3.1 COMPARISON WITH RANGE-INDEPENDENT ENVIRONMENTS

Some comparisons were made against a waveguide program called MLAYER, using several range-independent environments. MLAYER was developed at NOSC by Baumgartner [18] and Pappert[1]. Figures 6 and 7 show excellent agreement between PEPC and MLAYER for a 300-meter surface-based duct at L band, and a 20-meter evaporation duct at X band, respectively. Field strength in dB relative to free space is plotted versus height. A standard atmosphere at S band was also used for comparison, but results between the two models were indistinguishable, so that case is not shown here.

A radiometeorological investigation was conducted jointly by the Departments of Scientific and Industrial Research of the United Kingdom and New Zealand under the name of the Canterbury Project in Canterbury Province in the South Island of New Zealand [10]. Transmitters were placed in aircraft that flew a sawtooth pattern from over 100 km offshore inward toward the receiving ground stations located at Wakanui Beach. Data were taken from the Canterbury Project for the afternoon of 5 August 1947. This case was chosen because the environment varied little with range. A strong surface duct was present from 20 km offshore out to 100 km, as shown by figure 8. Slant paths were used for the model to represent different "legs" of the aircraft flight paths. Figures 9 and 10 show the X-band and S-band cases, respectively, against the observed radio data. Both figures display field strength in dB relative to free space versus height for one "leg" from 65 to 75 nautical miles, in which the aircraft descended from 1000 ft (at 65 nmi) to near the ocean surface (at 75 nmi). The model compares well with the observed data.

3.2 COMPARISON WITH RANGE-DEPENDENT ENVIRONMENTS

Three profiles, along with their corresponding ranges, were specified as inputs to PEPC to simulate an environment that varied from a standard atmosphere at the antenna, to a 300-meter surface-based duct at 100 km, and back to a standard atmosphere at 200 km. Figure 11 shows a lateral heterogeneous raytrace for this environment, using a program developed at NOSC [2]. The dotted portion of the plot shows how the trapping layer varies with range in height and thickness. The PE model requires a profile at each range step. The three 4-point profiles and their ranges were specified as inputs and, internal to the program, linear interpolation was used to obtain the height and M-unit value for each point at each range step based on the two nearest specified profiles. This method of interpolation provides for logical and smooth transitioning of the various features between specified profiles. Figure 12 shows the PEPC coverage diagram for this environment. Comparing figures 11 and 12, one can see that the field contours from PEPC follow the ray paths in figure 11.

---

[1] Pappert, R. A. 1984. "Field Strength and Path-loss in a Multilayer Tropospheric Waveguide Environment," NOSC TN 1366 (October). Naval Ocean Systems Center, San Diego, California. NOSC Technical Notes are working documents and do not represent an official policy statement or the Naval Ocean Systems Center. For further information, contact the author.

3.2.1 Guadalupe Island Measurements

Radio and meteorological data were measured concurrently in over-water paths from Guadalupe Island to San Diego during 1947 and 1948 [9]. Figures 13 through 15 show the data records for 3 days of measurements. In this experiment, receivers were located on the ground and the transmitting and meteorological equipment was located in the aircraft. The flight paths are shown in the upper portion of the figures. The aircraft took radio measurements on both ascending and descending paths, but only made meteorological measurements on the ascending paths. An attempt was made to represent the "slant" profiles vertically at ranges corresponding to the optimum coupling height. (The optimum coupling height is the height at which the base of the inversion layer is measured, and at which placement of an antenna will yield maximum angular trapping.)

The measurements of 12 March 1948 show a slowly increasing trapping layer from 40 to 200 nmi. Five linear segments were taken of each profile. In figure 16, the five profiles are displayed in M-units at each range corresponding to the optimum coupling height. The change in thickness and height of the most important features of the profiles are shown. Comparisons between PEPC with observed data are shown in figures 17 through 25 for the 170-, 520-, and 3300-MHz cases. Again, slant paths were used for the model to simulate the flight paths of the aircraft. All height-gain plots are displayed in dB relative to free space versus height. Standard atmosphere is shown as a reference.

At 170 and 520 MHz, there is excellent agreement at all three slant paths between PEPC and the observed data. For the S-band case, figures 23 and 24 agree well, while at greater ranges (figure 25) PEPC begins to deviate at low heights from the measured data. This discrepancy may be attributable to the undetected presence of an evaporation duct, which would affect higher-frequency signals. Accounting for an evaporation duct would give higher signal levels at the lower receiver heights. Figures 26 through 28 are PEPC coverage diagrams for the 170-, 520-, and 3300-MHz cases, respectively. In the S-band case (figure 28), it is more apparent how the environment changes. Comparing figures 16 and 28, it is easy to see how the field follows the trapping layer as it varies with range.

To assume a homogeneous environment will not give a clear picture of what is really happening. Figure 29 shows a coverage diagram for a homogenous environment at S band, using the profile at 39 nmi in figure 16. While the coverage diagram may match that of figure 28 at close ranges, it differs greatly at large ranges. One may try to "average" the profiles and assume that, at all ranges, the field is "close to" the field under actual range-dependent conditions, but using the "average" profile is also unsuitable. The average profile was taken from the data record in figure 13 for two height-gain plots for 170 and 3300 MHz (figures 30 and 31, respectively). The difference between the predicted and the measured fields are substantial.

Height-gain plots are shown in figures 32 through 43 for the environment on 8 April 1948. Again, there is good agreement between PEPC and the measured data at low frequencies. At S band, there is a big discrepancy for large ranges and high receiver elevations. One can only speculate that the presence of an elevated trapping layer went undetected, yielding low signal levels at large ranges. The corresponding coverage diagrams for the three frequencies are shown in figures 44 through 46.

Figures 47 through 55 are the height-gain plots for the environment of 13 November 1947. There is excellent agreement at all frequencies and ranges. The coverage diagrams are shown in figures 56 through 58.

3.2.2 Canterbury Project Measurements

Figures 59 and 60 show two days of refractivity measurements from the Canterbury project. The aircraft flight paths are shown on the right-hand side. The frequencies used in this experiment were predominantly S and X band, although some measurements were also made at 60 MHz. Two antenna heights were used on the receiving ground station, at 26.5 and 86 ft. In the following plots, S1 channel will refer to S band with antenna height of 26.5 ft, and S2 channel will refer to S band with antenna height of 86 ft. Similarly, X1 and X2 channels will refer to X band with antenna heights of 26.5 and 86 ft, respectively.

Figures 61 through 63 show height-gain plots for the environment measured on 19 June 1947. The slant path used corresponded to flight leg M→N. There is excellent agreement in all three cases. The corresponding coverage diagrams are shown in figures 64 through 66.

For the environment of 11 July 1947, two flight legs were chosen. Figures 67 and 68 show leg G→H for the X1 and X2 channels, respectively, and figures 69 and 70 show the same channels for leg H→I. Good agreement is shown for leg G→H, with somewhat good agreement for leg H→I. The corresponding coverage diagrams are shown in figures 71 and 72.
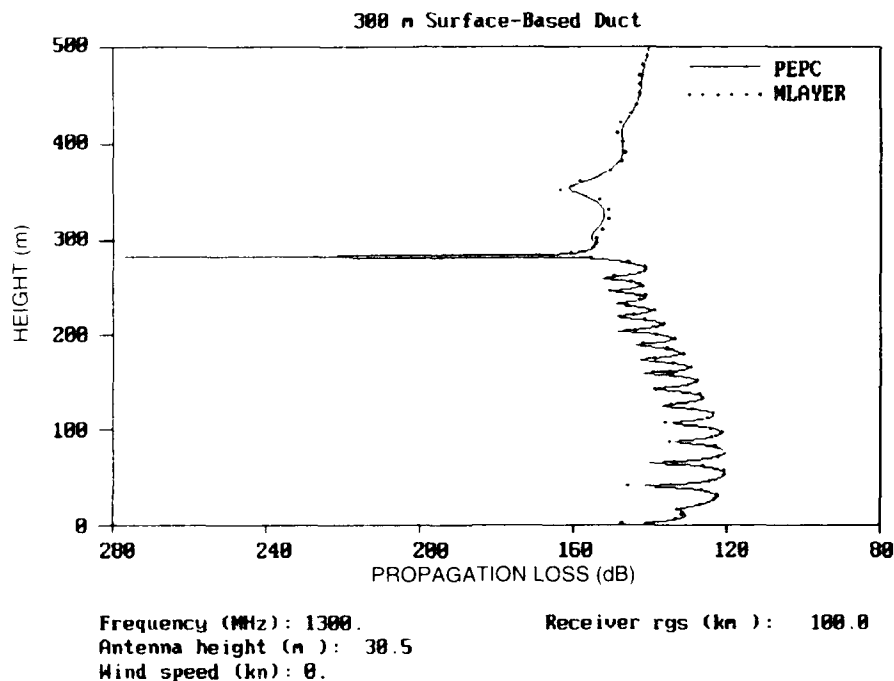

Figure 6. Height-gain plot comparison of PEPC and MLAYER for 300-m surface-based duct.

20 m Evaporation Duct

Frequency (MHz): 9600.
Antenna height (m): 30.5
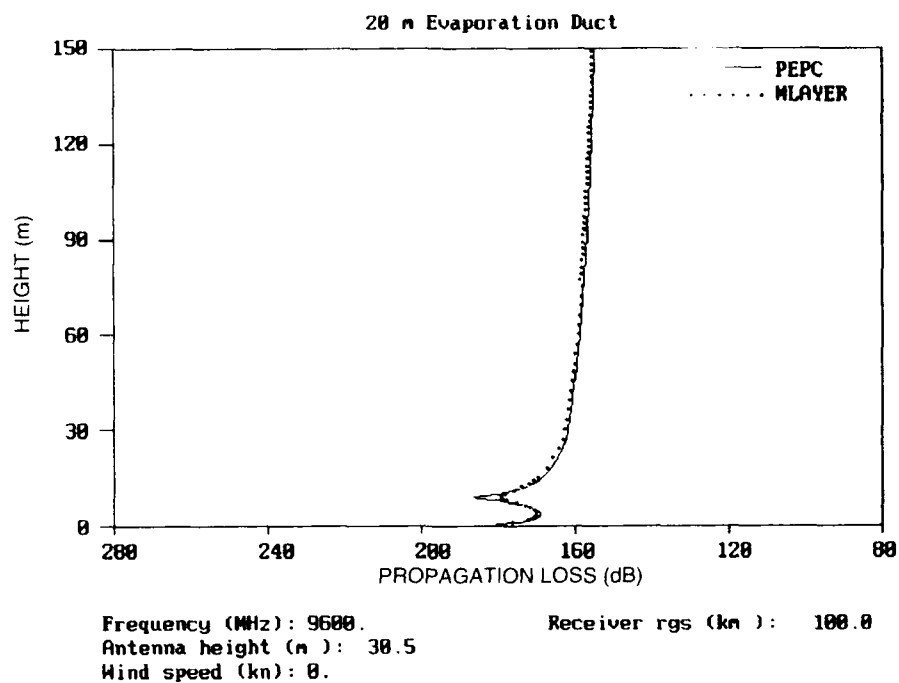Wind speed (kn): 0.

Receiver rgs (km):   100.0

Figure 7. Height-gain plot comparison of PEPC and MLAYER for 20-m evaporation duct.
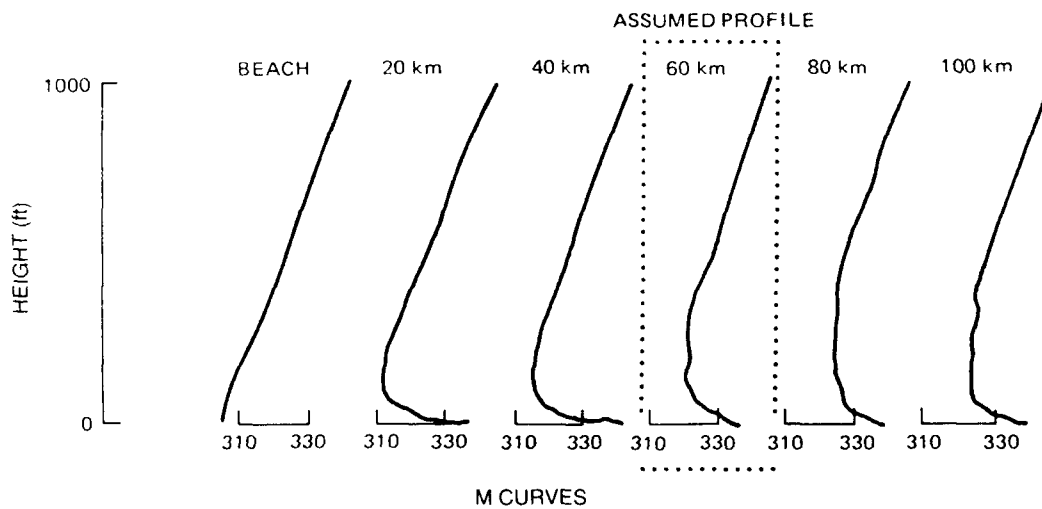

Figure 8. Measured M-unit-versus-height profiles from Canterbury Project environmental measurements for 5 August 1947.
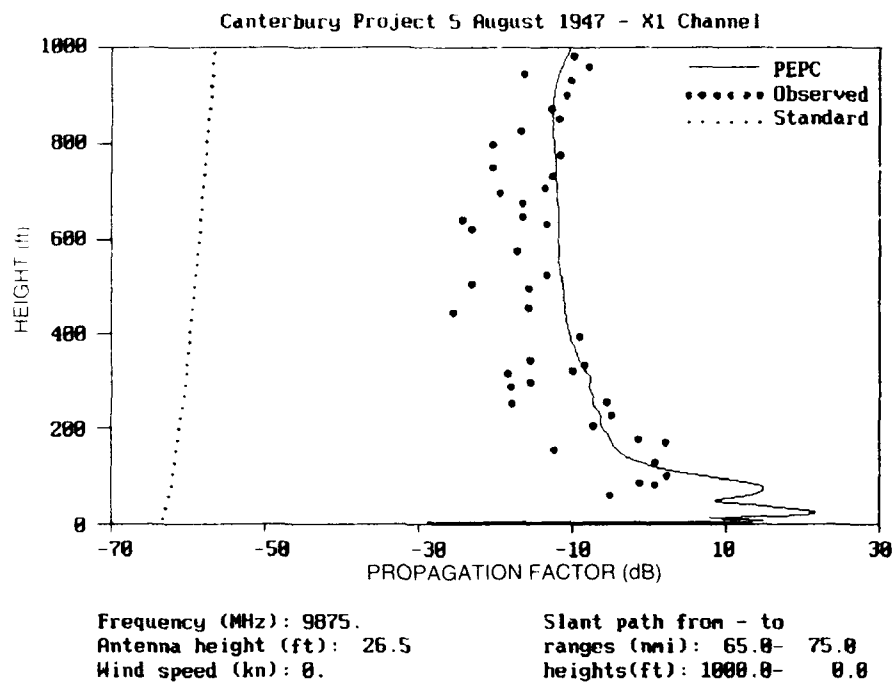
Figure 9. X-band comparison between PEPC and Canterbury Project measurements for 5 August 1947.
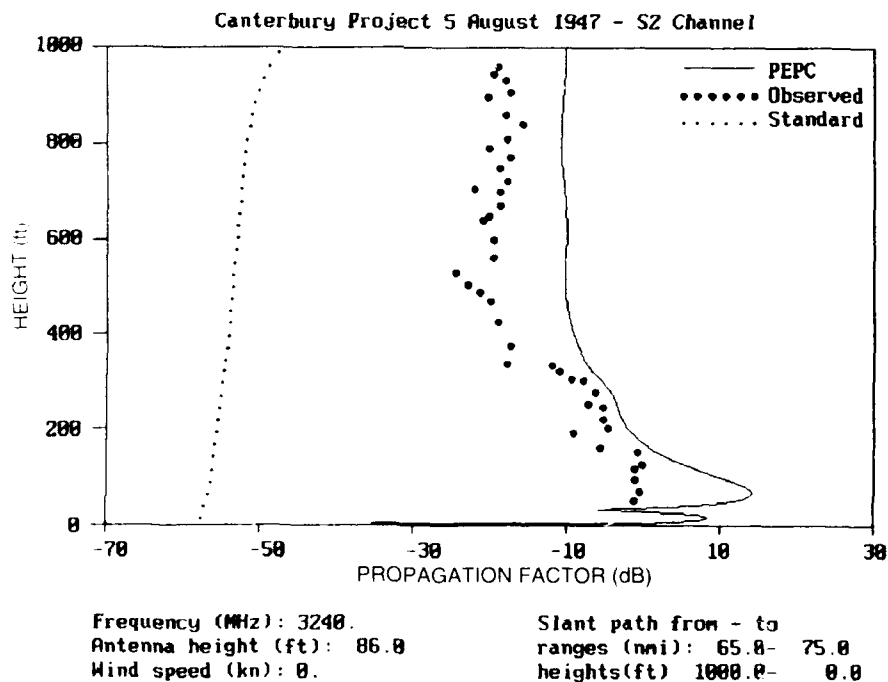

Figure 10. S-band comparison between PEPC and Canterbury Project measurements for 5 August 1947.
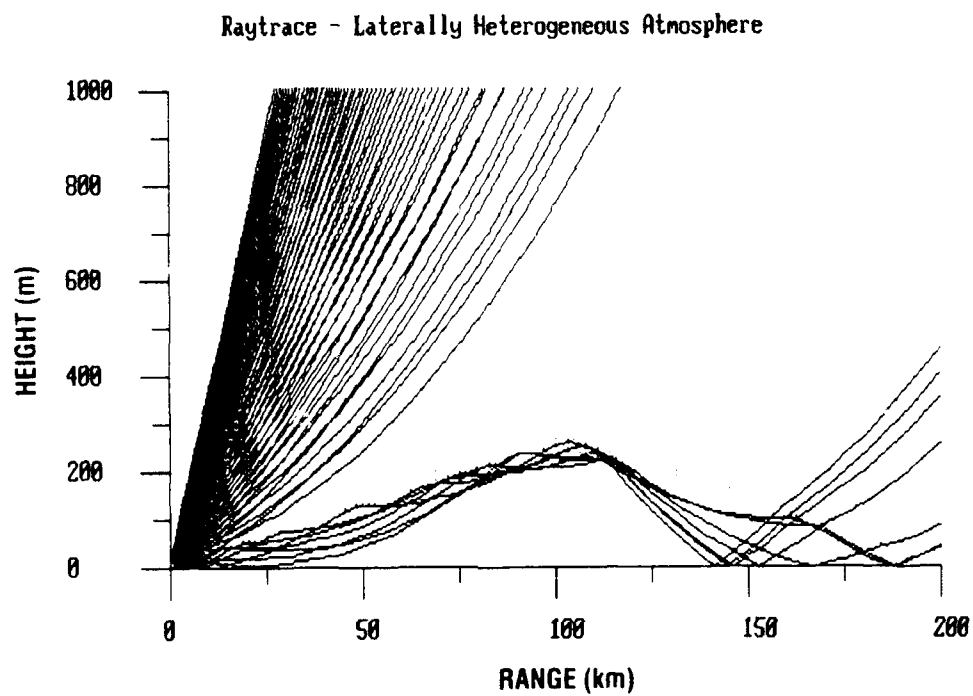
Figure 11. Range-dependent ray trace with trapping layer (represented by shaded area) varying with range. Antenna height is 25 m.

Standard to 300 m Surface-Based Duct to Standard

PEPC Ver: 1.0

Freq MHz 1300.
AntHt m 25.0
Wind kn 0.

LOSS:0 ▮110 ▮115 120 ▮125 ▮130 ▮135 140 ▮145 150 999 dB

Figure 12. Coverage diagram for environment of figure 11.

Figure 13. Environment and radio data record from Guadalupe Island measurements for 12 March 1948.

20

Figure 14. Environment and radio data record from Guadalupe Island measurements for 8 April 1948.
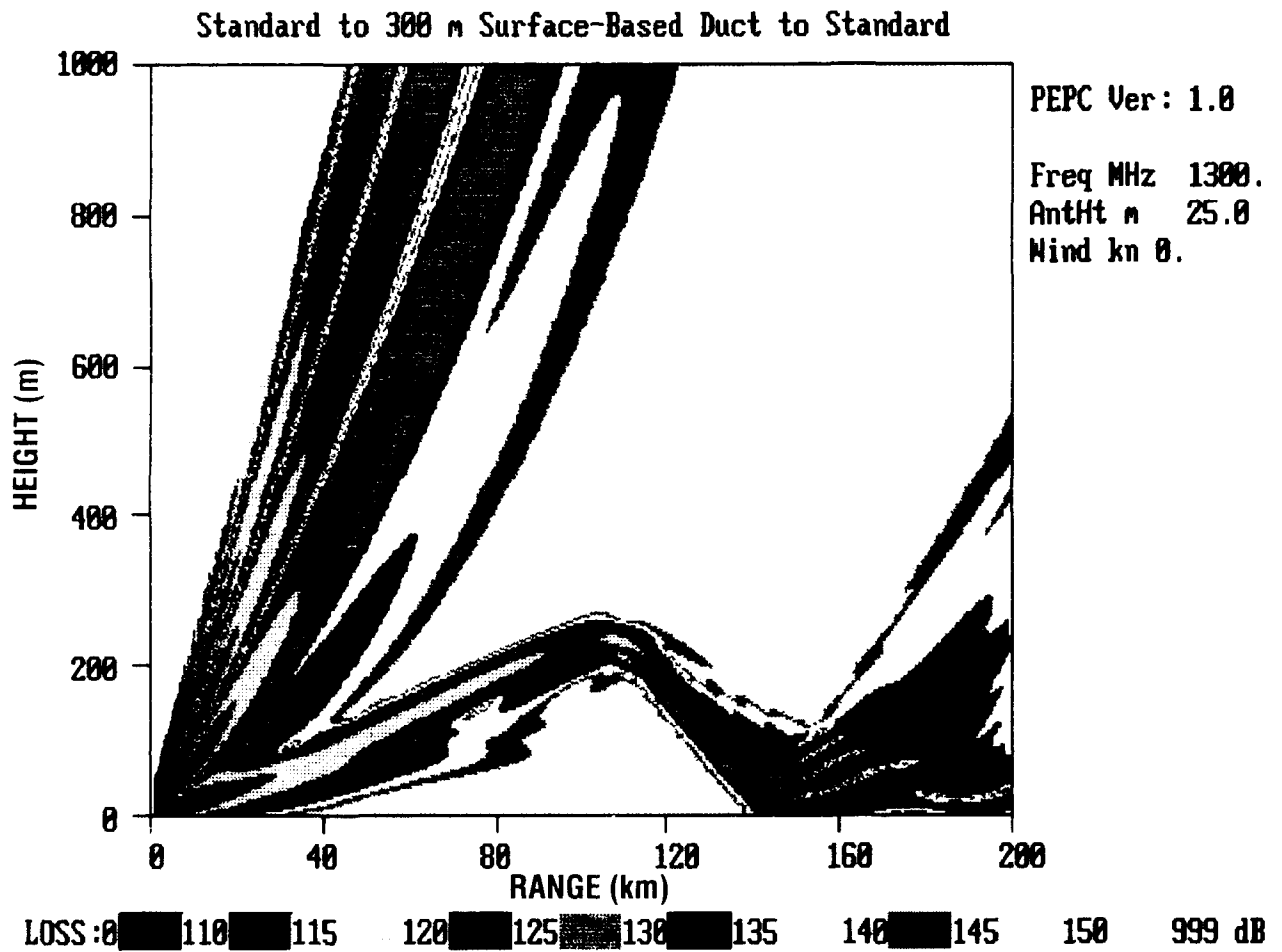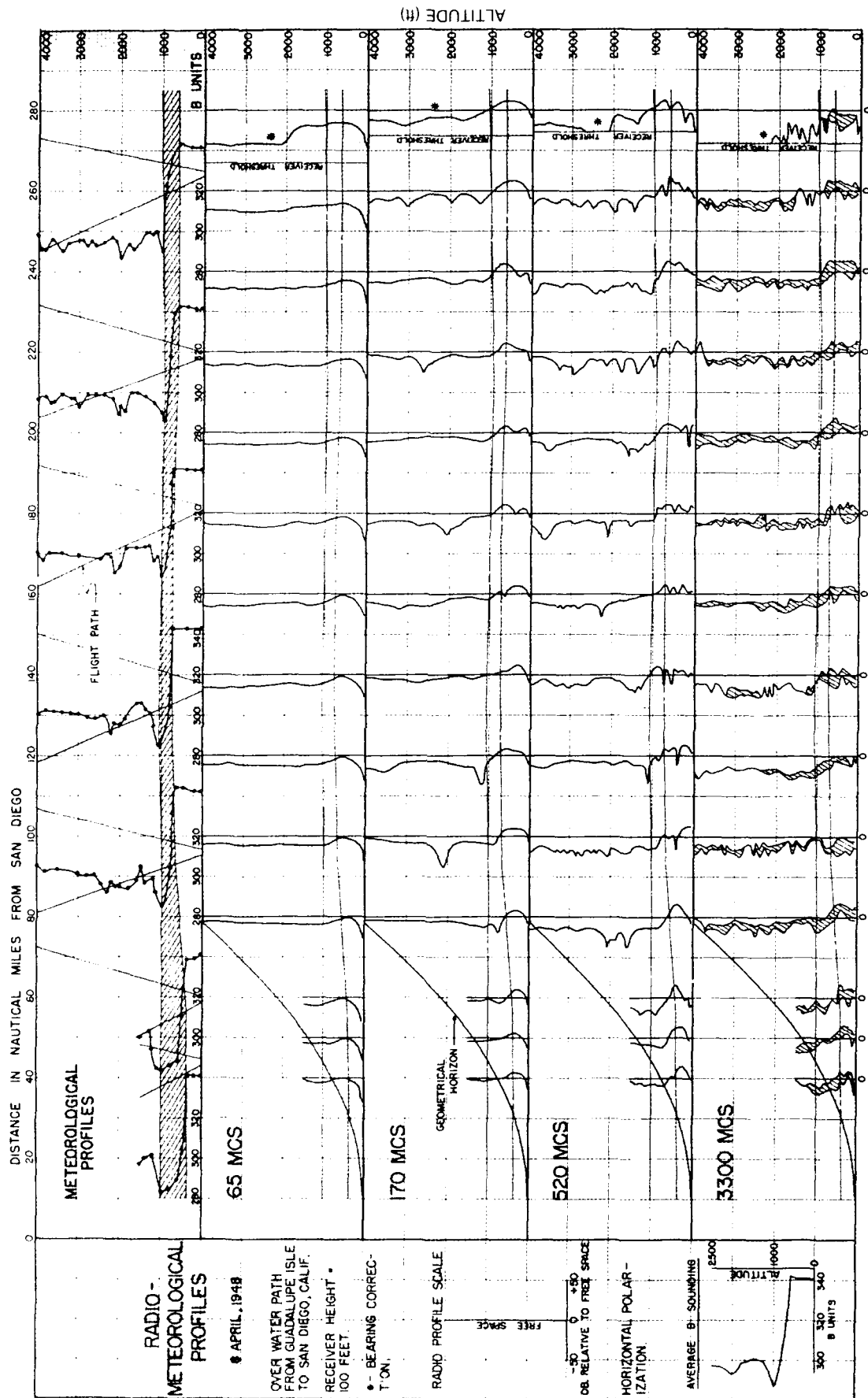
21
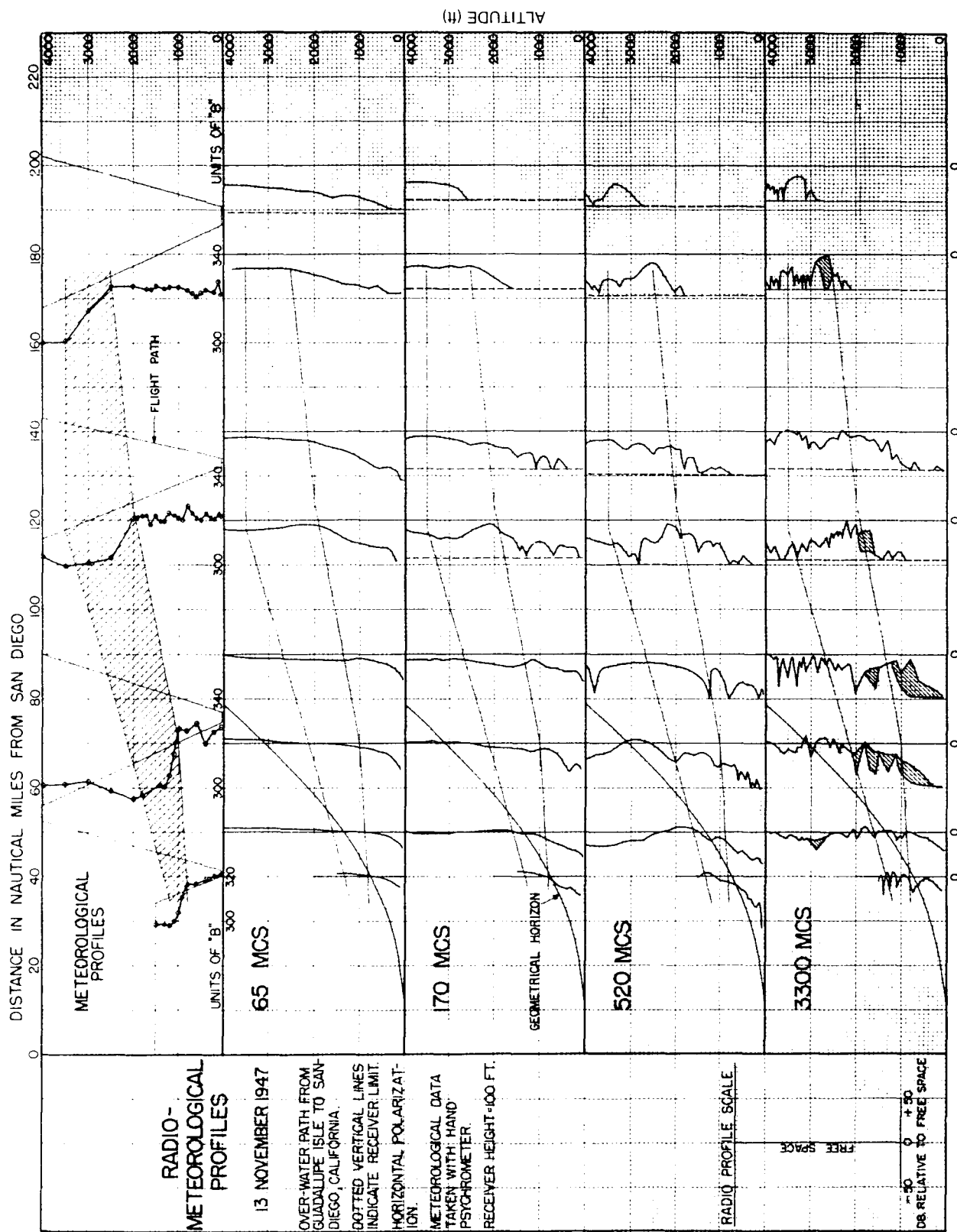
Figure 15. Environment and radio data record from Guadalupe Island measurements for 13 November 1947.

22

GUADALUPE ISLAND PROFILES
12 MARCH 1948
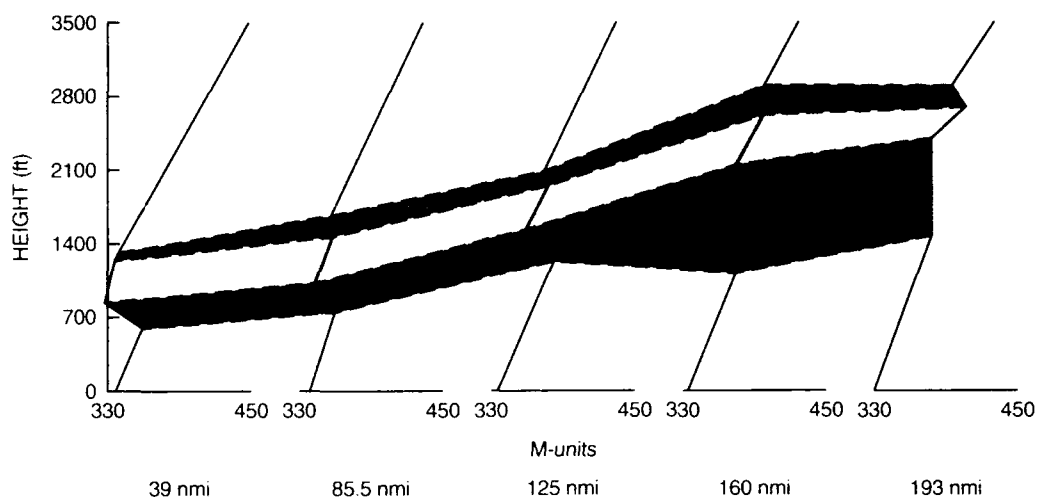
Figure 16. Interpolated M-unit-versus-height profiles for fixed ranges from 12 March 1948, with variation in trapping layer height and thickness represented by shaded areas.

Figure 17. Comparisons between PEPC and measured radio data at 170 MHz for 12 March 1948, along slant path from 69 to 89 nmi.

Figure 18. Comparisons between PEPC and measured radio data at 170 MHz for 12 March 1948, along slant path from 91 to 101 nmi.

Figure 19. Comparisons between PEPC and measured radio data at 170 MHz for 12 March 1948, along slant path from 115 to 130 nmi.

Guadalupe Island - 12 March 1948

Frequency (MHz): 520.
Antenna height (ft): 100.0
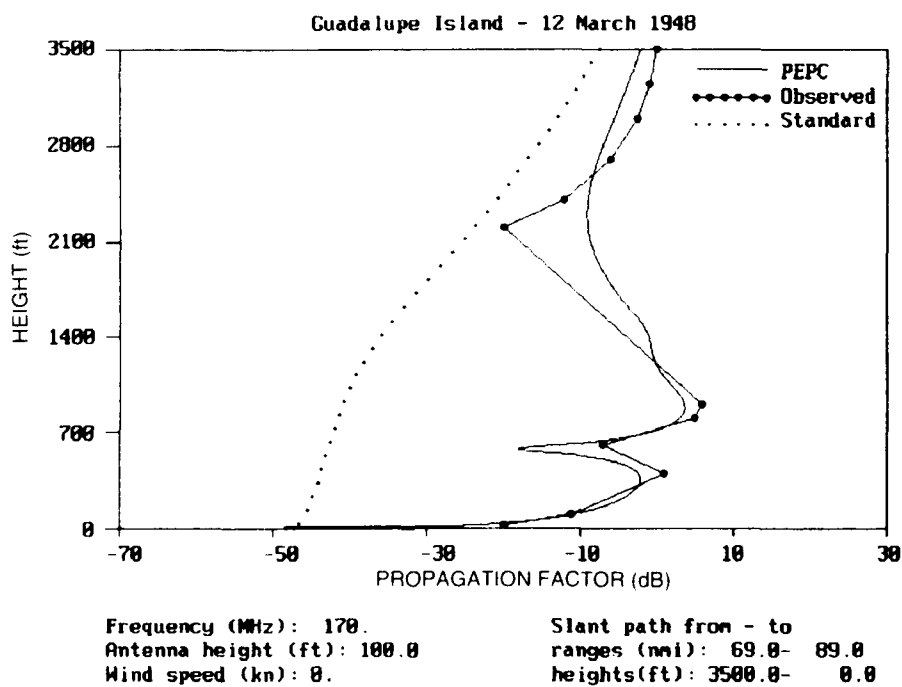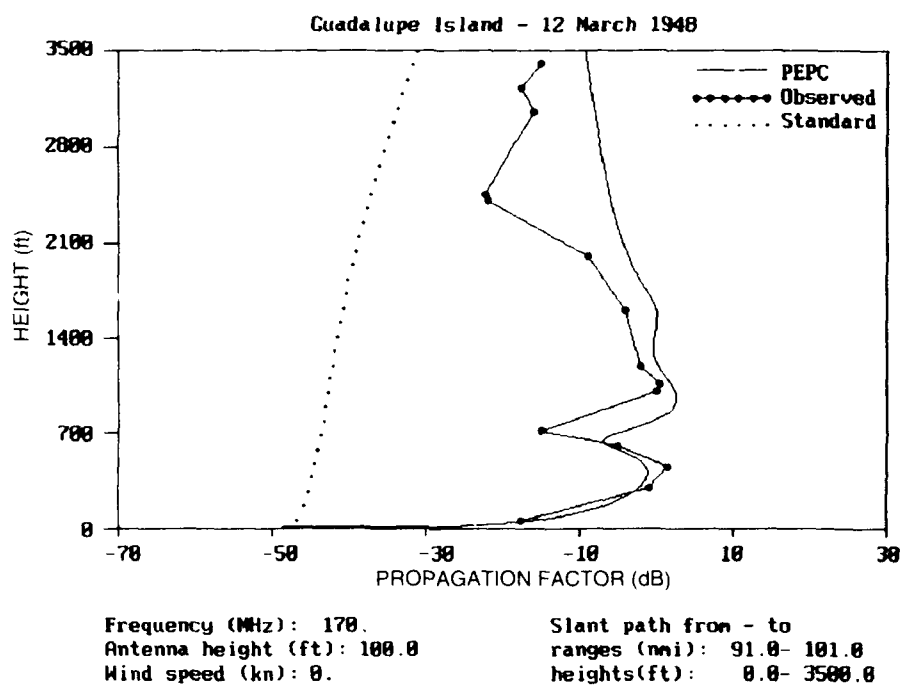Wind speed (kn): 0.

Slant path from - to
ranges (nmi): 69.0- 89.0
heights(ft): 3500.0-   0.0

Figure 20. Comparisons between PEPC and measured radio data at 520 MHz for 12 March 1948, along slant path from 69 to 89 nmi.

Guadalupe Island - 12 March 1948

Frequency (MHz): 520.
Antenna height (ft): 100.0
Wind speed (kn): 0.

Slant path from - to
ranges (nmi): 91.0- 101.0
heights(ft):   0.0- 3500.0

Figure 21. Comparisons between PEPC and measured radio data at 520 MHz for 12 March 1948, along slant path from 91 to 101 nmi.
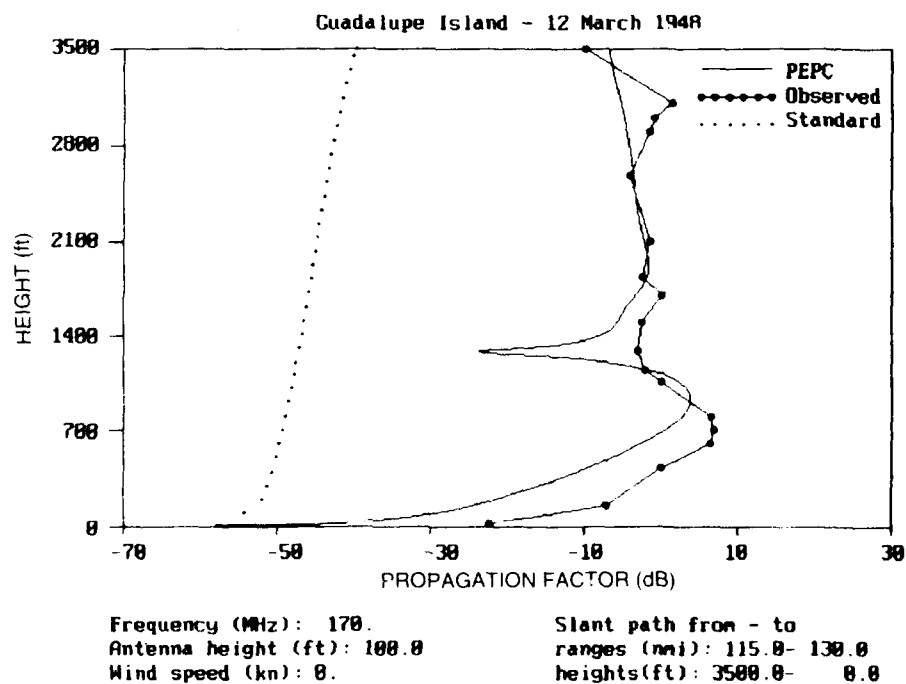
25

Figure 22. Comparisons between PEPC and measured radio data at 520 MHz for 12 March 1948, along slant path from 115 to 130 nmi.
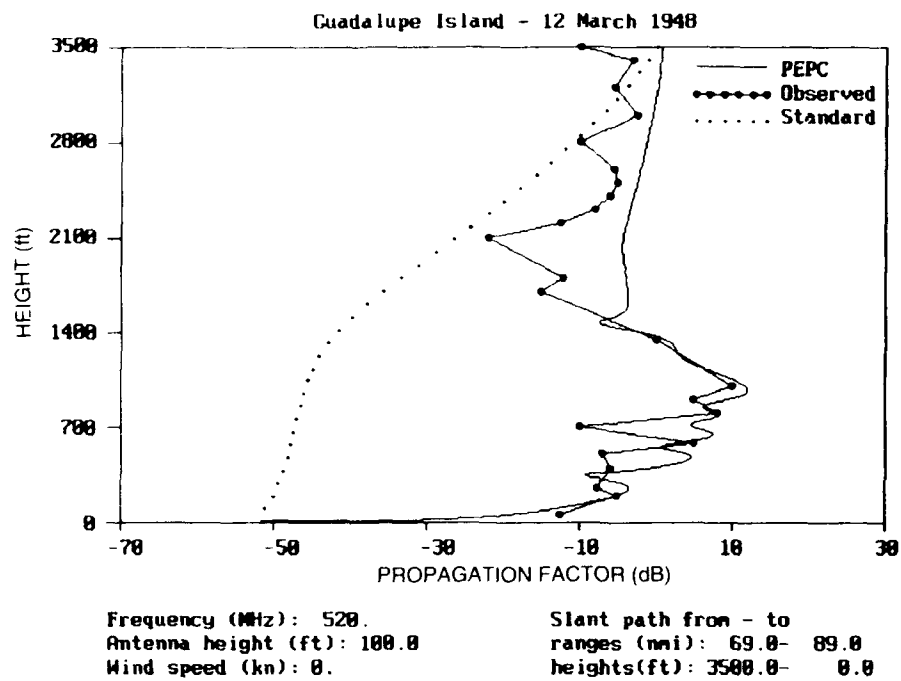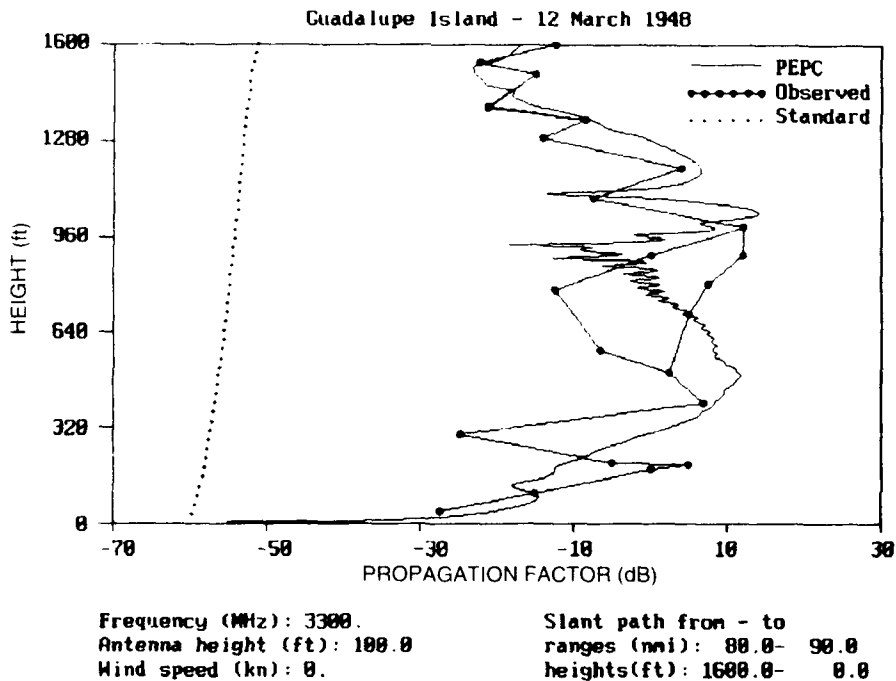

Figure 23. Comparisons between PEPC and measured radio data at 3300 MHz for 12 March 1948, along slant path from 80 to 90 nmi.
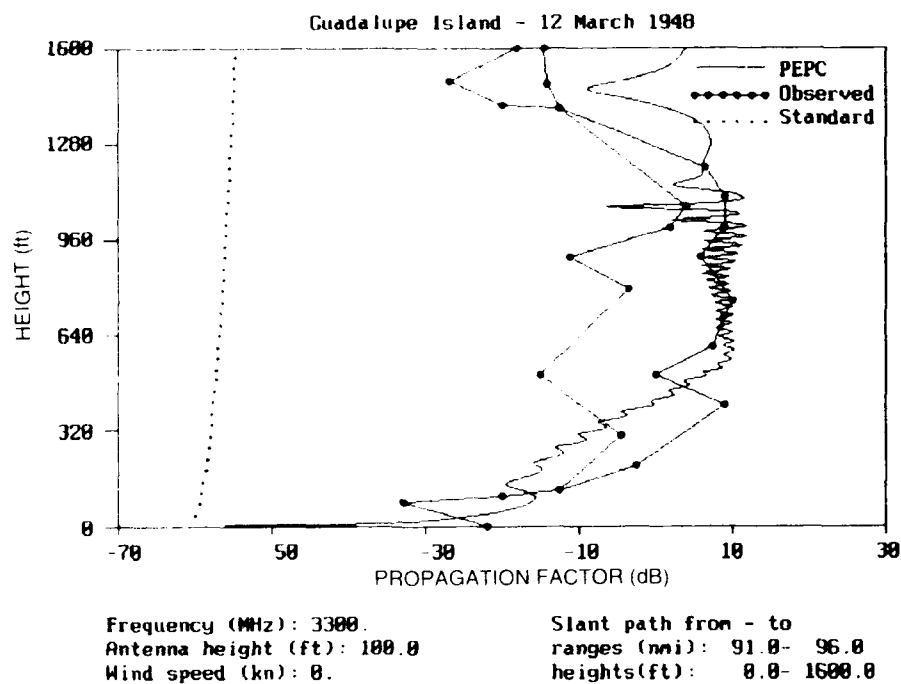
Figure 24. Comparisons between PEPC and measured radio data at 3300 MHz for 12 March 1948, along different slant paths (91 to 96 nmi).
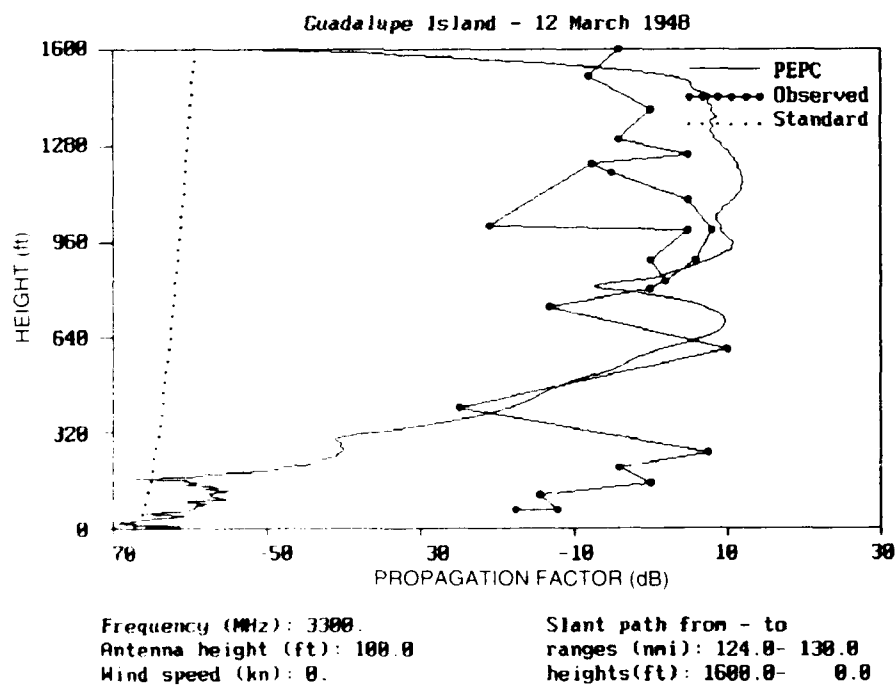
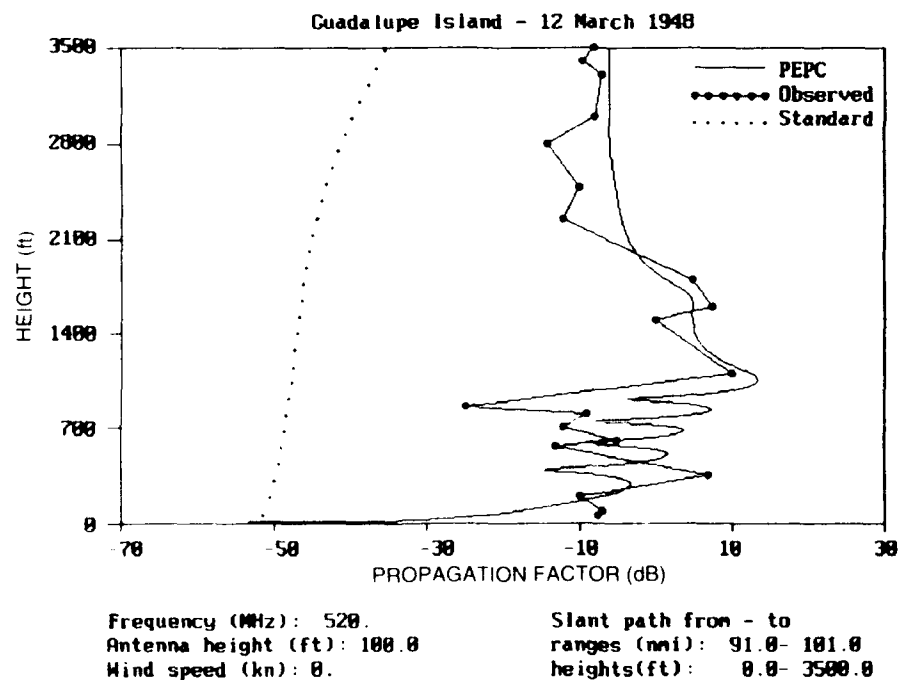Figure 25. Comparisons between PEPC and measured radio data at 3300 MHz for 12 March 1948, along slant path from 124 to 130 nmi.
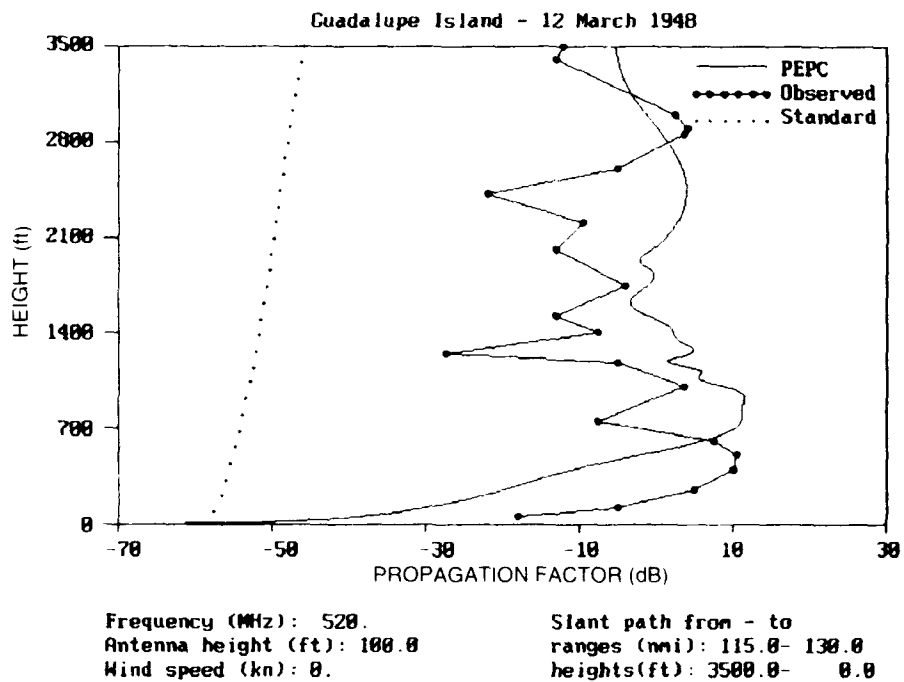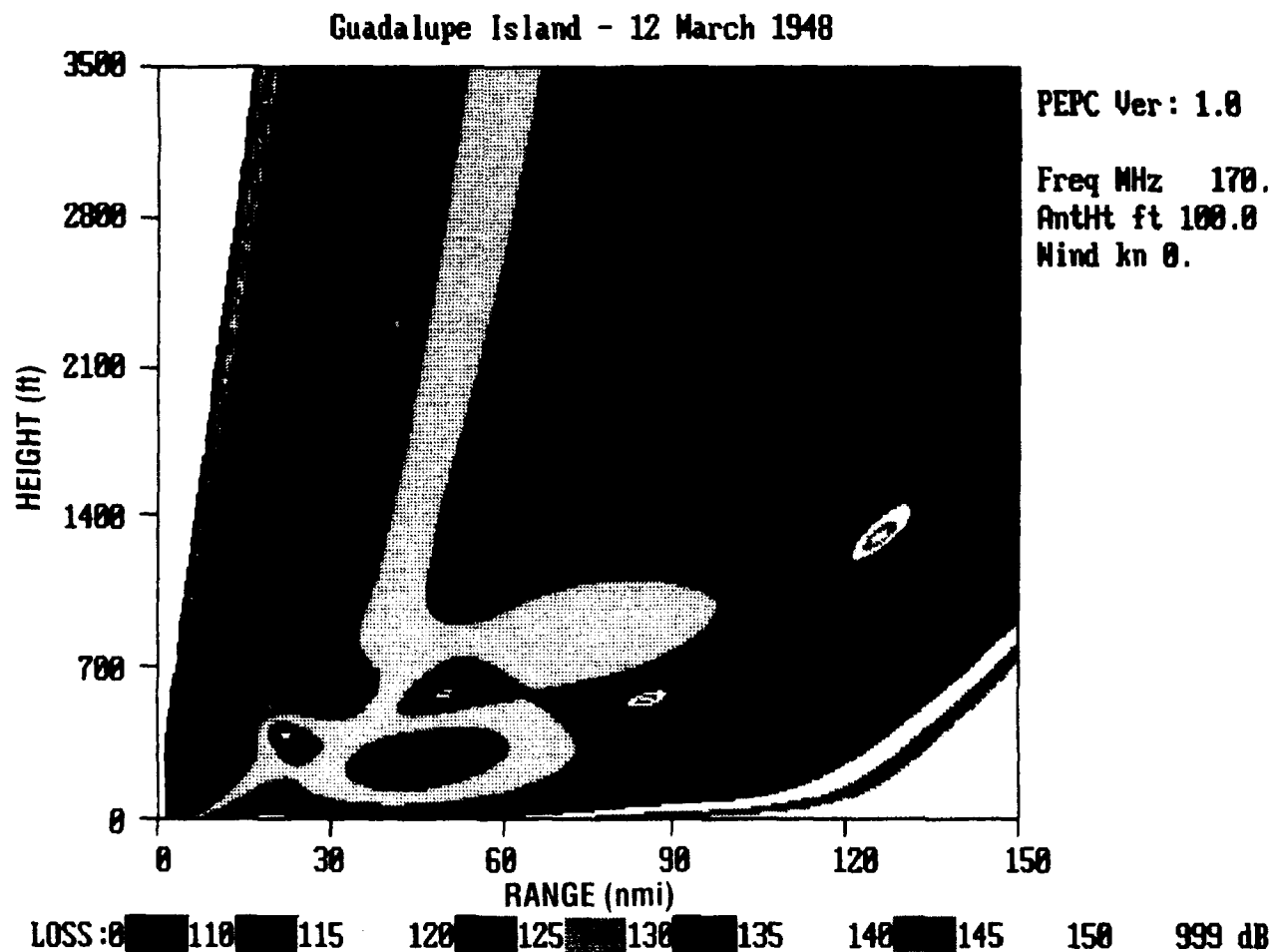
Figure 26. Coverage diagram for environment of 12 March 1948 at 170 MHz.
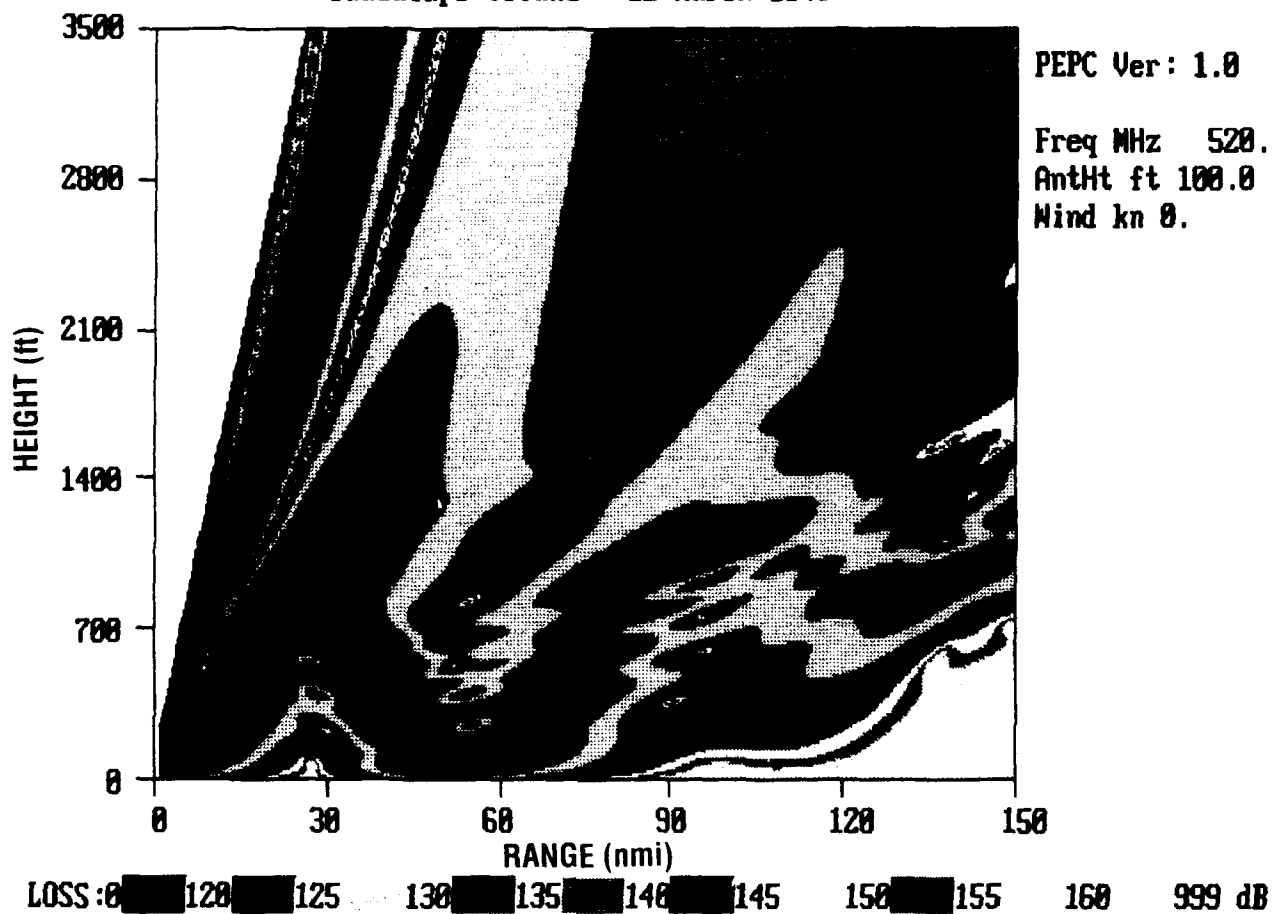
Figure 27. Coverage diagram for environment of 12 March 1948 at 520 MHz.
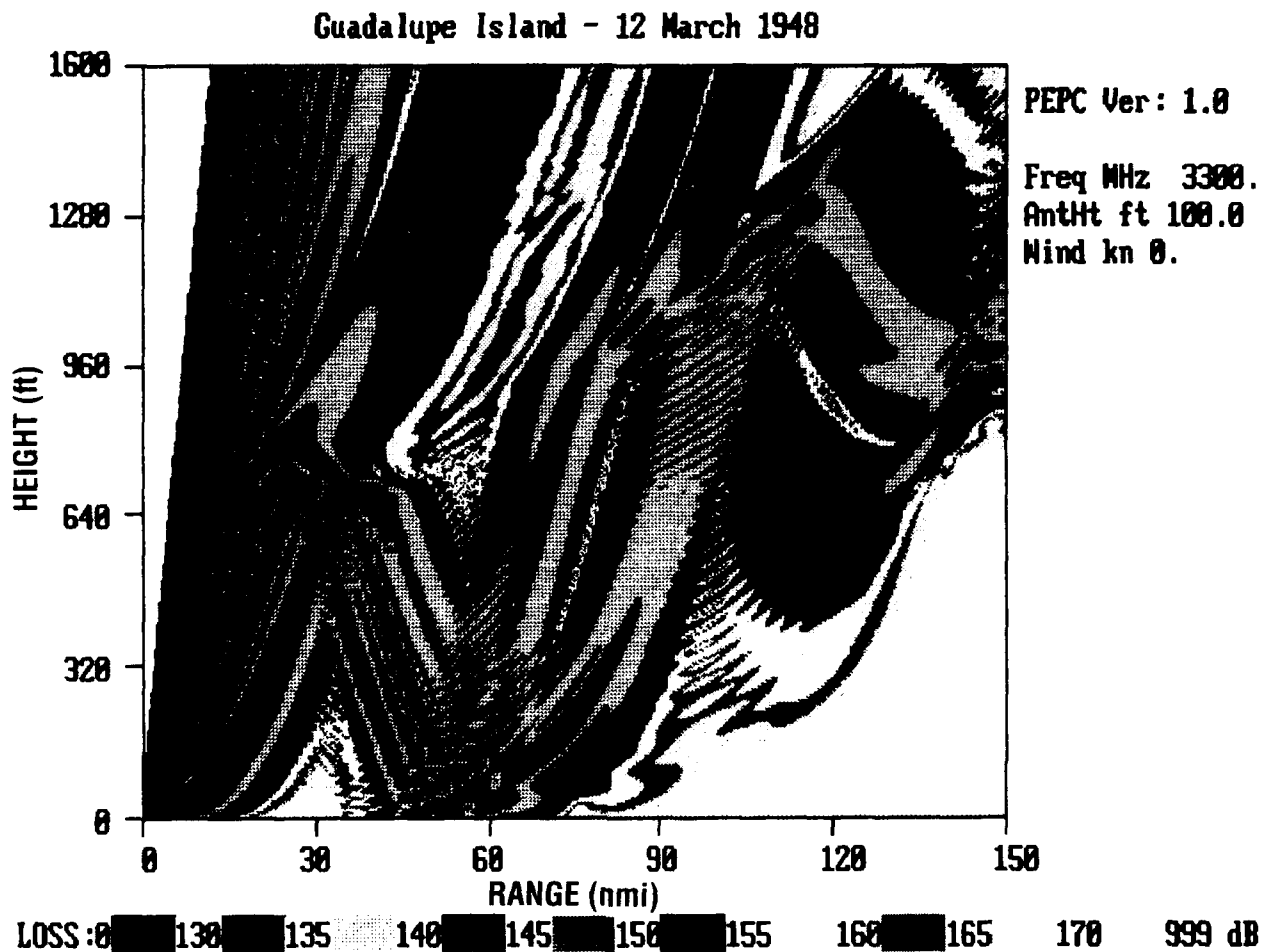
Figure 28. Coverage diagram for environment of 12 March 1948 at 3300 MHz.

Guadalupe Island Homogeneous - 12 March 1948

PEPC Ver: 1.0

Freq MHz 3300.
AntHt ft 100.0
Wind kn 0.
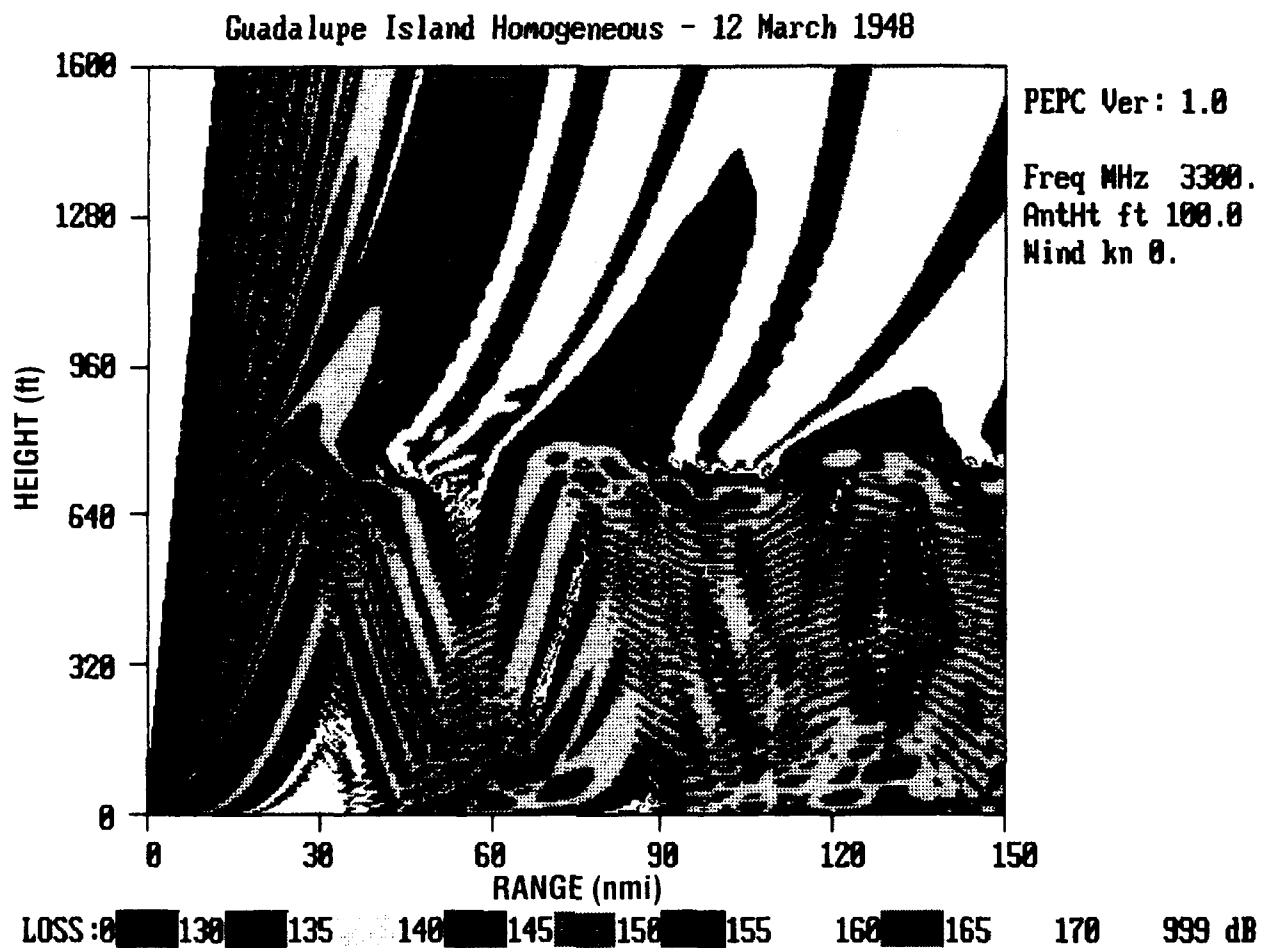
Figure 29. Coverage diagram using homogeneous profile measured at 39 nmi
taken from the 12 March 1948 data record.

Guadalupe Island Average Profile - 12 March 1948

Frequency (MHz): 170.
Antenna height (ft): 100.0
Wind speed (kn): 0.

Slant path from - to
ranges (nmi): 91.0- 101.0
heights(ft): 0.0- 3500.0
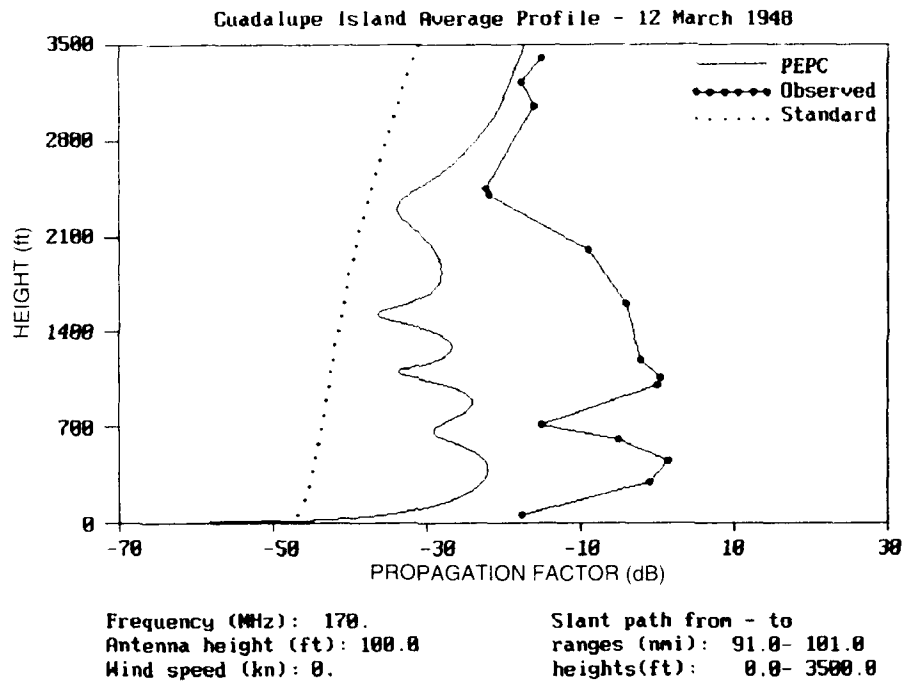
Figure 30. Comparisons between PEPC and measured radio data, using the average profile from the 12 March 1948 data record for 170 MHz.

Guadalupe Island Average Profile - 12 March 1948

Frequency (MHz): 3300.
Antenna height (ft): 100.0
Wind speed (kn): 0.

Slant path from - to
ranges (nmi): 91.0- 96.0
heights(ft): 0.0- 1600.0
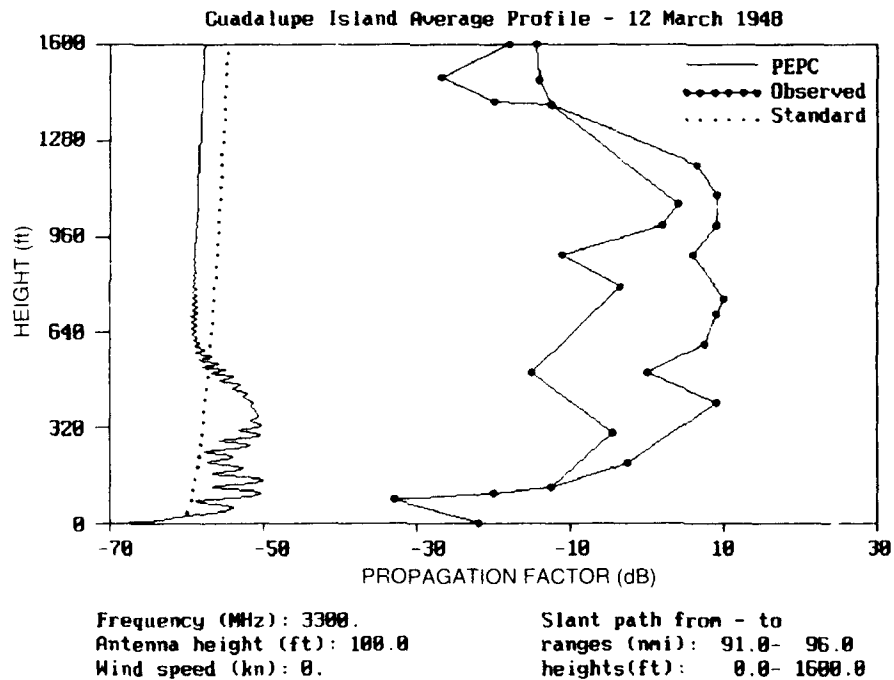
Figure 31. Comparisons between PEPC and measured radio data, using the average profile from the 12 March 1948 data record for 3300 MHz.

32

Guadalupe Island – 8 April 1948

Frequency (MHz): 170.
Antenna height (ft): 100.0
Wind speed (kn): 0.

Slant path from – to
ranges (nmi): 60.0– 72.0
heights(ft): 0.0– 4000.0

Figure 32. Comparisons between PEPC and measured radio data at 170 MHz for 8 April 1948, along slant path from 60 to 72 nmi.

Guadalupe Island – 8 April 1948

Frequency (MHz): 170.
Antenna height (ft): 100.0
Wind speed (kn): 0.

Slant path from – to
ranges (nmi): 81.0– 95.0
heights(ft): 4000.0– 0.0

Figure 33. Comparisons between PEPC and measured radio data at 170 MHz for 8 April 1948, along slant path from 81 to 95 nmi.

33

Figure 34. Comparisons between PEPC and measured radio data at 520 MHz for 8 April 1948, along slant path from 60 to 72 nmi.

Figure 35. Comparisons between PEPC and measured radio data at 170 MHz for 8 April 1948, along slant path from 118 to 136 nmi.

Figure 36. Comparisons between PEPC and measured radio data at 170 MHz for 8 April 1948, along slant path from 97 to 107 nmi.

Figure 37. Comparisons between PEPC and measured radio data at 520 MHz for 8 April 1948, along slant path from 81 to 95 nmi.

Guadalupe Island - 8 April 1948

Figure 38. Comparisons between PEPC and measured radio data at 520 MHz for 8 April 1948, along slant path from 97 to 107 nmi.

Guadalupe Island - 8 April 1948
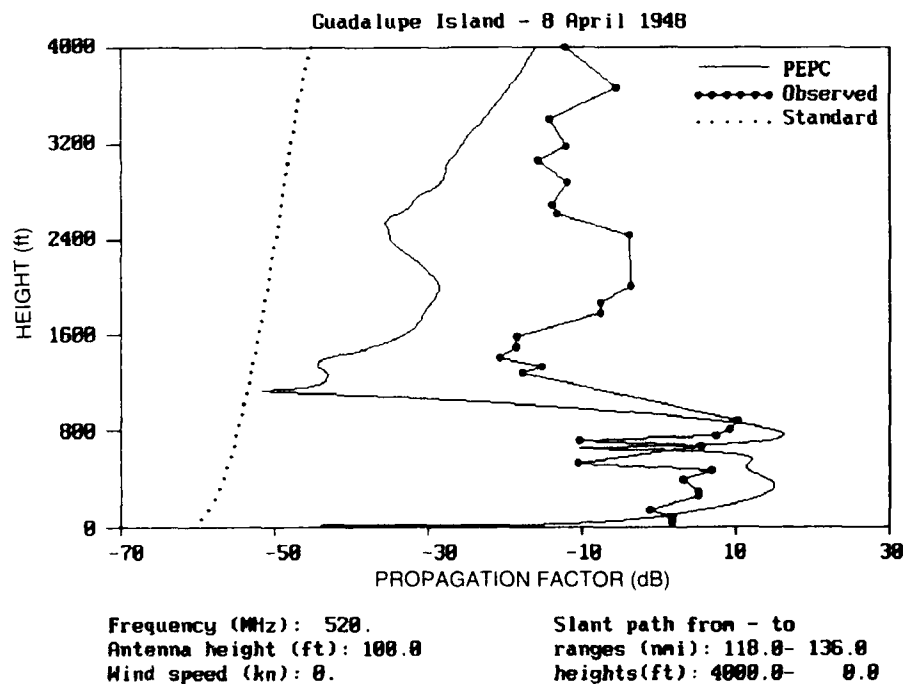
Figure 39. Comparisons between PEPC and measured radio data at 520 MHz for 8 April 1948, along slant path from 118 to 136 nmi.
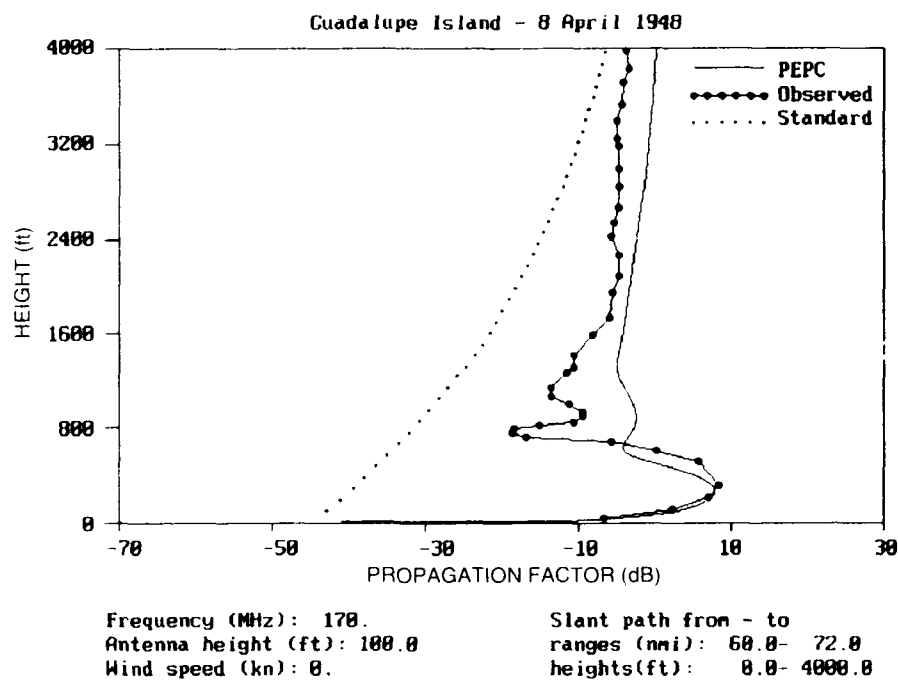
36
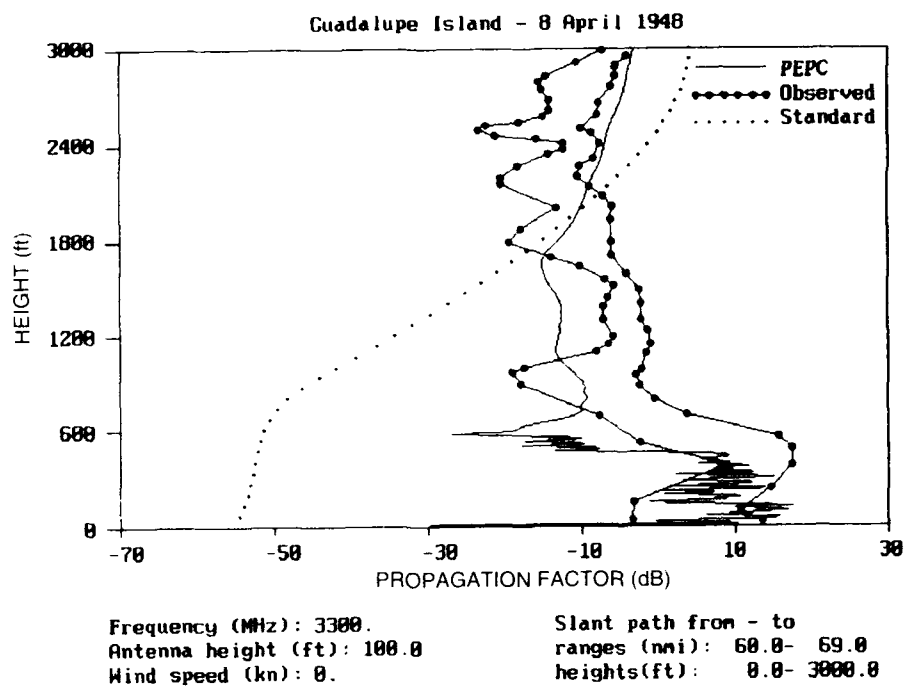
Figure 40. Comparisons between PEPC and measured radio data at 3300 MHz for 8 April 1948, along slant path from 60 to 69 nmi.
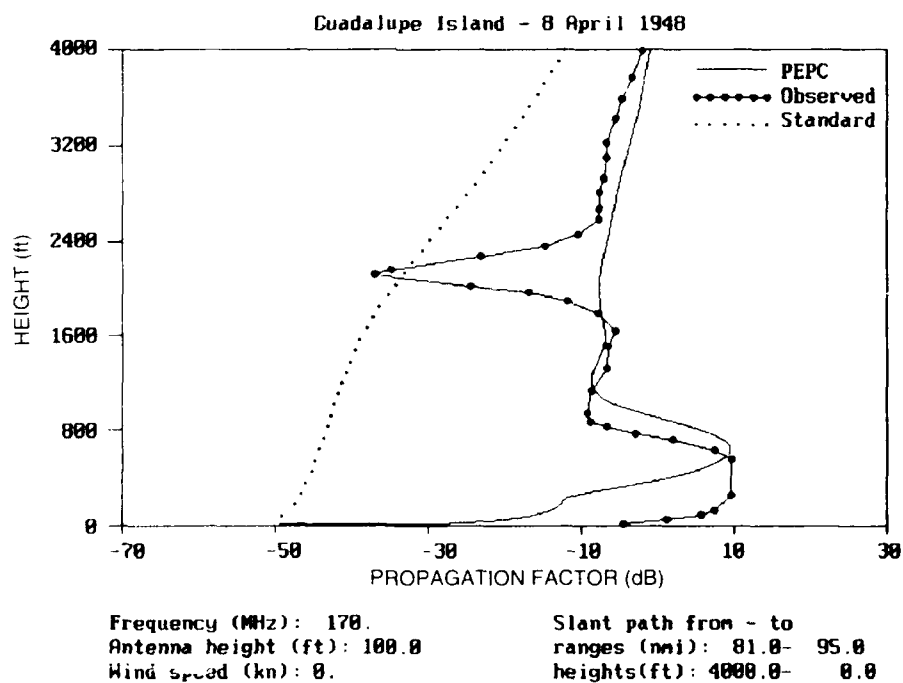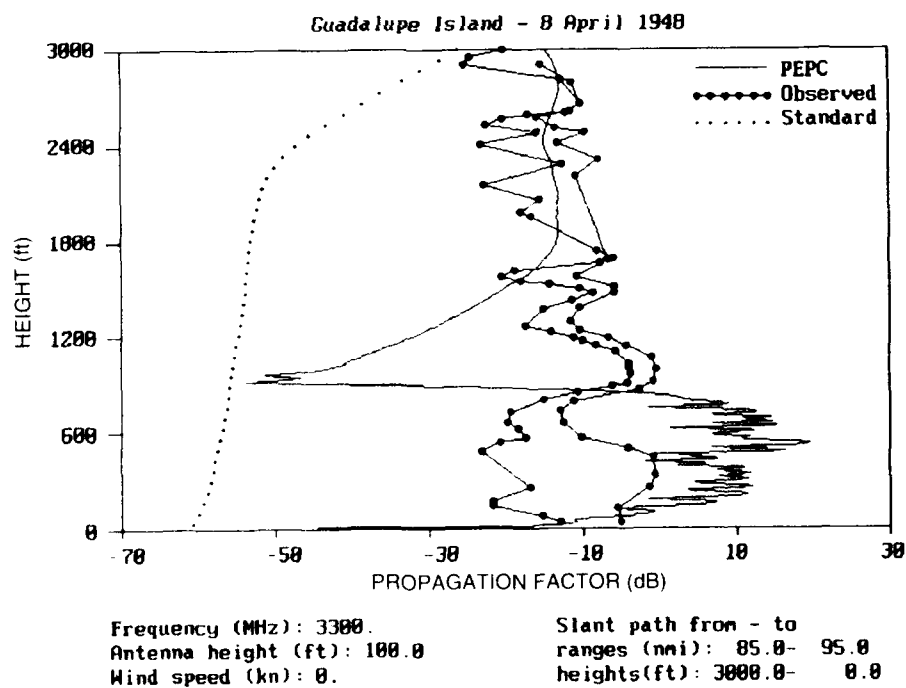

Figure 41. Comparisons between PEPC and measured radio data at 3300 MHz for 8 April 1948, along slant path from 85 to 95 nmi.
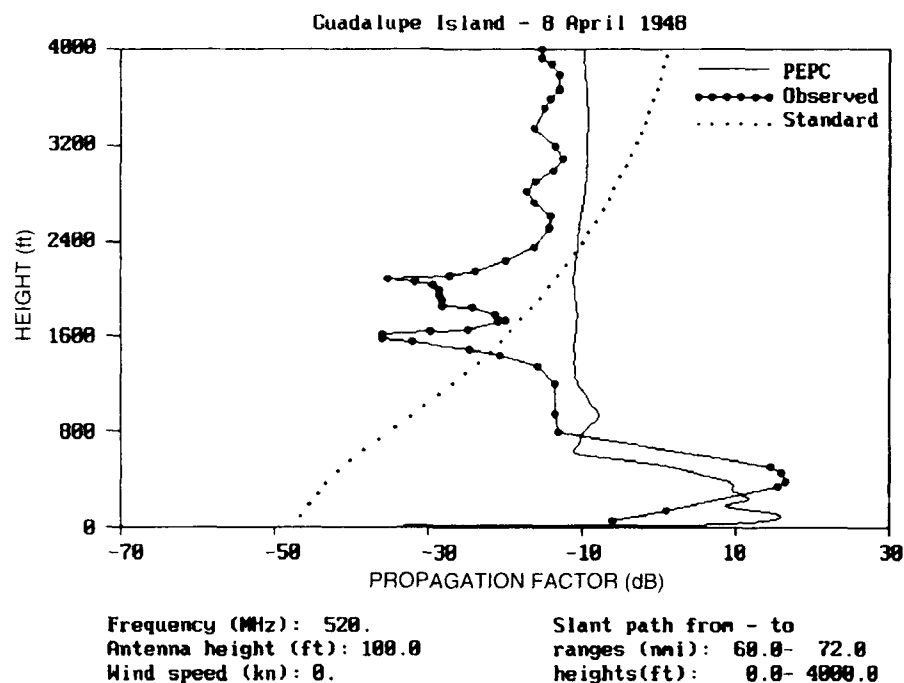
Figure 42. Comparisons between PEPC and measured radio data at 3300 MHz for 8 April 1948, along slant path from 97 to 104 nmi.
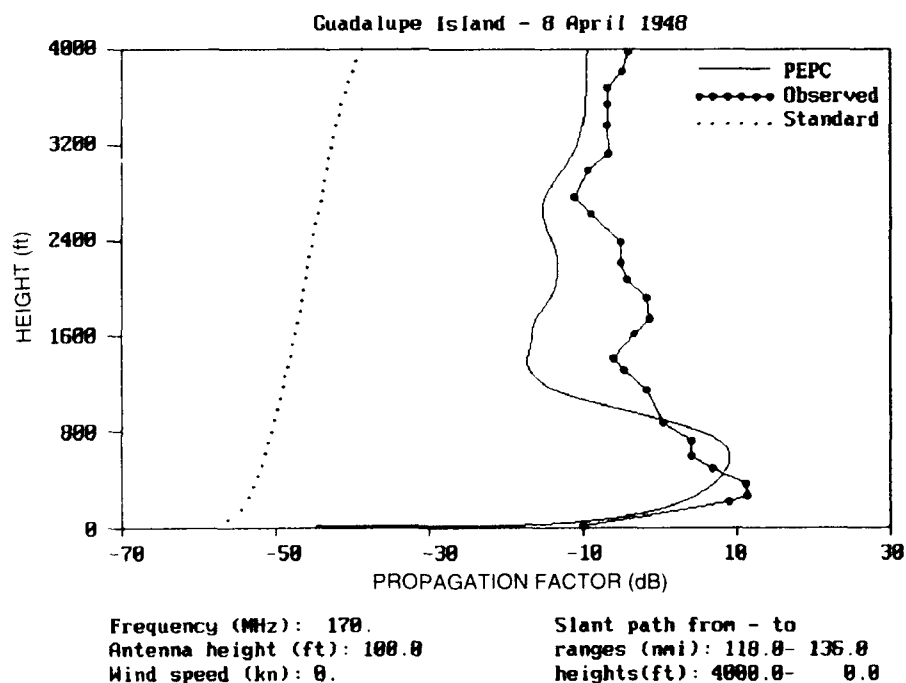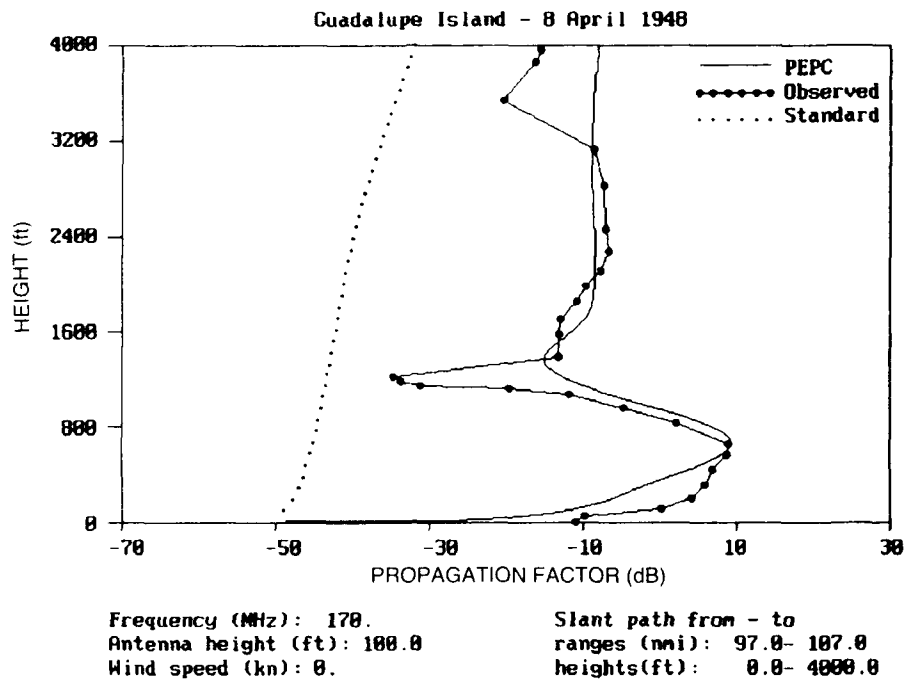

Figure 43. Comparisons between PEPC and measured radio data at 3300 MHz for 8 April 1948, along slant path from 126 to 136 nmi.

38

Figure 44. Coverage diagram for environment of 8 April 1948 at 170 MHz.
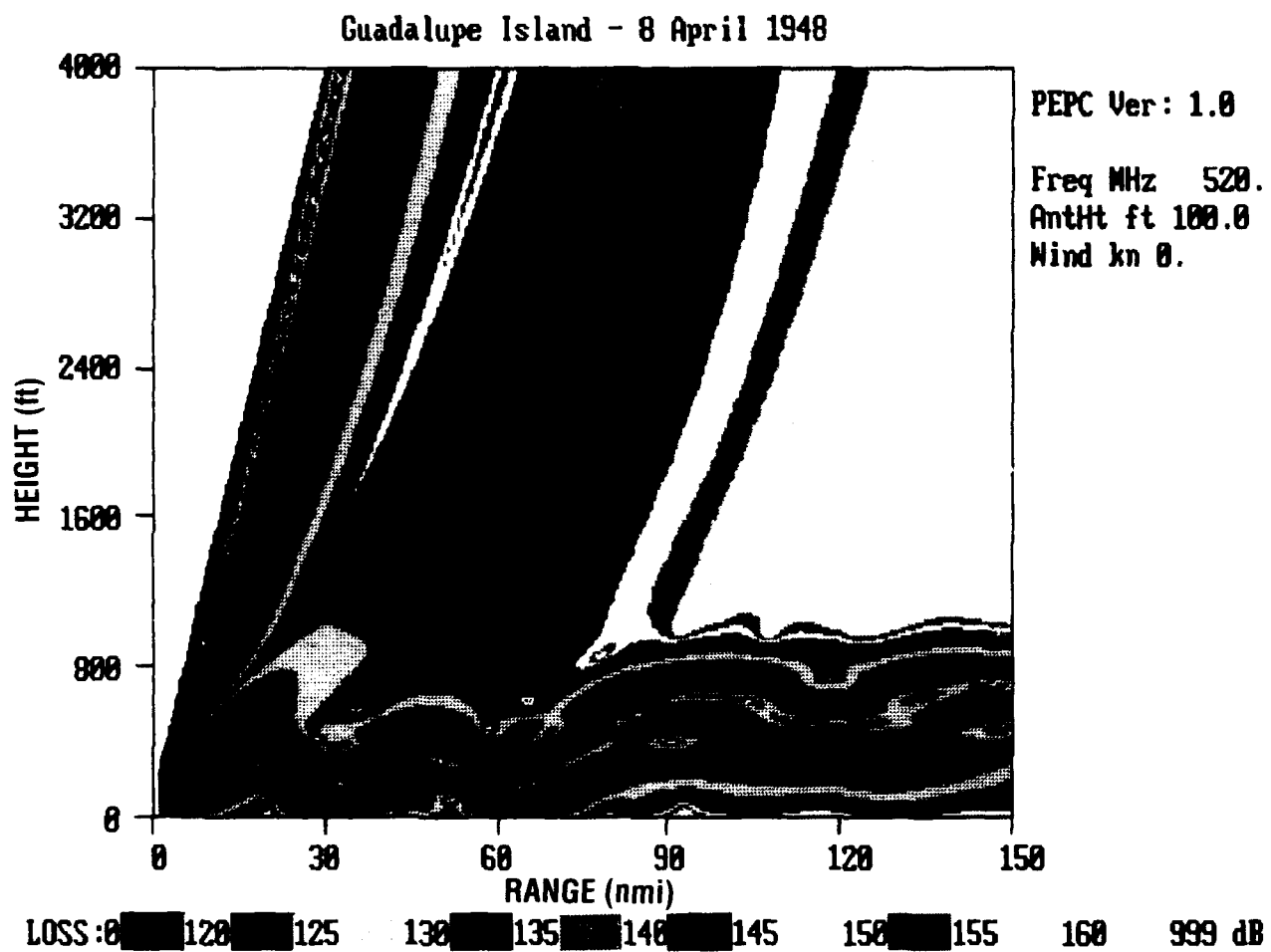
Figure 45. Coverage diagram for environment of 8 April 1948 at 520 MHz.
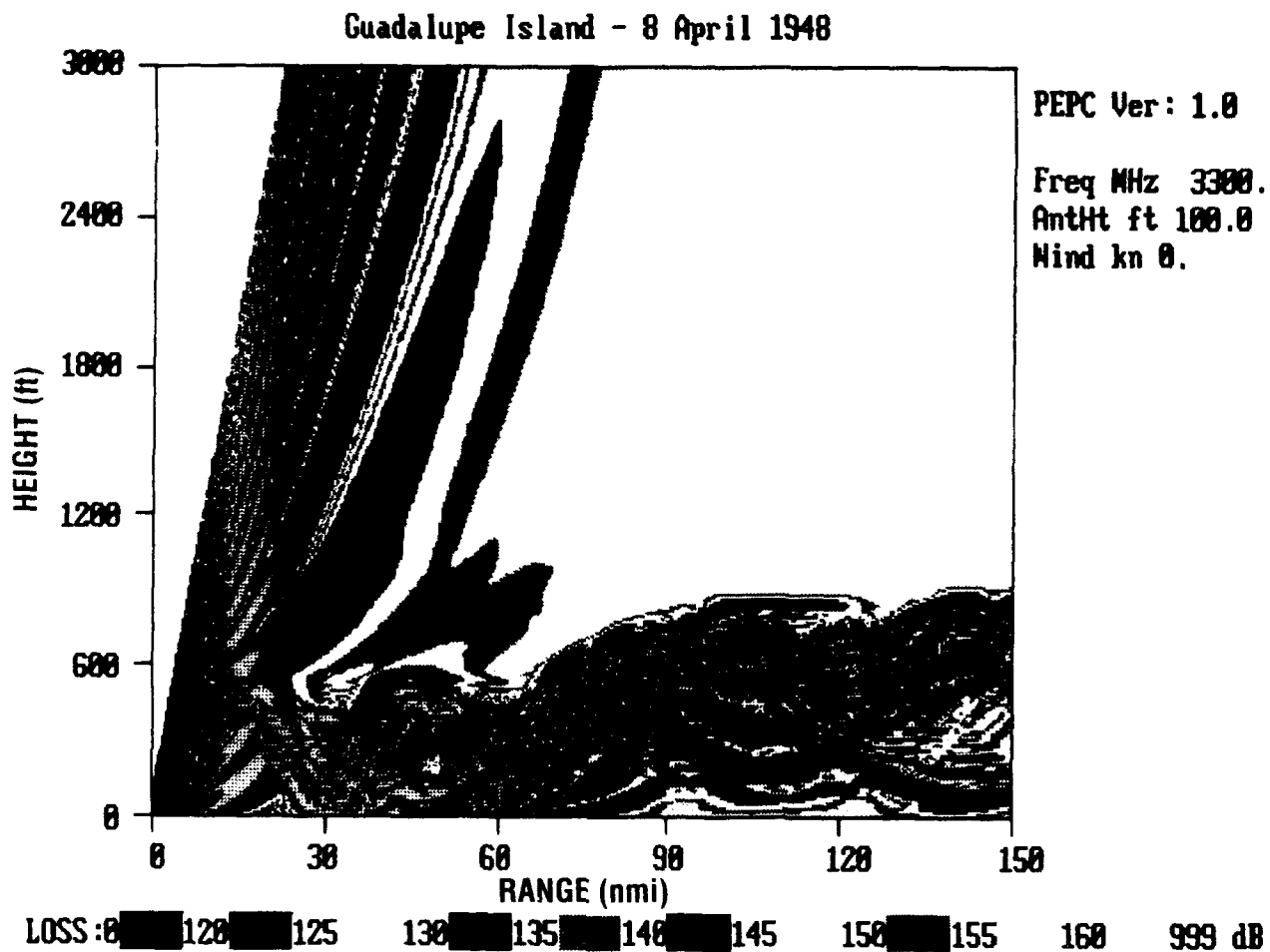
Figure 46. Coverage diagram for environment of 8 April 1948 at 3300 MHz.
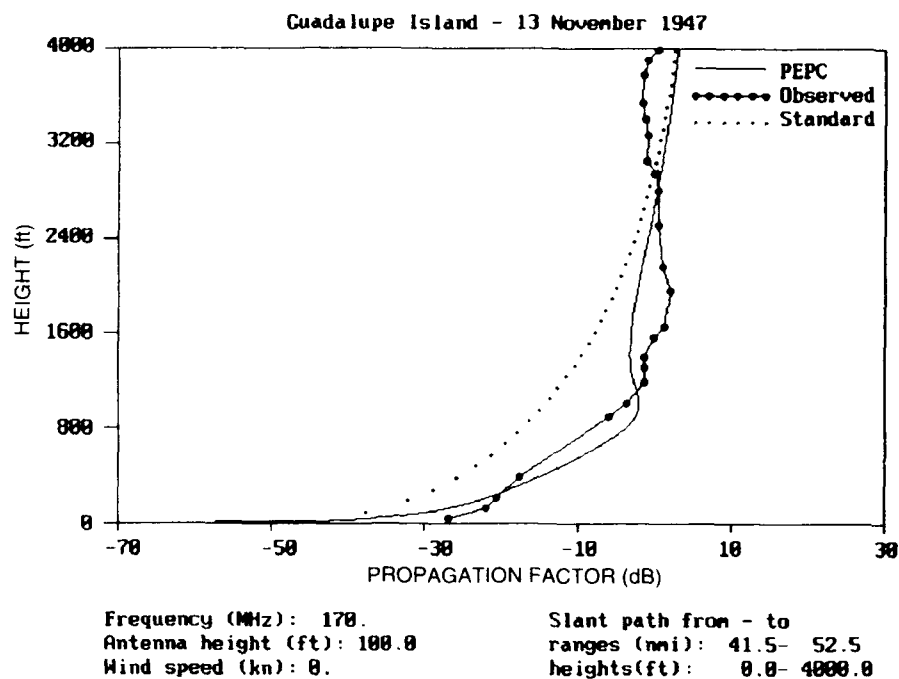
Figure 47. Comparisons between PEPC and measured radio data at 170 MHz for 13 November 1947, along slant path from 41.5 to 52.5 nmi.
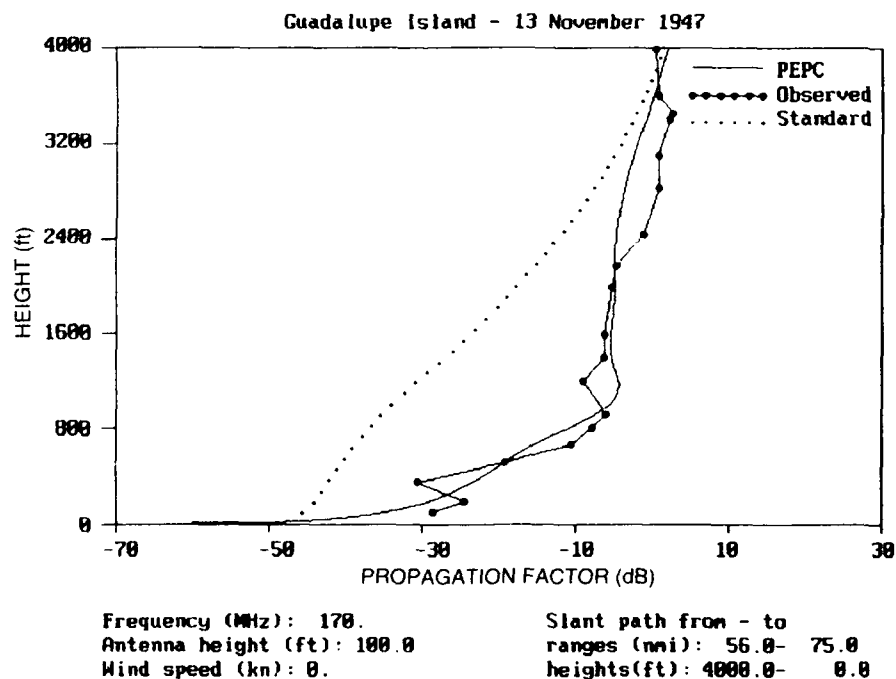
Figure 48. Comparisons between PEPC and measured radio data at 170 MHz for 13 November 1947, along slant path from 56 to 75 nmi.
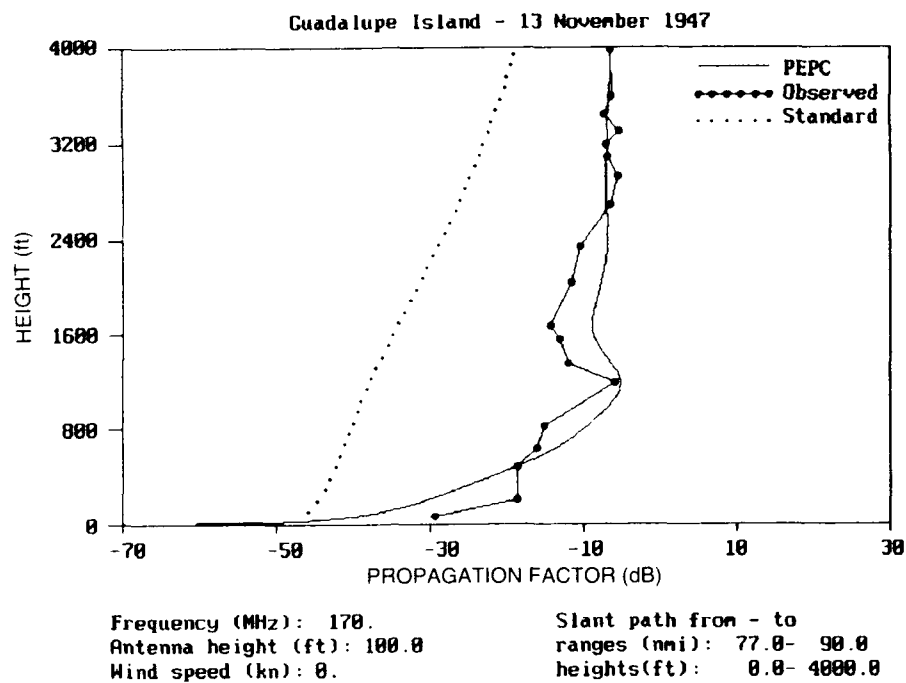
Figure 49. Comparisons between PEPC and measured radio data at 170 MHz for 13 November 1947, along slant path from 77 to 90 nmi.
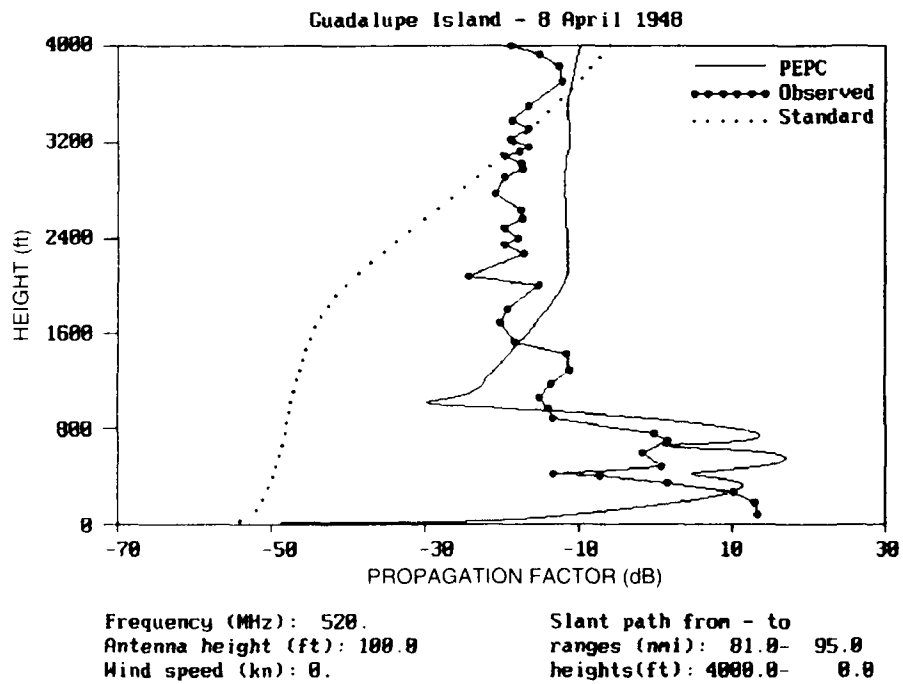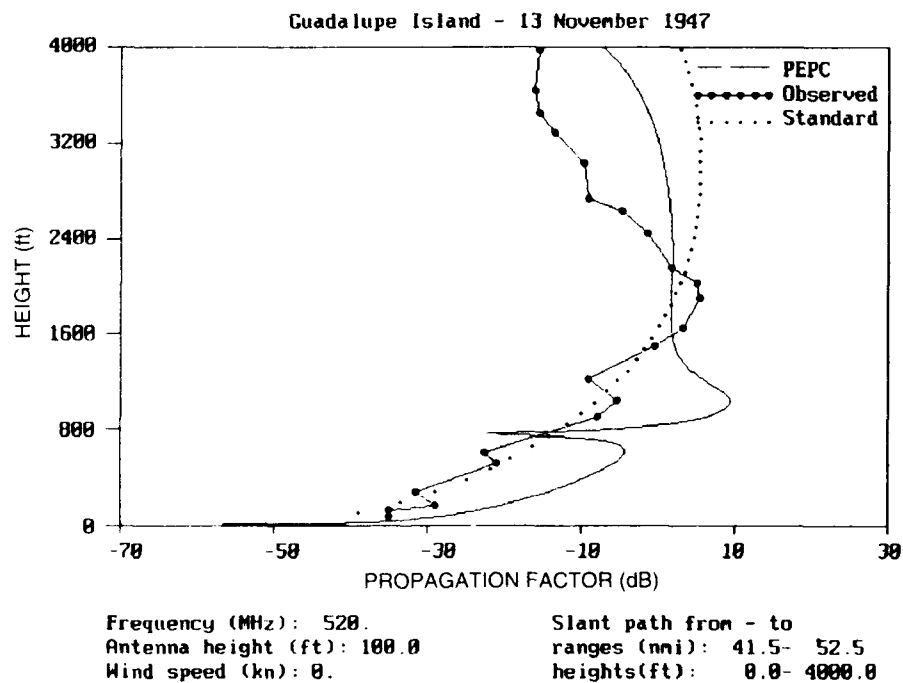

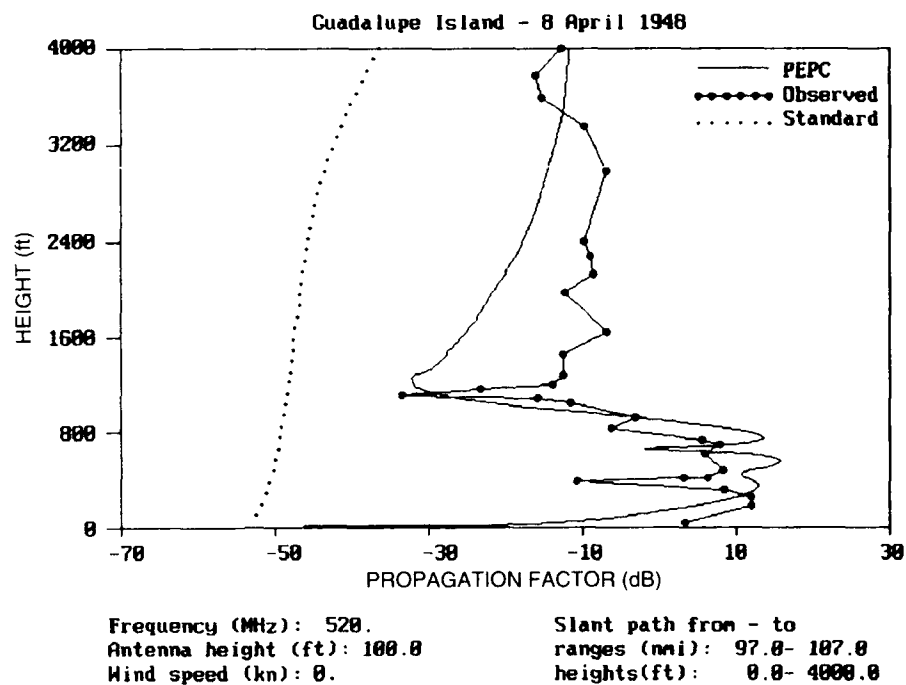Figure 50. Comparisons between PEPC and measured radio data at 520 MHz for 13 November 1947, along slant path from 41.5 to 52.5 nmi.
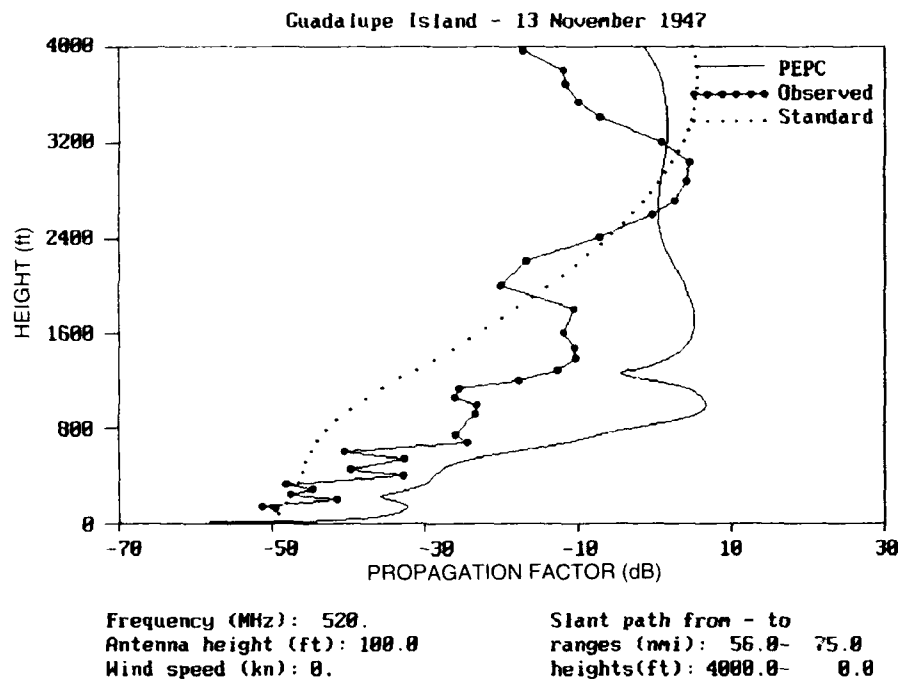
Figure 51. Comparisons between PEPC and measured radio data at 520 MHz for 13 November 1947, along slant path from 56 to 75 nmi.
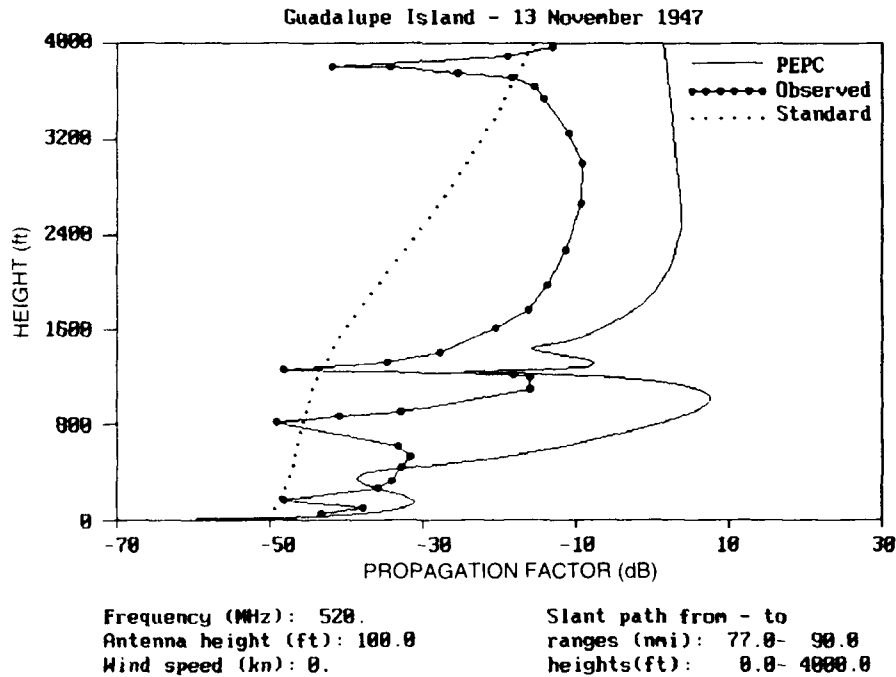
Figure 52. Comparisons between PEPC and measured radio data at 520 MHz for 13 November 1947, along slant path from 77 to 90 nmi.

44

Guadalupe Island - 13 November 1947

Frequency (MHz): 3300.
Antenna height (ft): 100.0
Wind speed (kn): 0.

Slant path from - to
ranges (nmi): 41.5- 50.0
heights(ft): 0.0- 3000.0
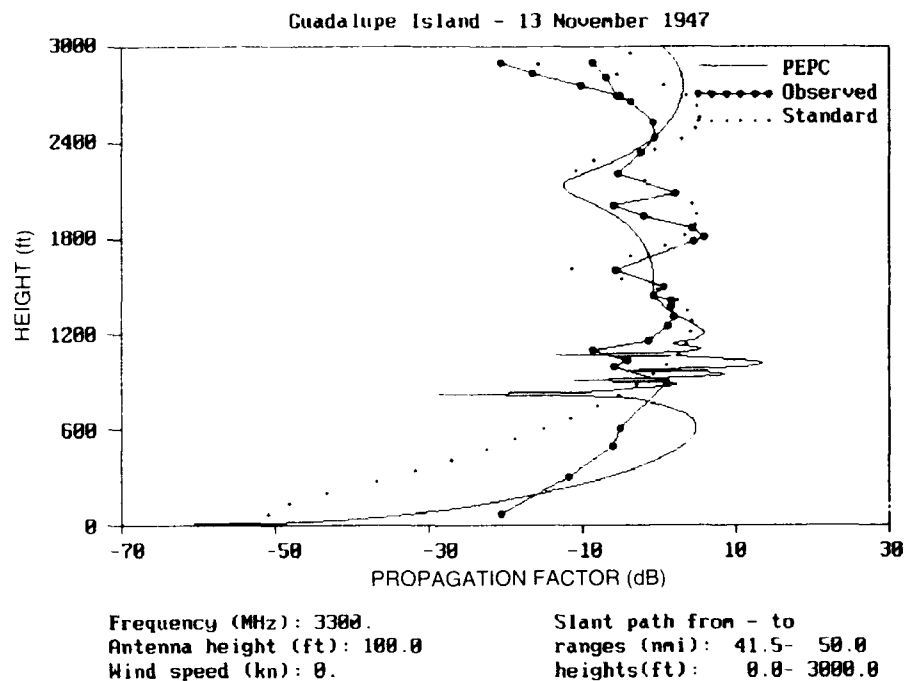
Figure 53. Comparisons between PEPC and measured radio data at 3300 MHz for 13 November 1947, along slant path from 41.5 to 50 nmi.

Guadalupe Island - 13 November 1947

Frequency (MHz): 3300.
Antenna height (ft): 100.0
Wind speed (kn): 0.

Slant path from - to
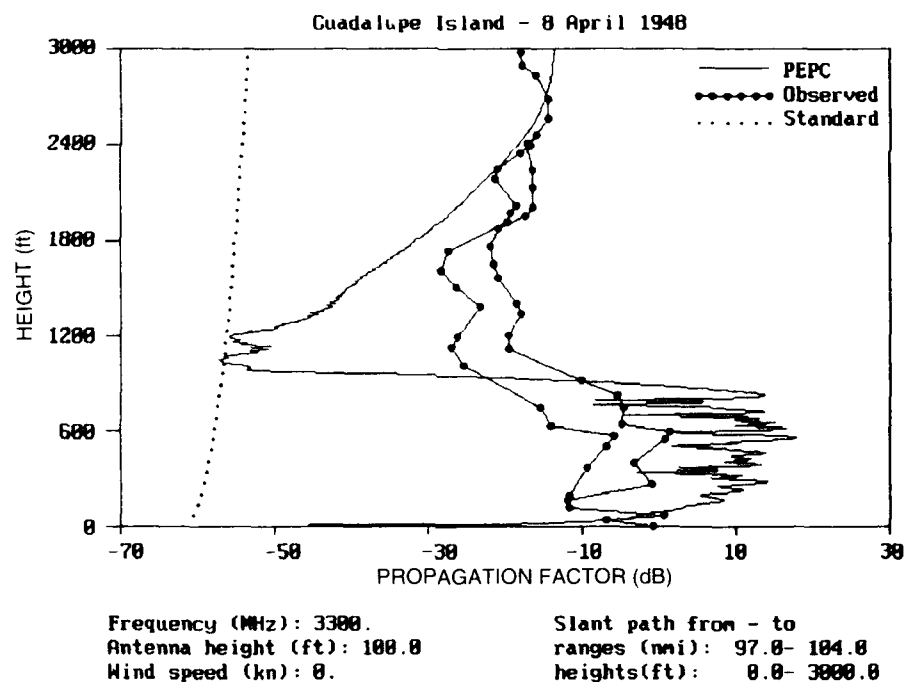ranges (nmi): 61.0- 75.0
heights(ft): 3000.0- 0.0
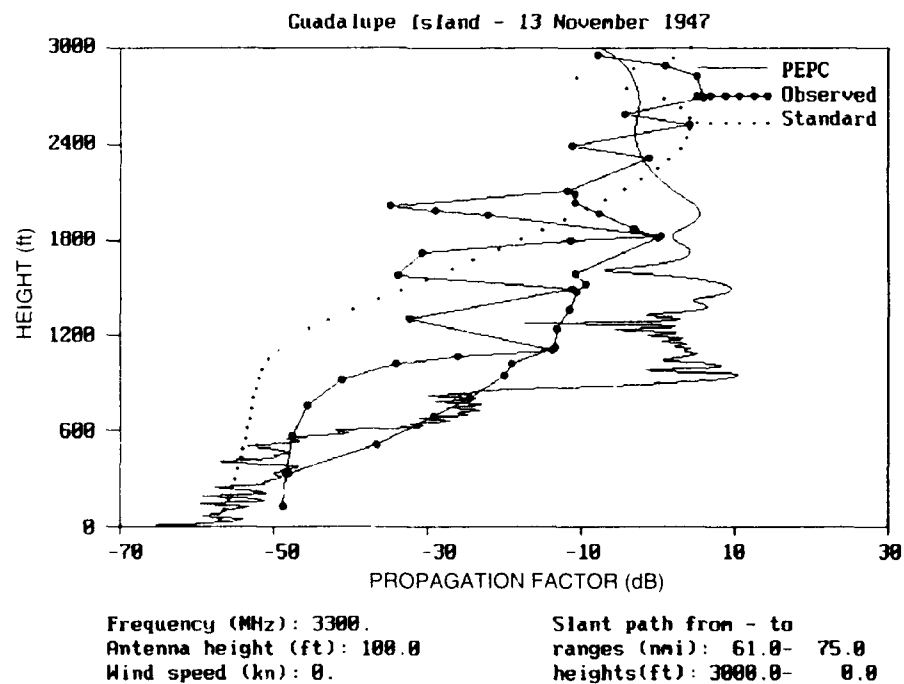
Figure 54. Comparisons between PEPC and measured radio data at 3300 MHz for 13 November 1947, along slant path from 61 to 75 nmi.

45
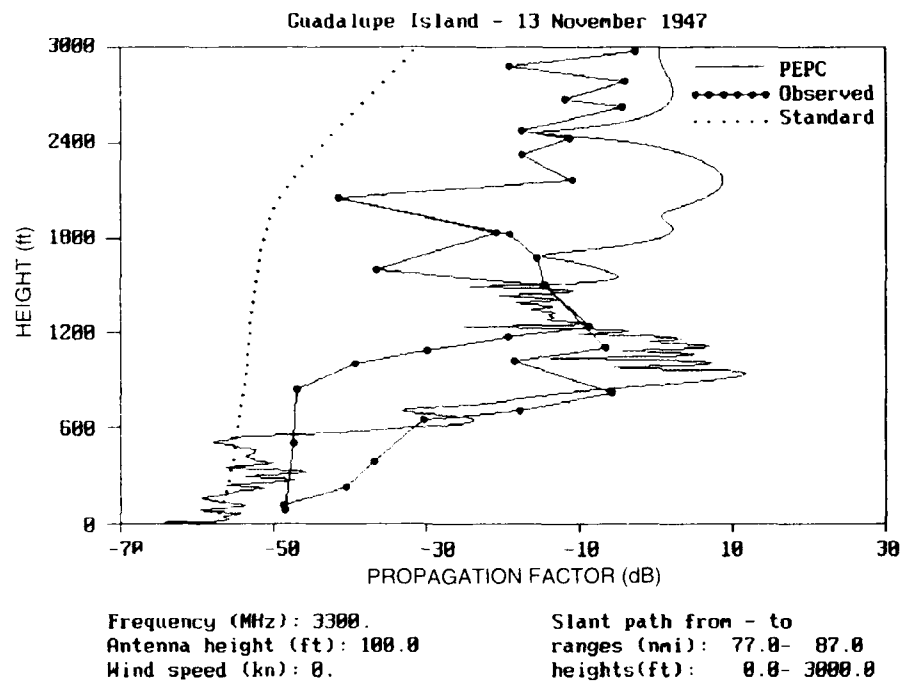
Figure 55. Comparisons between PEPC and measured radio data at 3300 MHz for 13 November 1947, along slant path from 77 to 87 nmi.
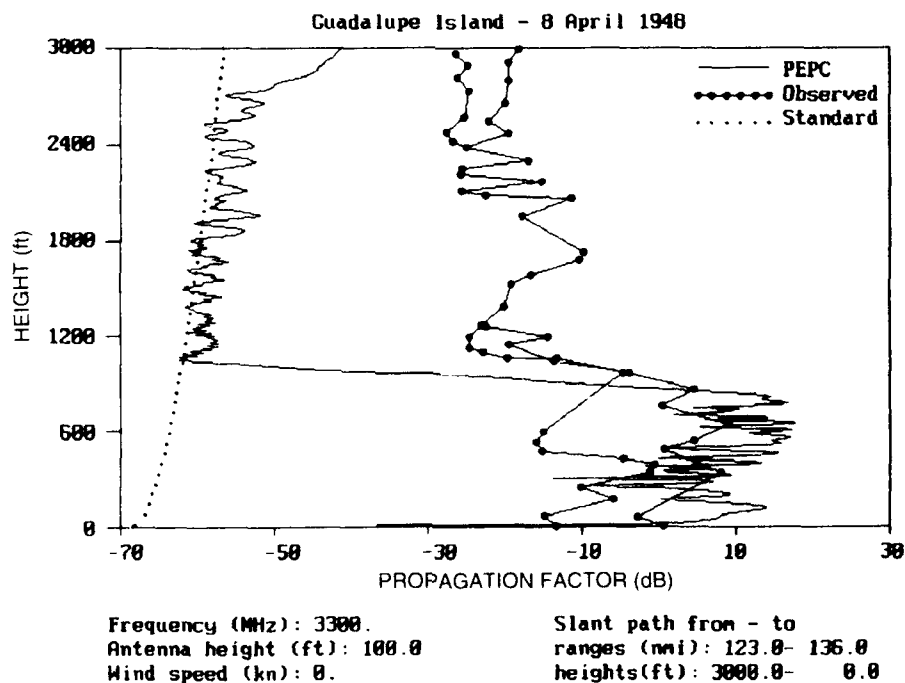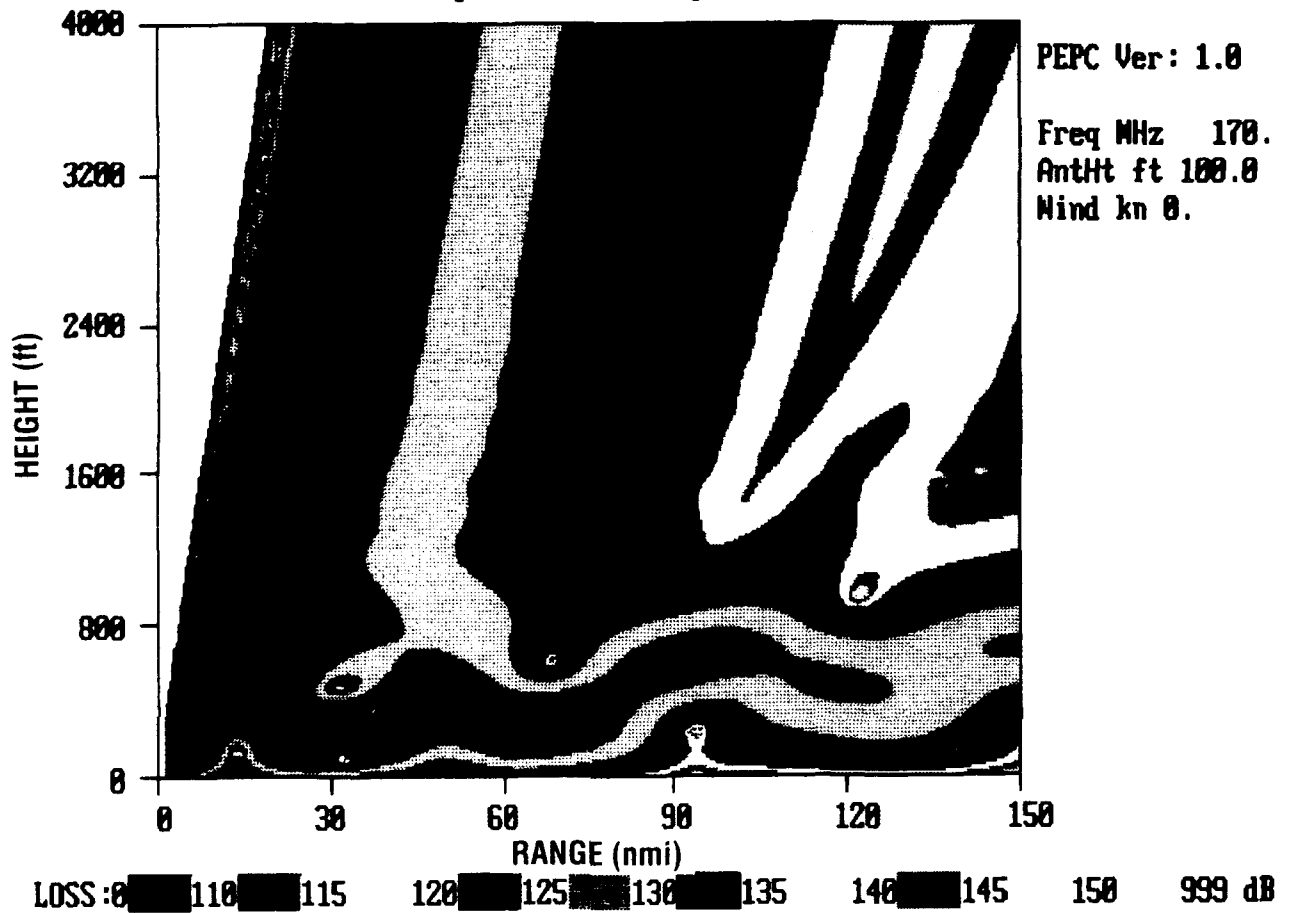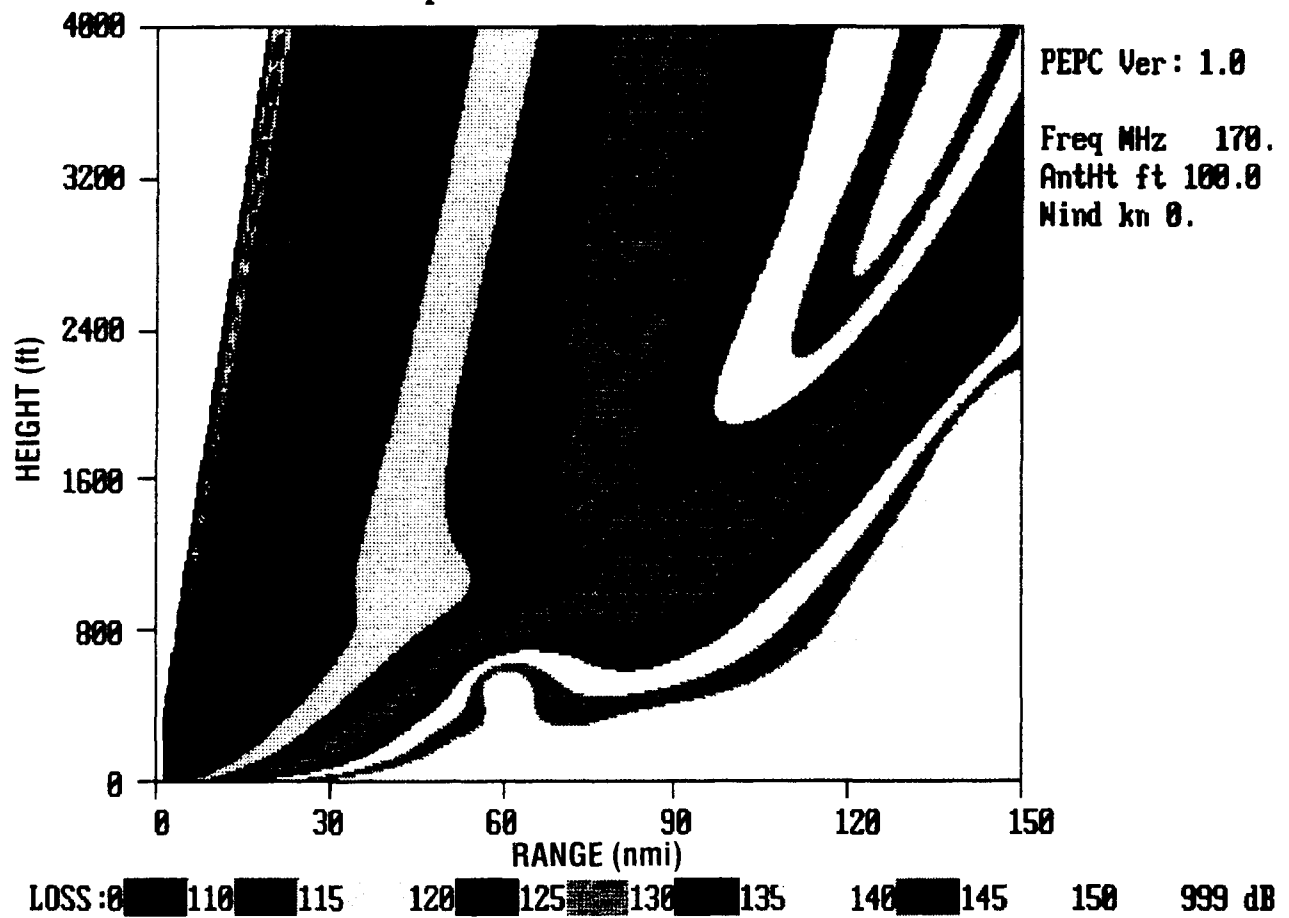
Figure 56. Coverage diagram for environment of 13 November 1947 at 170 MHz.
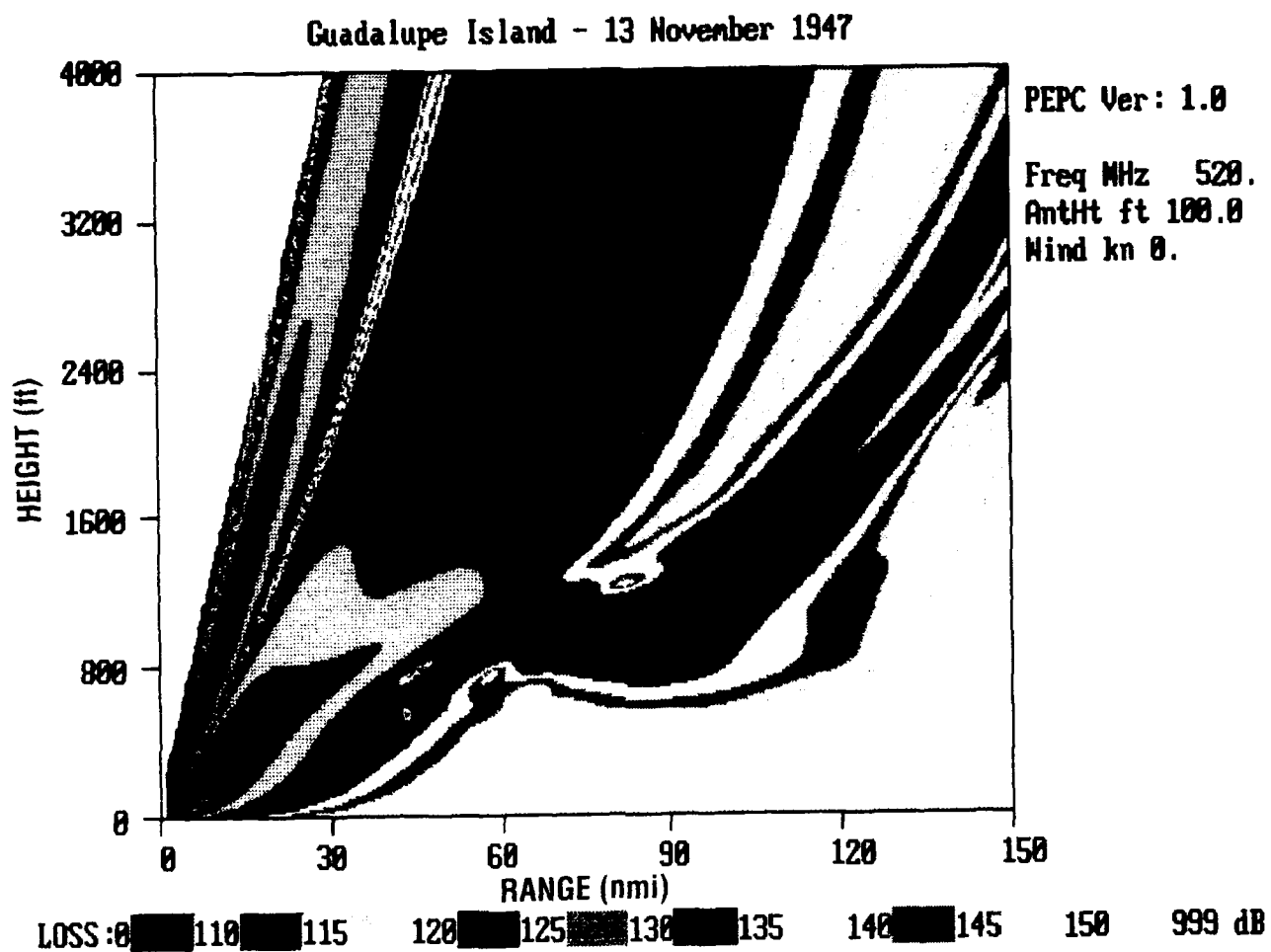
Figure 57. Coverage diagram for environment of 13 November 1947 at 520 MHz.
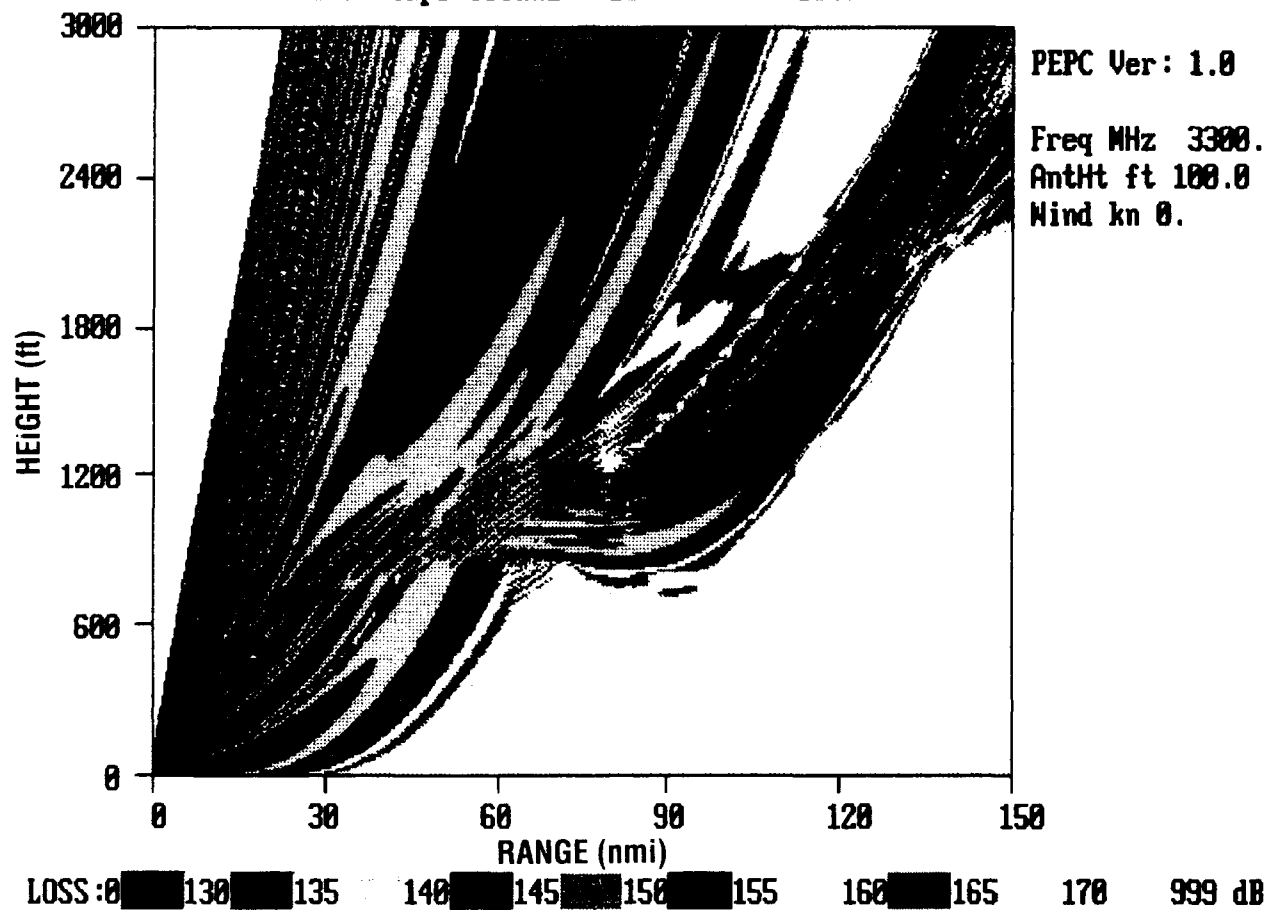
Figure 58. Coverage diagram for environment of 13 November 1947 at 3300 MHz.

Figure 59. Data records from Canterbury Project for 19 June 1947.

ISOPLETHS OF MODIFIED REFRACTIVE INDEX

RADAR A/C FLIGHT PLAN - ANSON 417
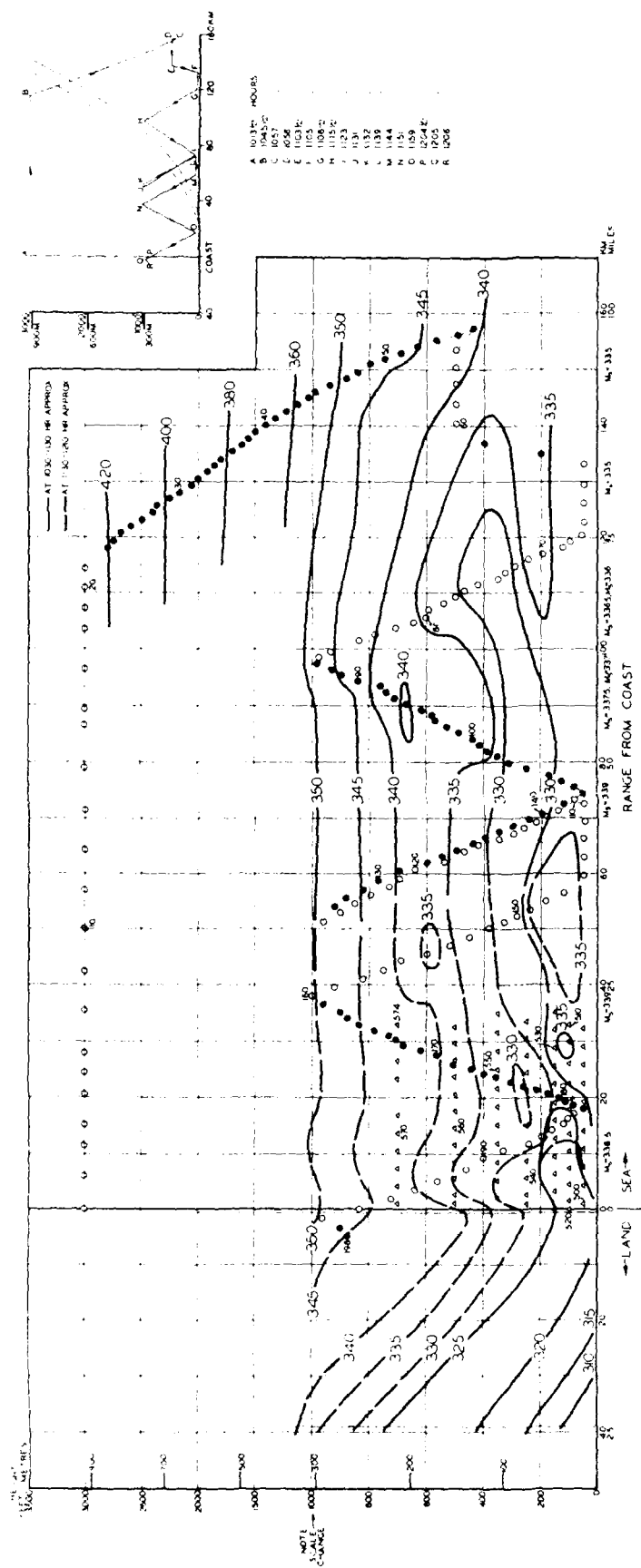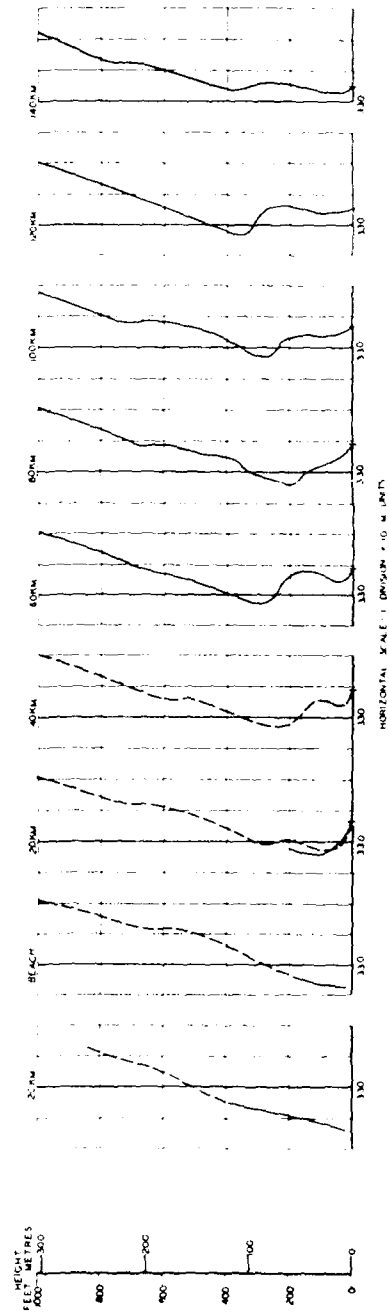
AIRCRAFT TRACK - ANSON 417

M CURVES
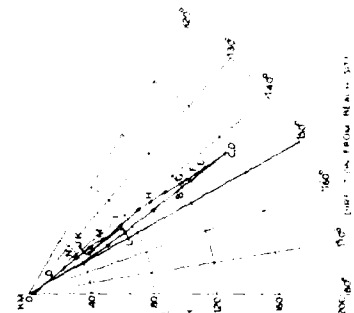
Figure 60. Data records from Canterbury Project for 11 July 1947.

Canterbury Project 19 June 1947 - S2 Channel

Frequency (MHz): 3240. Slant path from - to
Antenna height (ft): 86.0 ranges (nmi): 26.0- 38.0
Wind speed (kn): 0. heights(ft): 0.0- 1000.0
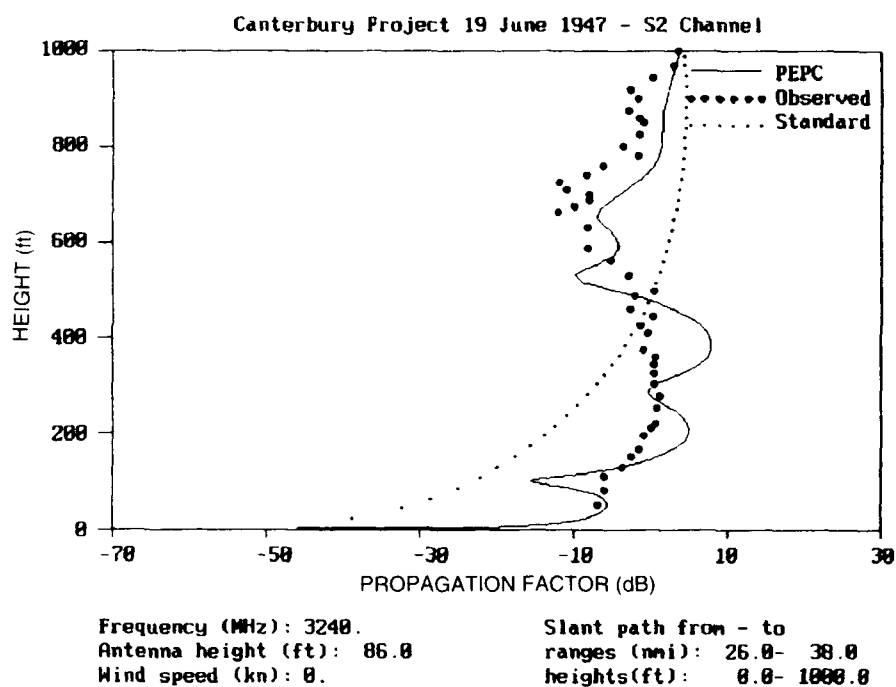
Figure 61. Comparison between PEPC and measured radio data at 3240 MHz from Canterbury Project data record for 19 June 1947.

Canterbury Project 19 June 1947 - X1 Channel

Frequency (MHz): 9875. Slant path from - to
Antenna height (ft): 26.5 ranges (nmi): 26.0- 38.0
Wind speed (kn): 0. heights(ft): 0.0- 1000.0
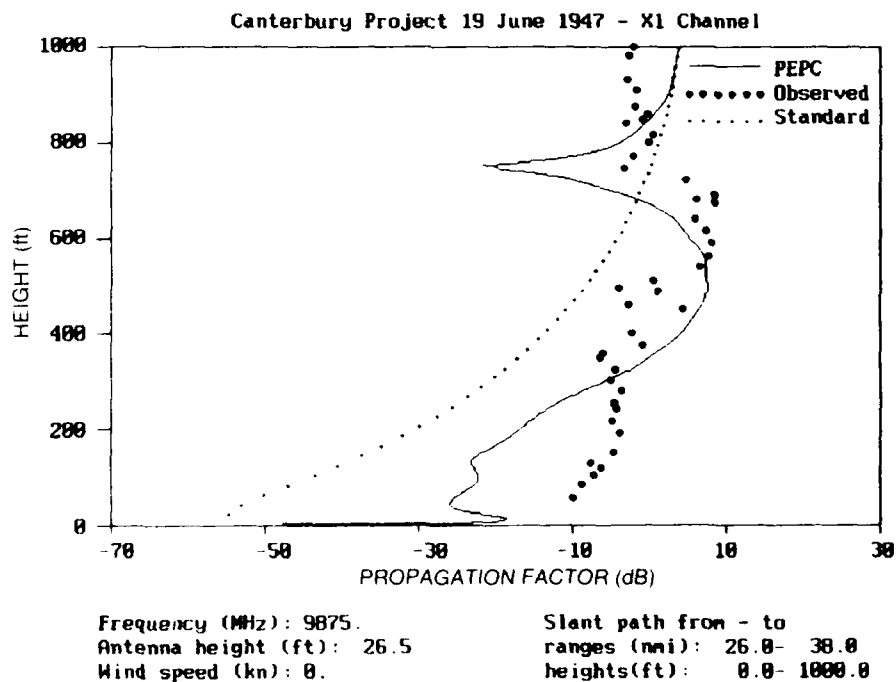
Figure 62. Comparisons between PEPC and measured radio data at 9875 MHz from Canterbury Project data record for 19 June 1947, with antenna height at 26.5 feet.

52
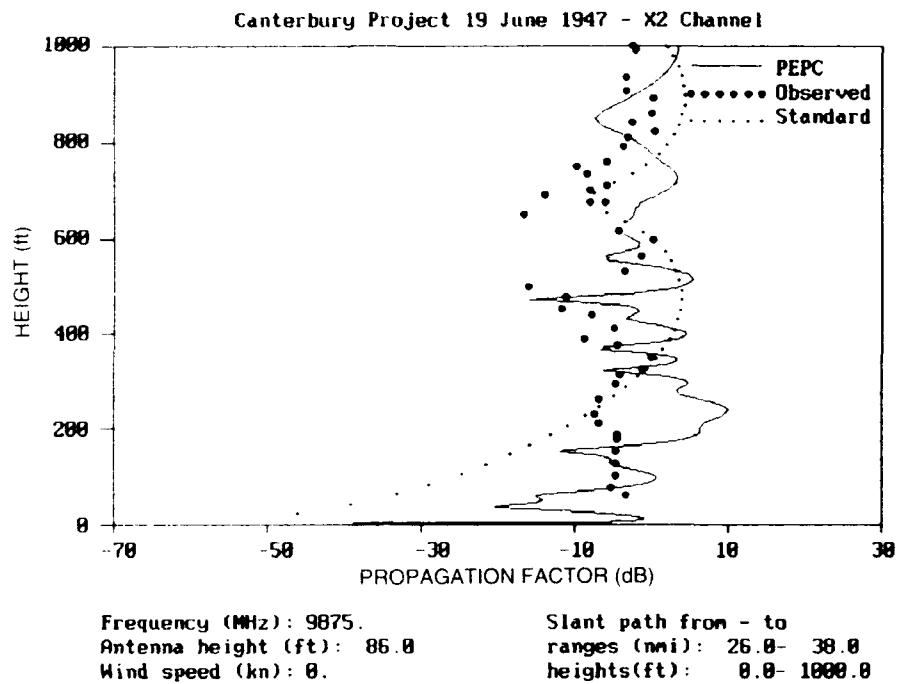
Figure 63. Comparisons between PEPC and measured radio data at 9875 MHz from Canterbury Project data record for 19 June 1947, with antenna height at 86 feet.

Figure 64. Coverage diagram for frequency and environment from figure 61.
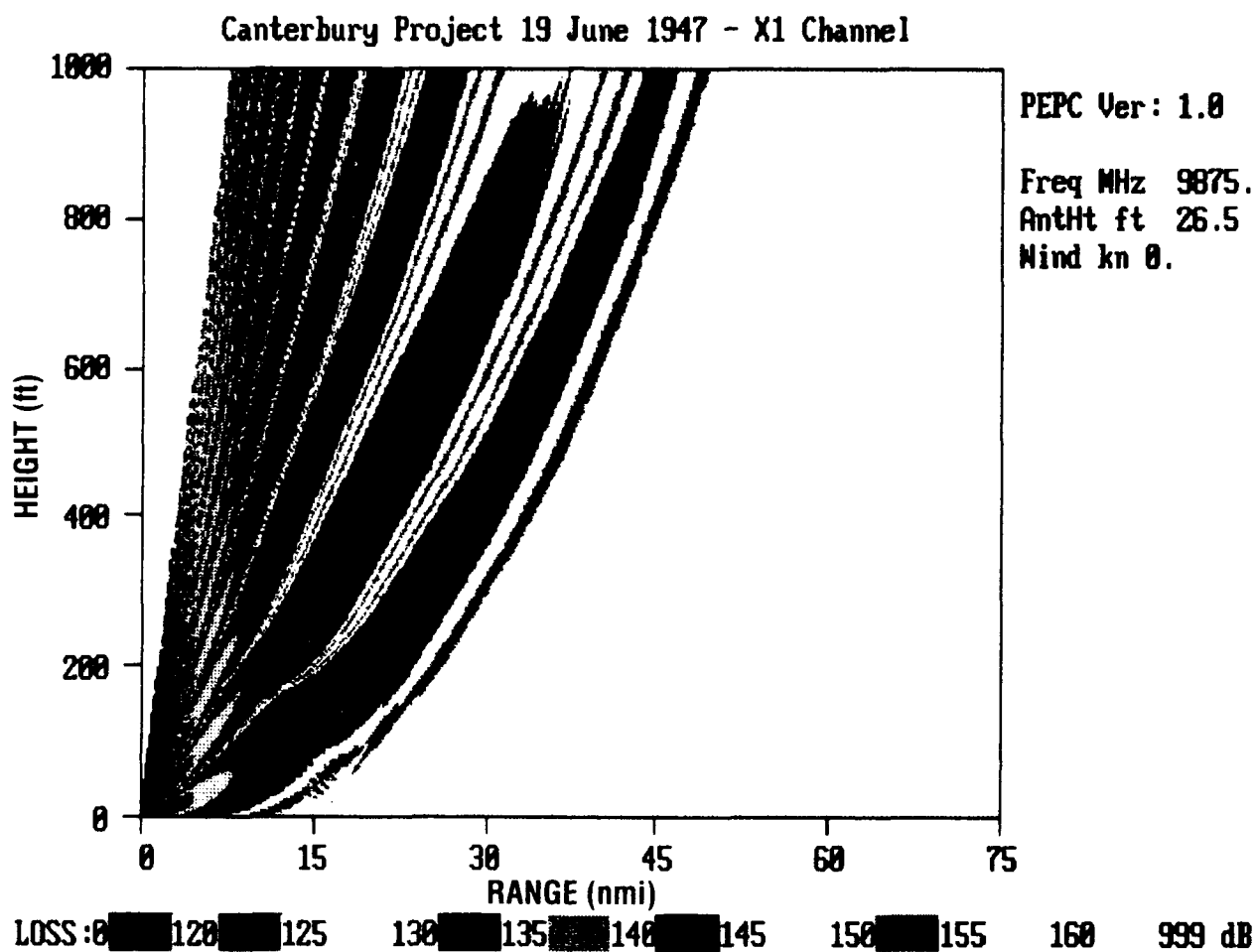
Figure 65. Cover diagram for frequency and environment from figure 62.

Figure 66. Cover diagram for frequency and environment from figure 63.

Canterbury Project 11 July 1947, Leg G->H

Frequency (MHz): 9875.
Antenna height (ft): 26.5
Wind speed (kn): 0.

Slant path from - to
ranges (nmi): 53.0- 65.0
heights(ft): 1000.0- 0.0
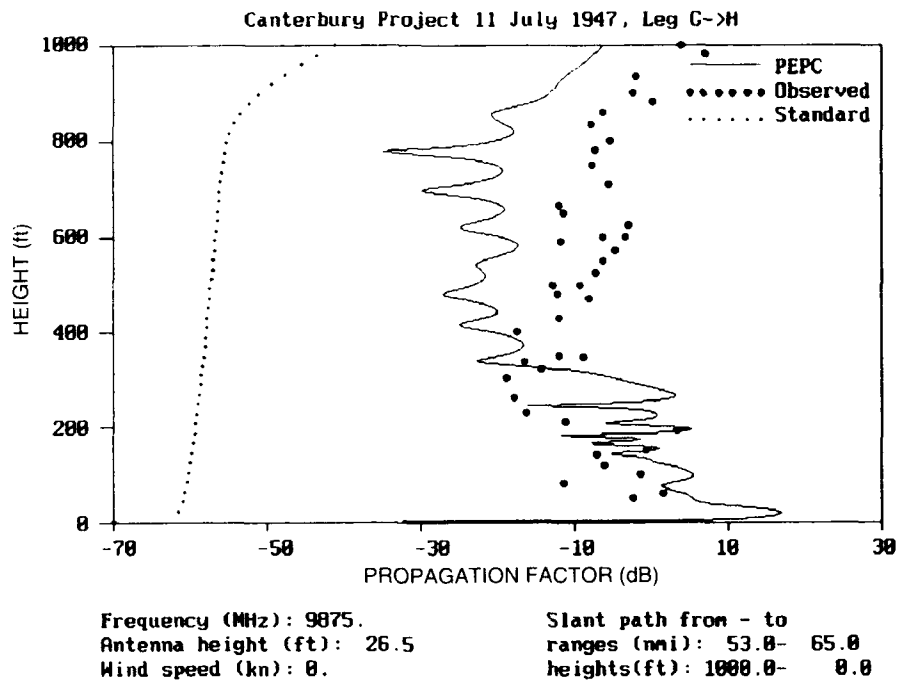
Figure 67. Comparisons between PEPC and measured radio data for flight path labeled GH from Canterbury Project data record of 11 July 1947, for antenna height at 26.5 feet.

Canterbury Project 11 July 1947, Leg G->H

Frequency (MHz): 9875.
Antenna height (ft): 86.0
Wind speed (kn): 0.

Slant path from - to
ranges (nmi): 53.0- 65.0
heights(ft): 1000.0- 0.0
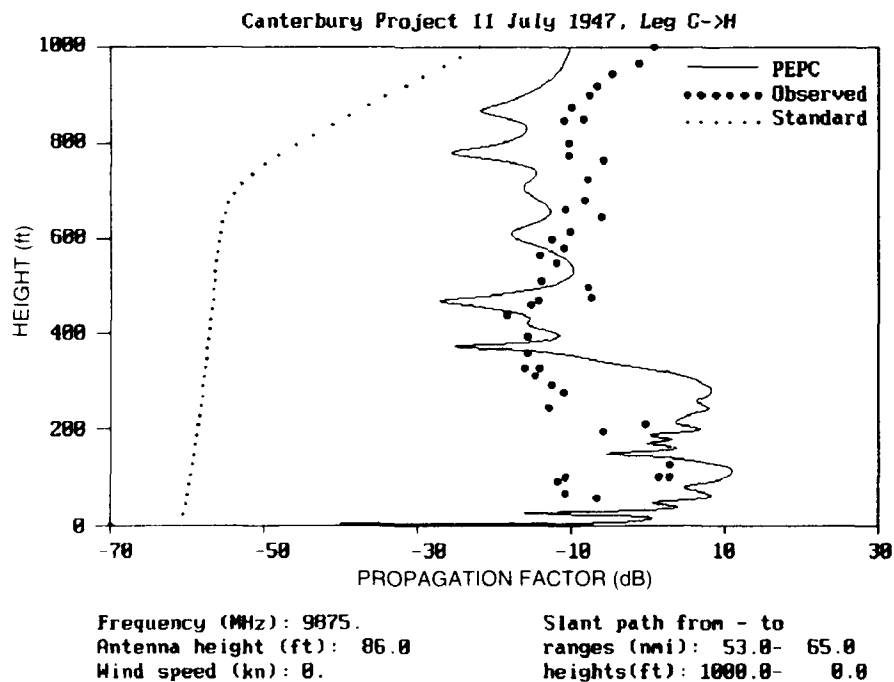
Figure 68. Comparisons between PEPC and measured radio data for flight path labeled GH from Canterbury Project data record of 11 July 1947, for antenna height at 86 feet.

57

Canterbury Project 11 July 1947, Leg H->I

Frequency (MHz): 9875.
Antenna height (ft): 26.5
Wind speed (kn): 0.

Slant path from - to
ranges (nmi): 40.0- 53.0
heights(ft): 0.0- 1000.0
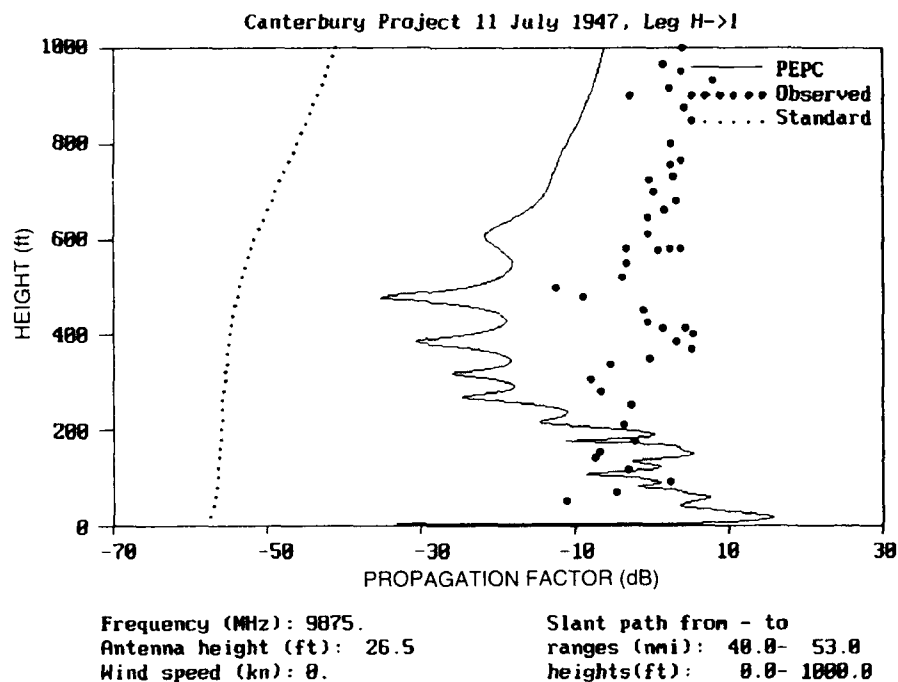
Figure 69. Comparisons between PEPC and measured radio data for flight path labeled HI from Canterbury Project data record of 11 July 1947, for antenna height at 26.5 feet.

Canterbury Project 11 July 1947, Leg H->I

Frequency (MHz): 9875.
Antenna height (ft): 86.0
Wind speed (kn): 0.

Slant path from - to
ranges (nmi): 40.0- 53.0
heights(ft): 0.0- 1000.0
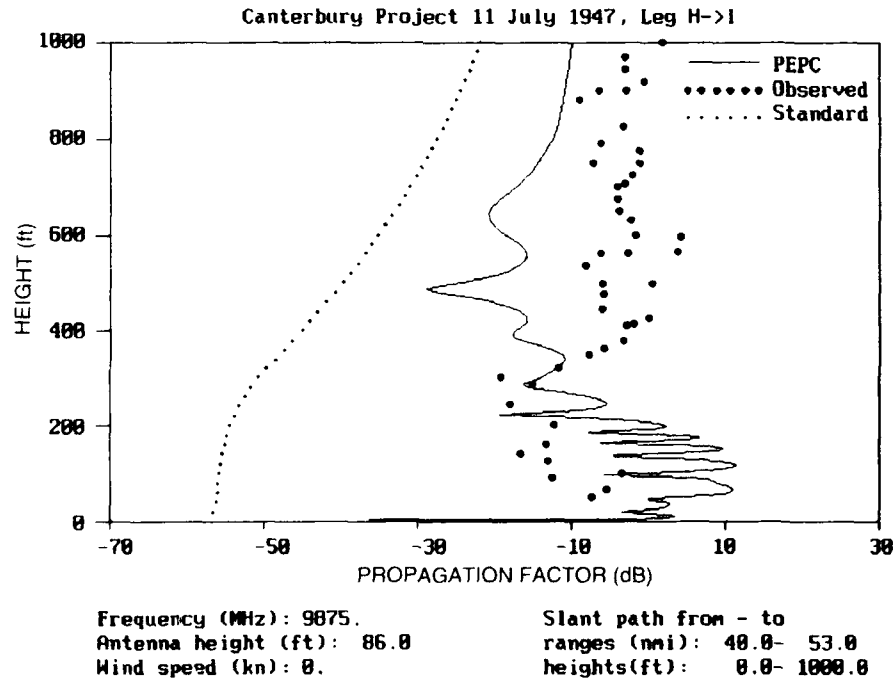
Figure 70. Comparisons between PEPC and measured radio data for flight path labeled HI from Canterbury Project data record of 11 July 1947, for antenna height at 86 feet.

Canterbury Project 11 July 1947, X1 Channel

PEPC Ver: 1.0

Freq MHz 9875.
AntHt ft 26.5
Wind kn 0.
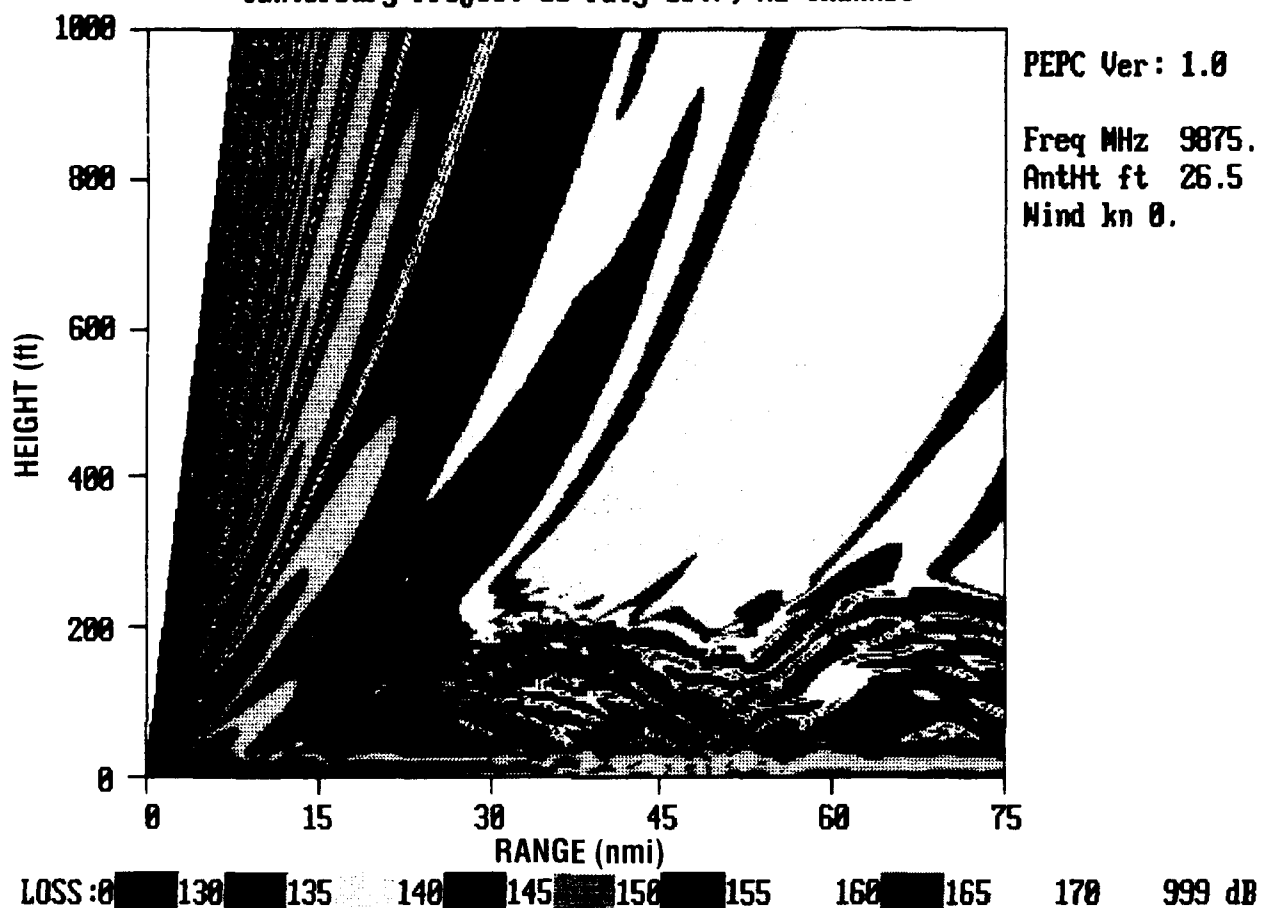
Figure 71. Coverage diagram for frequencies and environments from figures 67–70, antenna height at 26.5 feet.
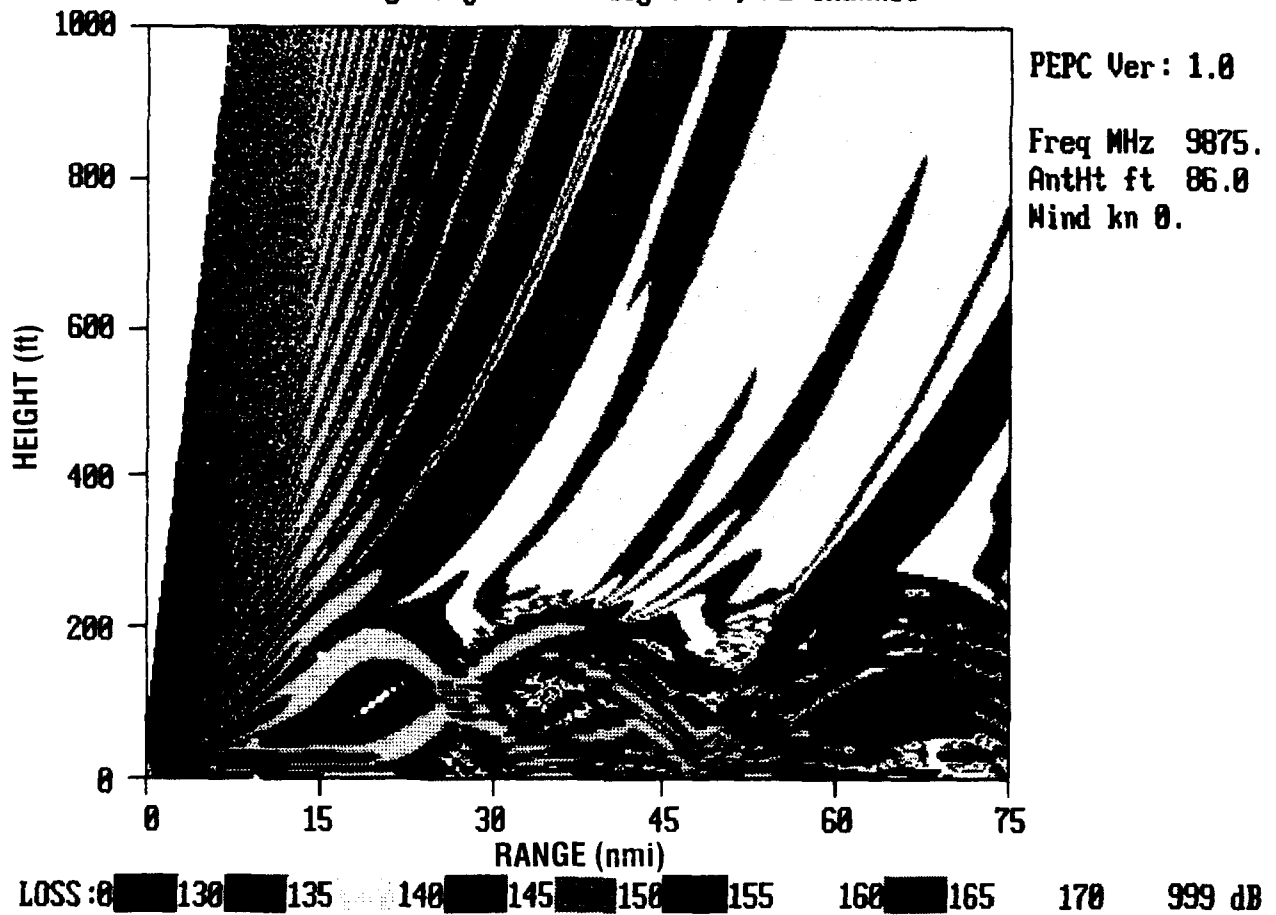
Figure 72. Coverage diagram for frequencies and environments from figures 67–70, antenna height at 86 feet.

4.0 CONCLUSIONS

The parabolic equation model, PEPC, has been shown to predict, with reasonably good accuracy, field strengths for range-dependent and range-independent environments. While improvements must be made to account for surface roughness and other environmental effects, for the simplest case used here PEPC agreed quite well with experimental data.

As mentioned before, horizontal homogeneity occurs in the troposphere almost 86% of the time. When the environment is inhomogeneous, the model presented here provides a means by which the field strengths can be predicted within these environments. The comparisons given in this report between predicted field strengths and measured data within measured range-dependent environments show the importance of including horizontal inhomogeneity in field prediction models. Care must be taken, however, in applying meteorological measurements to the models. A detailed knowledge of the refractivity structure involved is needed to make the best possible estimate of how the environment is changing.

REFERENCES

1. Hitney, H. V., J. H. Richter, R. A. Pappert, K. D. Anderson, and G. B. Baumgartner, Jr. 1985. "Tropospheric Radio Propagation Assessment," *Proc. of the IEEE*, vol. 73, no. 2 (February).

2. Patterson, W. L. 1987. "A Raytrace Method for a Laterally Heterogeneous Environment," NOSC TR 1180 (July). Naval Ocean Systems Center, San Diego, California.

3. Fock, V. A. 1965. *Electromagnetic Diffraction and Propagation Problems*, chap. 11–14. Elmsford, NY. Pergamon Press.

4. Hardin, R. H., and F. D. Tappert. 1973. "Application of the split-step Fourier method to the numerical solution of nonlinear and variable coefficient wave equations," SIAM Rev. 15, p. 423.

5. Ko, H. W., J. W. Sari, and J. P. Skura. 1983. "Anamolous Microwave Propagation Through Atmospheric Ducts," *John Hopkins APL Tech. Dig. 4*, pp. 12–16.

6. Dockery, G. D., and G. C. Konstanzer. "Recent Advances in Prediction of Tropospheric Propagation Using the Parabolic Equation," *Johns Hopkins APL Tech. Dig. 8*, pp. 404–412.

7. Ryan, F. J. 1989. "RPE: A Parabolic Equation Radio Assessment Model," in *AGARD Operational Decision Aids for Exploiting or Mitigating Electromagnetic Propagation Effects*, Electromagnetic Wave Propagation Panel Symposium, San Diego, CA, 15–16 May 1989. [Advisory Group for Aerospace Research and Development, Neuilly Sur Seine (Paris), France.]

8. Craig, K. H. 1989. "Propagation Modeling in the Troposphere: Parabolic Equation Method," *Elec. Lett. 24*, pp. 1136–1139.

9. NEL Report 173. 1949. Symposium on Tropospheric Wave Propagation (25–29 July). Naval Electronics Laboratory, San Diego, California.

10. Department of Scientific and Industrial Research. 1951. "Report of Factual Data from the Canterbury Project," DSIR, vol. I, II, III. Wellington, New Zealand.

11. Tappert, F. D. 1977. "The Parabolic Approximation Method," in *Wave Propagation and Underwater Acoustics*, Lecture Notes in Physics, vol. 70, ed. by J. B. Keller and J. S. Papadakis, pp. 224–287. Springer-Verlag, Berlin.

12. Feit, M. D., and J. A. Fleck, Jr. 1978. "Light Propagation in Graded-Index Fibers," *Appl. Opt. 17*, pp. 3990–3998.

13. Thomson, D. J., and N. R. Chapman. 1983. "A Wide-Angle Split-Step Algorithm for the Parabolic Equation," *J. Acous. Soc. Am. 74*, pp. 1848–1854.

14. Dockery, G. D. 1988. "Modeling Electromagnetic Wave Propagation in the Troposphere Using the Parabolic Equation," *IEEE Trans. on Ant. and Prop.*, vol. 36, no. 10 (October), pp. 1464—1470.

15. Yeh, L. P. 1960. "Simple Methods for Designing Troposcatter Circuits," *IRE Trans. CS-8*, 193—198.

16. Rice, P. L., A. G. Longley, K. A. Norton, and A. P. Barsis. 1965. National Bureau of Standards Technical Note 101, "Transmission Loss Predictions for Tropospheric Communication Circuits," vol. 1 & 2, U.S. Department of Commerce, Washington, D.C.

17. Patterson, W. L., C. P. Hattan, H. V. Hitney, R. A. Paulus, A. E. Barrios, G. E. Lindem, and K. D. Anderson. 1990. "Engineer's Refractive Effects Prediction System (EREPS) Revision 2.0," NOSC TD 1342 (February). Naval Ocean Systems Center, San Diego, California.

18. Baumgartner, G. B. 1983. "XWVG: A Waveguide Program for Trilinear Tropospheric Ducts," NOSC TD 610. (June.) Naval Ocean Systems Center, San Diego, California.

RELATED READING

1. Kuttler, J. R., and G. D. Dockery. 1991. "Theoretical Description of the Parabolic Approximation/Fourier Split-Step Method of Representing Electromagnetic Propagation in the Troposphere," *Radio Science.* (March—April.) Pp. 381—393.

2. Craig, K. H., and M. F. Levy, Radio Communications Research Unit, Rutherford Appleton Laboratory, Chilton, Didcot, U.K. "Parabolic Equation Modeling of the Effects of Multipath and Ducting on Radar Systems," Unpublished notes. Available to qualified requesters. Contact author of this TR for additional information.

3. Ryan, F. J., Ocean and Atmospheric Sciences Division (Code 541), Naval Ocean Systems Center, San Diego, CA. "A Theoretical Analysis of Tropospheric Radiowave Propagation Using the Parabolic Wave Equation," preliminary draft, 1991. Available to qualified requesters. Contact author of this TR for additional information.

4. Hattan, C. P. 1988. "Evaporation Duct Effects on the Detection of Low-Altitude Targets," NOSC TR 1201 (January). Naval Ocean Systems Center, San Diego, California.

APPENDIX

GUADALUPE ISLAND PROFILE TABLES

Table A-1. M-unit versus height profiles and corresponding
ranges from Guadalupe Island data record tor 12 March 1948.

Environment for 12 March 1948

Profile #1 - Range at 0 nmi
Height(ft)   M-units
   0.   337.
  540.   358.44
  803.407   324.736
 1217.17   334.888
 1231.   334.494
 3500.   447.400

Profile #2 - Range at 39 nmi
Height(ft)   M-units
   0.   337.
  540.   358.44
  803.407   324.736
 1217.17   334.888
 1231.   334.494
 3500.   447.400

Profile #3 - Range at 85.5 nmi
Height(ft)   M-units
   0.   337.169
  740.   365.34
 1080.63   343.702
 1490.61   356.039
 1652.63   351.889
 3500.00   430.919

Profile #4 - Range at 125. nmi
Height(ft)   M-units
   0.   335.819
 1190.   382.84
 1574.55   357.962
 1889.38   371.111
 2096.94   371.011
 3500.00   430.957

Profile #5 - Range at 160. nmi
Height(ft)   M-units
   0.   333.676
 1145.00   378.220
 2140.00   370.715
 2584.38   398.294
 2923.08   404.423
 3500.00   429.802

Profile #6 - Range at 193. nmi
Height(ft)   M-units
   0.   331.056
 1420.00   382.920
 2387.50   383.544
 2718.44   410.029
 2892.62   399.773
 3500.00   430.849

Table A-2. M-unit versus height profiles and corresponding
ranges from Guadalupe Island data record for 8 April 1948.

Environment for 8 April 1948

Profile #1 - Range at 0 nmi
Height(ft)	M-units
0.0	340.007
349.827	352.781
574.223	309.753
968.295	317.703
1207.64	345.040
1488.62	351.822
1503.41	358.671
1809.71	359.083
2194.20	375.590
2293.07	374.704
2563.72	393.768
4000.00	447.772

Profile #2 - Range at 41.1 nmi
Height(ft)	M-units
0.0	340.007
349.827	352.781
574.223	309.753
968.295	317.703
1207.64	345.040
1488.62	351.822
1503.41	358.671
1809.71	359.083
2194.20	375.590
2293.07	374.704
2563.72	393.768
4000.00	447.772

Profile #3 - Range at 56.9 nmi
Height(ft)	M-units
0.0	341.728
368.239	352.042
577.280	308.902
1005.35	320.349
1260.99	348.064
1475.73	352.767
1503.41	358.671
1809.71	359.083
2194.20	375.590
2293.07	374.704
2563.72	393.768
4000.00	447.772

Profile #4 - Range at 93.2 nmi
Height(ft)	M-units
0.0	341.806
672.037	368.492
983.245	320.817
1231.19	343.194
1388.96	347.223
1503.41	358.671
1809.71	359.083
2194.20	375.590
2293.07	374.704
2563.72	393.768
4000.00	447.772

Profile #5 - Range at 132.7 nmi
Height(ft)	M-units
0.0	342.668
733.564	369.305
1059.78	323.572
1251.12	345.108
1539.68	361.967
2030.24	368.838
2153.73	373.425
2182.62	371.732
2363.42	384.754
4000.00	443.040

Table A-3. M-unit versus height profiles and corresponding
ranges from Guadalupe Island data record for 13 November 1947.

Environment for 13 November 1947

Profile #1 - Range at 0 nmi

Height(ft)	M-units
0.	317.9
216.865	314.73
1617.62	362.87
3084.17	420.63
4000.	456.18

Profile #2 - Range at 37.5 nmi

Height(ft)	M-units
0.	322.762
795.918	345.177
1116.23	340.451
1553.31	354.080
3182.06	414.038
4000.00	440.863

Profile #3 - Range at 71.4 nmi

Height(ft)	M-units
0.0	331.331
393.097	335.389
618.075	351.704
820.575	355.378
1008.75	362.805
1359.41	348.897
2155.46	371.392
3182.06	414.038
4000.00	440.863

Profile #4 - Range at 126.9 nmi

Height(ft)	M-units
0.0	306.607
518.528	321.198
790.755	336.550
926.370	335.692
1214.22	348.295
2017.49	373.394
2556.49	374.805
3684.10	410.625
4000.00	425.710

Environment for 11 July 1947 from Canterbury Project

Profile #1 - Range at 0 nmi
Height(ft)	M-units
0.	322.5
140.	324.
530.	342.5
1000.	351.

Profile #2 - Range at 10.8 nmi
Height(ft)	M-units
0.	335.5
60.	327.
200.	330.
270.	329.
1000.	350.

Profile #3 - Range at 21.6 nmi
Height(ft)	M-units
0.	337.5
25.	333.5
105.	336.
200.	327.
1000.	350.

Profile #4 - Range at 32.4 nmi
Height(ft)	M-units
0.	338.
40.	334.
165.	339.
285.	327.
1000.	350.

Profile #5 - Range at 43.2 nmi
Height(ft)	M-units
0.	339.
150.	331.
195.	326.
350.	330.
1000.	351.

Profile #6 - Range at 56 nmi
Height(ft)	M-units
0.	336.
80.	333.
200.	333.
270.	327.
1000.	347.5

Table A-5. M-unit versus height profiles and corresponding
ranges from Guadalupe Island data record for 19 June 1947.

Environment for 19 June 1947

Profile #1 - Range at 0 nmi
Height(ft)	M-units
0.	304.
220.	307.
515.	315.5
1000.	318.1

Profile #2 - Range at 10.8 nmi
Height(ft)	M-units
0.	315.
10.	309.
130.	314.
195.	306.
405.	323.
500.	317.5
1000.	335.8

Profile #3 - Range at 21.6 nmi
Height(ft)	M-units
0.	315.
25.	312.
345.	325.
425.	323.5
520.	326.
600.	325.
1000.	339.6

Profile #4 - Range at 32.4 nmi
Height(ft)	M-units
0.	320.
20.	313.
220.	322.
330.	322.5
500.	329.5
730.	336.
1000.	347.

Profile #5 - Range at 43.2 nmi
Height(ft)	M-units
0.	307.
375.	320.
480.	322.
650.	330.
780.	328.
1000.	339.

REPORT DOCUMENTATION PAGE

Form Approved
OMB No. 0704-0188

1. AGENCY USE ONLY *(Leave blank)*	2. REPORT DATE	3. REPORT TYPE AND DATES COVERED
	May 1991	Final: Oct 1990—May 1991

4. TITLE AND SUBTITLE
RADIO WAVE PROPAGATION IN HORIZONTALLY INHOMOGENEOUS
ENVIRONMENTS BY USING THE PARABOLIC EQUATION METHOD

5. FUNDING NUMBERS
PE: 0604230N
Proj: MP67
Task: X1752
WU: DN305 062

6. AUTHOR(S)
A. E. Barrios

7. PERFORMING ORGANIZATION NAME(S) AND ADDRESS(ES)
Naval Ocean Systems Center
San Diego, CA 92152–5000

8. PERFORMING ORGANIZATION REPORT NUMBER
NOSC TR 1430

9. SPONSORING/MONITORING AGENCY NAME(S) AND ADDRESS(ES)
Space and Naval Warfare Systems Command (PMW141)
Washington, DC 20362-5100

10. SPONSORING/MONITORING AGENCY REPORT NUMBER

11. SUPPLEMENTARY NOTES

12a. DISTRIBUTION/AVAILABILITY STATEMENT
Approved for public release; distribution is unlimited.

12b. DISTRIBUTION CODE

13. ABSTRACT *(Maximum 200 words)*

The validity of a parabolic equation (PE) model for predicting radio field strengths in horizontally inhomogeneous environments was investigated by performing comparisons between the model and experimental data. Excellent agreements were found at VHF and UHF frequencies with good agreement in S- and X-bands. In some cases, the predicted curves for the S-band comparisons underestimated that of the measured data at large ranges. This may be the result of phenomena such as surface roughness, backscatter, etc., not accounted for in the model. Discrepancies may also result from the presence of evaporation ducts not included in the environmental inputs to the model because of a lack of detailed measurements. This would account for lower predicted signal levels at higher frequencies.

14. SUBJECT TERMS
Tactical Environment Support System (TFSS)   horizontally inhomogeneous environments
electronic propagation models   parabolic equations
radio wave propagation

15. NUMBER OF PAGES
81

16. PRICE CODE

17. SECURITY CLASSIFICATION OF REPORT	18. SECURITY CLASSIFICATION OF THIS PAGE	19. SECURITY CLASSIFICATION OF ABSTRACT	20. LIMITATION OF ABSTRACT
UNCLASSIFIED	UNCLASSIFIED	UNCLASSIFIED	SAME AS REPORT

UNCLASSIFIED

21a. NAME OF RESPONSIBLE INDIVIDUAL	21b. TELEPHONE *(include Area Code)*	21c. OFFICE SYMBOL
A. E. Barrios	(619) 553-1429	Code 543

UNCLASSIFIED